UiT

THE ARCTIC
UNIVERSITY
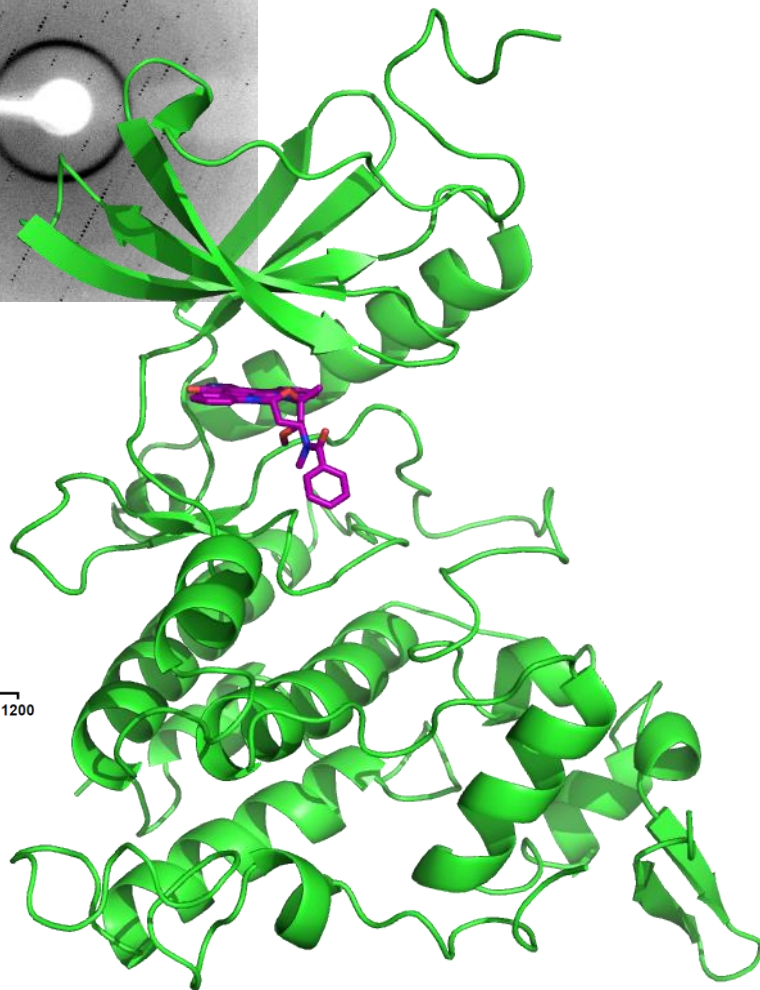OF NORWAY

Faculty of Science and Technology
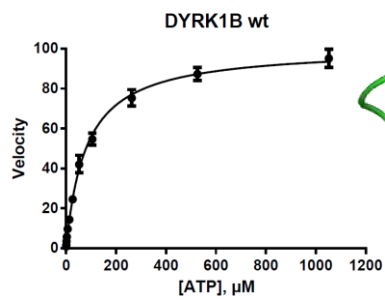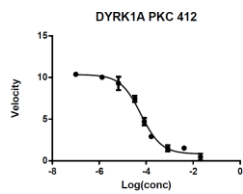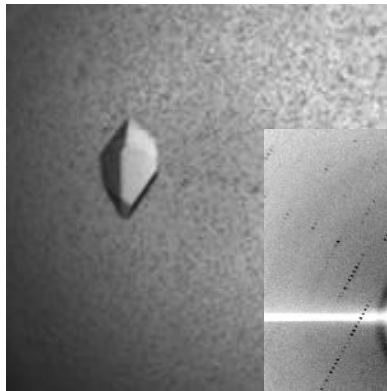
Biophysical characterization of the DYRK family

Studies on the kinases DYRK1A and DYRK1B

—

Marina Alexeeva
Master's Thesis in Chemistry KJE-3900   *November 2013*

DYRK1A PKC 412

DYRK1B wt

UNIVERSITY OF TROMSØ

PUBLICATIONS

Marina Alexeeva, Espen Åberg, Bjarne H. Johansen, Ole M. Seternes, Richard A. Engh, Ulli Rothweiler; PKC412 as Inhibitor for DYRK1A, (2013)

Manuscript is in the state of "in preparation prior submission".

The structure of DYRK1A in complex with PKC412 has been deposited to the protein data bank (PDB) under the code: **4NCT**

ABSTRACT

The dual-specificity tyrosine phosphorylation-regulated kinase family (DYRKs) has recently emerged as new therapeutic targets for different kinds of cancer and neurodegenerative diseases. In the latest studies it was shown that DYRK1B plays a key role in cancer cell survival, and its inhibition induces apoptosis of cancer cells. This thesis is about the biophysical characterization of DYRK1B and its comparison to DYRK1A, the closest homologue. This includes establishment of an expression and purification protocol for large-scale protein production of DYRK1B. Buffer optimization by screening with thermofluor was employed to further improve the stability and solubility of the protein. Enzyme kinetics of DYRK1B were characterized by determination of the Michaelis-Menten constant. Fifty small molecular weight molecules were screened for their ability to inhibit DYRK1B. The results of the screening were compared with DYRK1A to determine a selectivity profile of these inhibitors. A point mutation of DYRK1B to mimic DYRK1A was introduced to further investigate the selectivity profile. Finally, the crystal structure of DYRK1A in complex with PKC412 was solved by molecular replacement to a resolution of 2.6 Å. The structure shows for the first time the formation of a disulfide bridge between the catalytic loop and activation loop and it is the first structure published with the staurosporine analog PKC412.

ACKNOWLEDGEMENTS

ABBREVIATIONS

β-ME	β -mercaptoethanol
Δε	Extinction coefficient
A	Ampere
Amp	Ampicillin
ATP	Adenosine triphosphate
AU	Absorbance Unit
bp	base pair
Cam	Chloramphenicol
CV	Column Volume
Da	Dalton
DMSO	Dimethyl sulfoxide
dNTP	Deoxyribonucleotide
DTT	Dithiothreitol
DYRK	Dual-specificity tyrosine phosphorylation-regulated kinases
E. coli	*Escherichia coli*
EDTA	Ethylenediaminetetraacetic acid
FT	Flowthrough
HEPES	4-(2-hydroxyethyl)-1-piperazineethanesulfonic acid
IPTG	Isopropyl β-D-1-thiogalactopyranoside
Kan	Kanamycin
K_m	Michaelis-Menten constant for enzyme-substrate complex
LB	Lysogeny Broth
MPa	Mega Pascal
MES	2-(N-morpholino)ethanesulfonic acid
MilliQ water	Deionized water
MOPS	3-(N-morpholino)propanesulfonic acid
MST	Microscale thermophoresis
min	Minutes
OD	Optical density
o/n	overnight

PCR	Polymerase chain reaction
PEG	Polyethylene glycol
rpm	rounds per minute
SDS-PAGE	Sodium dodecyl sulfate - polyacrylamide gel electrophoresis
SEC	Size exclusion chromatography
si-RNAs	Small interference RNA
TAE	Tris-acetate-EDTA
TB	Terrific broth
TEV	*Tobacco Etch Virus*
Vmax	Maximum velocity of catalytic reaction
wt	wild type

CONTENTS

AIM OF STUDY

The aim of the study is the biophysical characterization of kinases from the DYRK family. This family has five members and, based on the expression test which had been done prior to this thesis, DYRK1A and DYRK1B were chosen for more detailed characterization. Both DYRK1A and DYRK1B have emerged recently as novel targets for a variety of diseases. DYRK1A plays a critical role in neuronal development and in consequence is implicated in diseases like Alzheimer and Parkinson and it also plays a role in mental retardation in patients suffering from Down syndrome due to its gene location on the DSCR on chromosome 21. DYRK1B is associated with ovarian cancers, pancreatic cancers and osteosarcoma, and the inhibition of DYRK1B leads to the apoptosis of cancer cells. Finding selective ATP competitive inhibitors for kinase is in general a challenge; the close similarity between DYRK1A and DYRK1B makes it even harder to find selective inhibitors for these two kinases. The focus in this thesis is on DYRK1B which has the highest sequence similarity in the kinase domain to DYRK1A among all DYRKs, but no structural details have been published. The aim of the first part is to develop an expression and purification protocol for DYRK1B that allows the characterization of this protein in terms of stability, phosphorylation pattern and kinase activity. The second part includes the screening for small molecular weight inhibitors and a comparison of the inhibitory activity of these inhibitors with DYRK1A. The third part of the thesis is the cloning of DYRK1B mutants to study the inhibitor selectivity profile and the residues involve in the enzyme kinetics. The last part is the crystallization of DYRK1B and/or DYRK1A with a small molecular weight inhibitor.

1 INTRODUCTION

1.1 Protein kinases

The kinases are a large group of phosphotransferases, i.e., enzymes which catalyze the transfer of the γ-phosphate group from an adenosine-5'-triphosphate (donor) to a hydroxyl-group (acceptor) of the specific substrates[1]. The divalent metal ions Mg^{2+} or Mn^{2+} are required for ATP binding and assistance of the phosphorylation reaction. Once phosphorylated, the kinase substrate may be functionally altered, and subsequently initiate the transmission of a biological signal to its own set of downstream targets.

Human kinases are involved in almost every cellular process, and are essential for signal transduction cascades in the cell. For example, protein kinase A (PKA, or cyclic AMP-dependent kinase), belonging to the AGC kinase group, controls the expression of large number of genes via the phosphorylation of transcription factor CREB[2], and, as a multiple substrate kinase, it is involved in the regulation of proliferation and differentiation of cells[3].

Human kinases have been extensively studied in the past, and are still an intensely investigated research field. Manning *et al.* in 2002 have classified the more than 500 human kinases, termed 'the human kinome', into seven groups based on the sequence similarity in the kinase domain[4]. Based on their ability to phosphorylate serine/threonine or tyrosine residues the protein kinases are divided into the two subdivisions: serine/threonine kinases (phosphorylate alcohol groups on serine or threonine) and tyrosine kinases (transfer the phosphate to the phenol group of tyrosine)[5]. However, there is a group of protein kinases, termed as 'dual-specificity' kinases, able to phosphorylate both serine/threonine and tyrosine residues on their targets[6].

From this perspective it is evident that abnormal function of kinases can lead to numerous diseases. For instance, mutation of the genes encoding growth factor receptors (e.g. EGF-R, epidermal growth factor receptor; VEGF-R, vascular endothelial growth factor receptor), which contain a tyrosine kinase domain responsible for transduction of the signal from the growth factors to cytoplasm in the cell, causes the alteration of structure of kinase domain leading to a ligand-independent activation of the growth factor receptor and dysregulation cell growth[7]. This type of dysregulation is often involved in tumor pathogenesis[8].

Protein kinases represent an interest for the pharmaceutical industry because they are considered as therapeutic targets for diseases including diabetes[9], neurodegenerative diseases as Alzheimer disease[10], *Herpes simplex* viral infection[11], malaria[12], and ischemic heart disease[13].

1.2 Structure of kinase domain

Kinases do not usually consist of the kinase domain alone, but have additional regulatory domains in the sequence required for their function, localization, and inter-protein interactions. Some kinases like CDKs need a second partner, cyclins, to be fully active[14]. Nevertheless, human kinases share a similar fold, the kinase domain, comprising an N-terminal lobe (N-lobe) with five antiparallel β-strands and a conserved regulatory αC-helix, and a larger C-terminal (C-lobe) consisting of α-helices[15]. The N-lobe and C-lobe are connected by a hinge region which is an important part of the ATP-pocket (**Figure 1**).
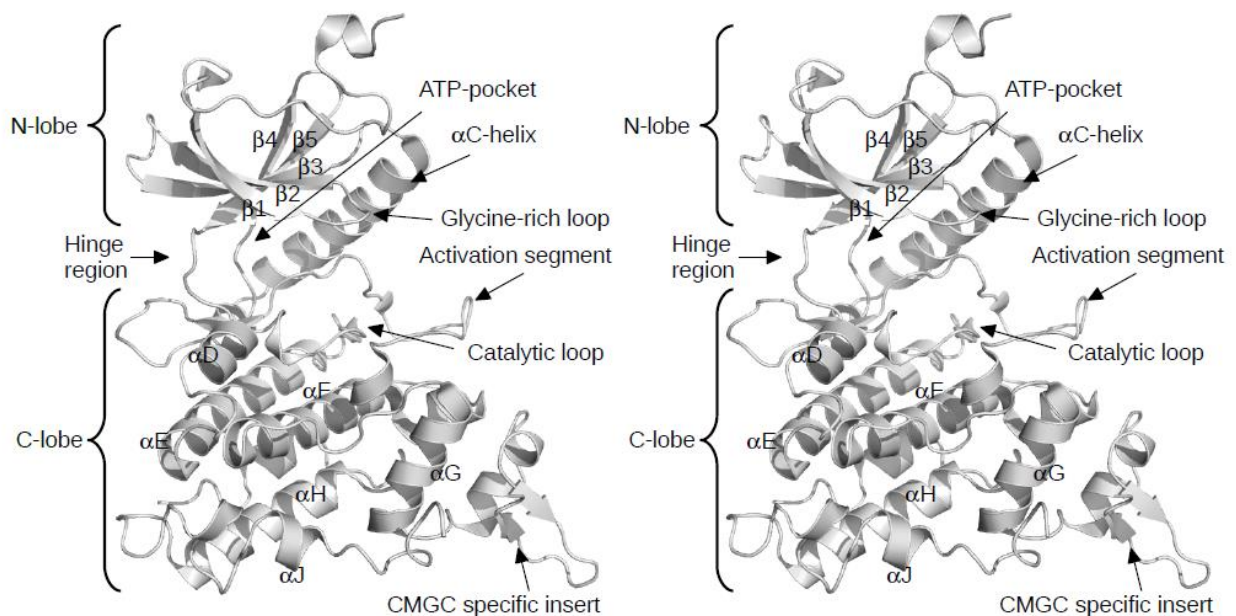
Figure 1. Stereo image of the kinase domain with several of its key features. The major structural elements are labeled. The structure of DYRK1A (3ANQ[16]) was used to illustrate the overview of kinase domain.

For most kinases, the αC-helix is located between β3 and β4. Kinases have in the activation loop one or more residues that can be phosphorylated. The activation loop is located at the C-lobe and starts from DFG-motif and ends with a conserved W/F/YRAPE motif (RFYRSPE in DYRKs)[17]. Depending on the kinase group and family, the phosphorylation is on a serine, threonine or tyrosine residue. This leads to an activation of kinase. In DYRK1A/B the phosphorylation occurs on the second tyrosine in the YQY motif during autoactivation immediately after translation by an intramolecular reaction[18-20]. The phosphorylated tyrosine of

the conserved YQY motif in DYRKs makes a contact with two arginines located at the end of the activation loop (R[325]FYR in DYRK1A and R[276]FYR in DYRK1B). In the DFG-motif the aspartate is the most conserved residue because it forms a contact with the phosphate groups of ATP either directly, or through magnesium. The phenylalanine in DFG is responsible for the hydrophobic interaction with the αC-helix and the correct orientation of aspartate in the DFG-motif[21]. In the literature, the active conformation of kinases is often referred to "DFG-in" conformation, while "DFG-out" corresponds to inactive state of protein kinases.

The catalytic loop is involved in transfer of the γ-phosphate to the substrate. A typical, highly conserved, motif of the catalytic loop in the kinome is HRD; however in the DYRK family a HCD motif is highly conserved in the catalytic loop instead. Another important part of the kinase domain is a glycine-rich loop. The glycine-rich loop comprises a GxGxxG motif (G[166]KGSFG in DYRK1A and G[118]KGSFG in DYRK1B). It is located between β1 and β2 and constitutes a part of ATP-pocket from the N-lobe. An important residue in the ATP-pocket is the "gatekeeper" which is responsible for the selectivity of inhibitors. DYRKs have a phenylalanine as a gatekeeper (F238 in DYRK1A and F190 in DYRK1B) which is located at the beginning of the hinge region.

1.2.1 Architecture of the ATP-pocket

Crystal structures of protein kinases have revealed that ATP binds at a specific region, called the ATP-pocket or cleft, between the N- and C-lobes of the kinase domain, connected by a hinge region. Protein kinases evolved to bind ATP, and therefore many residues forming the ATP-pocket are highly conserved among group and families of protein kinases. This makes it a challenge for the scientist to develop a selective inhibitor for a specific kinase, because the majority of the protein kinase inhibitors are ATP-competitive, i.e. the inhibitors have to mimic ATP and bind to the ATP-pocket. A. Vulpetti and R. Bosotti have studied the key structural features of ATP-pocket, involved in the binding of ATP and inhibitors by multiple sequence alignment of 478 protein kinases, comprising the human kinome[22]. They established that in the ATP-pocket, five regions responsible for the binding of different chemical group on the ATP molecule can be distinguished. First, the adenine region: the adenine ring forms two hydrogen bonds with the backbone of the hinge region and adenine core interacts with the hydrophobic residues via non-polar interactions. Second, the sugar ring: the ribose forms one hydrogen bond with a lysine, histidine or other polar residues of the C-lobe of kinase domain. Third, the phosphate region: the triphosphate group forms one hydrogen bond with a highly conserved

lysine. Fourth and fifth, the buried region and solvent accessible region are not occupied by ATP, but comprise a set of residues which are the source of sequence divergence among the kinases.

1.3 DYRK family

The <u>D</u>ual-specificity <u>tY</u>rosine phosphorylation-<u>R</u>egulated <u>K</u>inases (DYRKs) are called "dual-specificity" kinases because of their ability to become active by autophosphorylation of a tyrosine residue in the activation segment during translation, and after that, the members of DYRK family are capable of phosphorylate serine or threonine residues of exogenous substrates, losing a feature of a tyrosine kinase[18]. However, latest research showed that the tyrosine phosphorylation is not restricted to the autoactivation during translation but that the mature DYRK1A kinase remains some tyrosine phosphorylation activity[23].

DYRKs are an evolutionary conserved family whose members are found in different branches of life. DYRKs are found in yeast, for example, Yak1p from *Schizosaccharomyces pombe* which was primarily characterized by Garret S. *et al.*[24]. In nematodes: particularly *Caenorhabditis elegans*, where there are two genes, *mbk-1* and *mbk-2* encoding the kinases, MBK-1 and MBK-2 (homologs of minibrain kinases), which were identified as members of DYRK family[25]. However, the characterization by Tejedor F. *et al.* of the *mnb* (minibrain) gene encoding for MNB (minibrain kinase) kinase found in *Drosophila melanogaster* attracted the attention of the scientific world to these kinases as their dysfunction leads to the reduction of the brain size in the optic lobes of adult flies, notably indicating the role of MNB neurogenesis[26].

Human homologs of DYRKs belong to the CMGC group (according to the Manning G. *et al.* classification[4]) which also includes the cyclin-depended kinases (CDKs), mitogen-activated protein kinases (MAPKs), glycogen-synthase kinase-3 (GSK3) and CDK-like kinases. The human DYRK family includes five members: DYRK1A, DYRK1B, DYRK2, DYRK3 and DYRK4. DYRK kinases are further categorized as class I (DYRK1A and DYRK1B) and class II (DYRK2, DYRK3 and DYRK4)[27]. The comparison of the protein structure of human DYRKs is depicted in **Figure 2.** DYRK1A and DYRK1B have a DYRK homology (DH)-box typical for class I of DYRKs at the N-terminus, while the members of class II differ by the presence of an N-terminal autophosphorylation accessory region (NAPA) at the N-termini. Class I of DYRKs have a region rich in proline, glutamic acids, serine and threonine, called PEST (sequence common to rapidly degraded proteins), which in the DYRK1A is followed by a polyhistidine stretch (His) and then a

region enriched in serine and threonine residues (S/T). Members of the DYRK family are capable of phosphorylation of serine and threonine residues within the consensus sequence RXS/TP[28,29].
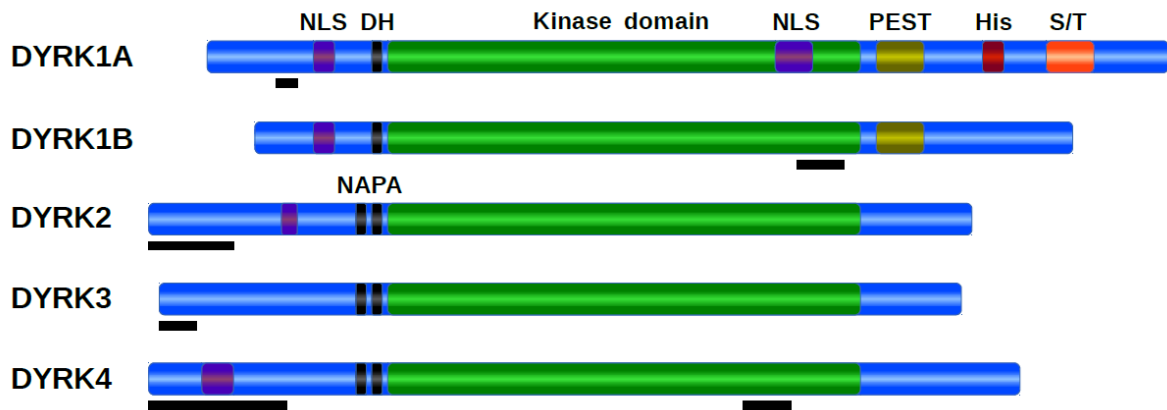
Figure 2. Protein structure scheme of the DYRKs. Kinase domain (green), N-terminus (blue) at the left of kinase domain, C-terminus (blue) at the right of kinase domain; NLS, nuclear localization signal; DH, DYRK-homology box; NAPA, N-terminal autophosphorylation accessory region; Kinase domain; PEST, motif rich in proline, glutamic acid, serine, and threonine residues; His, polyhistidine stretch; and S/T, region enriched in serine and threonine residues. Black lines indicate protein regions affected by alternative splicing events. The figure is modified from Aranda *et al.*[28]

1.3.1 DYRK1B

Leder S. *et al*. has performed the cloning of DYRK1B by cDNA and has analyzed its tissue distribution in human[30]. The *mirk* gene (in some literature the DYRK1B kinase is also called MIRK, or minibrain-related kinase, and, thus, gene *mirk* encodes for MIRK or DYRK1B; however, in this thesis the DYRK1B name is used to avoid confusion) is located in the 19q13.1 chromosome. S. Leder shows that DYRK1B has three splicing variants (629, 601, and 589 AA) and expresses at low levels in human tissues, except for the skeletal muscles where it is abundant. Later, a myogenesis (i.e. formation of muscular tissue) was exploited as a model system to investigate the functions of DYRK1B in myoblast differentiation by Lu J. *et al*.[31], Deng X. *et al*.[32] and Mercer S. *et al*.[33]. It was shown that the level of DYRK1B protein is low in dividing myoblasts; however, when the myoblasts enter into a differentiation stage the expression of DYRK1B increases at least 10-fold and remains elevated in mature cells. Deng X. *et al*. have shown that induction of the *mirk* gene in myoblasts is induced by Rho proteins (family of GTPases) and inhibitors of MEK (mitogen-activated protein kinase)[32]. Moreover, DYRK1B controls the cell cycle by an arrest of cycling myoblasts in a G0/G1 state through the phosphorylation of cyclin D and p27[33].

However, in spite of the low expression of *mirk* gene in normal tissues (except skeletal muscles), Lee K. *et al*. studies have found an elevated expression level of *mirk* in colon carcinoma cells, lung carcinoma cells, ovarian carcinoma cells, chronic myelogenous leukemia cells, lymphoblastic leukemia cells and melanoma cells[34].

Mercer S. studies have demonstrated that DYRK1B is also overexpressed in rhabdomyosarcoma cells (i.e. skeletal muscle-derived tumor), where the depletion of DYRK1B gene performed by small interference RNAs (siRNAs) leads to an induction of apoptosis of the cancer cells, indicating that DYRK1B functions as survival kinase for cancer cells under stress conditions[35].

Yang C. *et al*. have investigated the role of DYRK1B in osteosarcoma[36]. They have shown that the knockdown of the DYRK1B gene by siRNAs facilitates to the termination of the cancer cell growth and an increased number of cells entering to apoptosis. Yang C. *et al*. have also shown that that expression of DYRK1B is correlated with poor prognoses for patients and low survival, and noted that DYRK1B may serve as a biomarker for a prognosis[36].

Likewise, Gao J. *et al.* have studied the role of DYRK1B in non-small cell lung cancer cells (NSCLC) and found that DYRK1B is expressed at high levels in the majority of NSCLC. They have employed the similar siRNA knockdown of DYRK1B expression, and results have shown that NSCLC exhibited an inhibition of cell growth and induction of an apoptosis compared to non-depleted DYRK1B cells. Moreover, knockdown of DYRK1B enhanced the sensitivity of NSCLC to cisplatin-induced apoptosis[37]. Increased sensitivity of cancer cells to cisplatin was also demonstrated by Hu J. and Friedman E. in the study of ovarian cancer cells where DYRK1B depletion leads to increasing of ROS (reactive oxygen species) assisting to further elevation of ROS by cisplatin that, finally, kills the cancer cell[38].

E. Friedman has given an excellent review about the role of DYRK1B in the ovarian cancer[39] and pancreatic cancer[40]. This author has done a tremendous amount of work summarizing the role of mechanism of DYRK1B in tumor progression. The author explained that Mirk/DYRK1B, which is not mutated in cancer cells, sustains the quiescent state of the cancer cells through the phosphorylation-dependent destabilization of cyclin D1 at T288[41], and stabilization of the CDK (cyclin-dependent kinase) inhibitor p27 at S10[42]. DYRK1B in the cancer cells is activated by the oncogenic K-ras signaling[43]. This mechanism enables halting of the cell cycle at G0 stage (quiescence or resting stage), however, the inhibition of DYRK1B, as was shown in the study of Hu J. *et al.* [44], was able to induce the apoptosis of cancer cells (**Figure 3**).

Taken together, DYRK1B is a new emerging target for cancer therapy for osteocarcoma, lung cancer, pancreatic cancer, ovarian cancer etc. Therefore, the characterization of DYRK1B, and

investigation of binding features of this kinase with molecular weight inhibitors has become an urgent task.
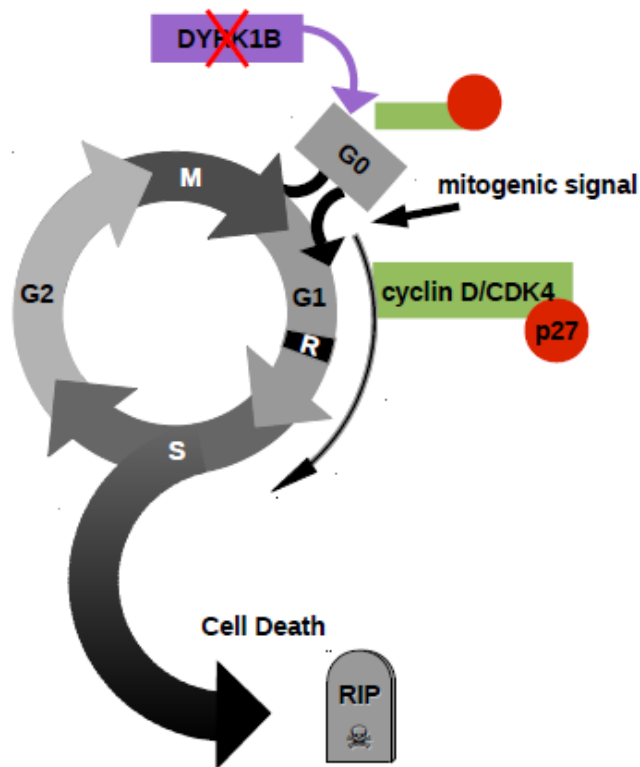
Figure 3. DYRK1B inhibition leads to the cell death. S (synthesis stage), M (mitosis), G1 (Gap 1), G2 (Gap 2), G0 (Gap0 or quiescent). The figure is adapted and modified from Friedman E. (2013)[39].

1.3.2 DYRK1A

The *DYRK1A* gene is located in the Down syndrome critical region (DSCR) on chromosome 21[45] and the overexpression of DYRK1A in patient suffering from Down syndrome (DS) is coupled to mental retardation[46]. Patients with Down syndrome develop an Alzheimer-like dementia[47] relatively early compared to the general population. Besides its involvement in DS, DYRK1A has attracted attention due to potential involvement in other neurodegenerative diseases like Alzheimer[47], Parkinson's disease[48] and Huntington's disease[49]. Regarding to the Alzheimer disease, as reviewed by Smith B. *et al*, DYRK1A directly phosphorylates tau protein promoting a following multiple site phosphorylation of tau by GSK 3β kinase and aggregation of the hyperphosphorylated tau into neurofibrillary tangles. This facilitates neuronal death and dementia severity[50].

1.3.3 Sequence alignment of DYRK1A and DYRK1B

The closest homolog to DYRK1B is DYRK1A. The identity over the whole enzyme is 73.9% (89.4% similarity) and in the kinase domain it is 85.0% (95.6% similarity). The pairwise sequence alignment was performed by the on-line software LALIGN[51]. Within the ATP pocket there is only one residue M240 in DYRK1A, L192 in DYRK1B at the hinge region, which is different between these two kinases (**Figure 4**).
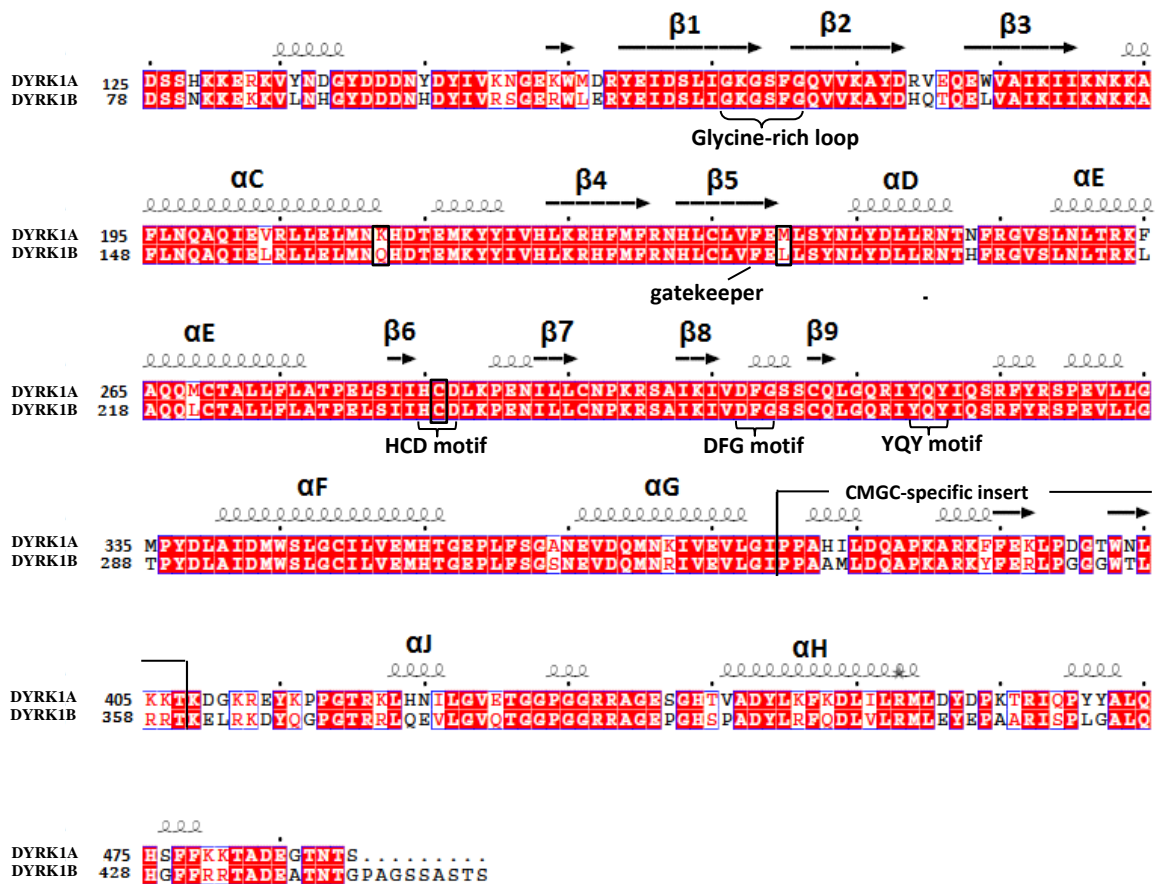
Figure 4. Pairwise sequence alignment of the DYRK1A (125-490 AA) and DYRK1B (78-451 AA). The sequences were obtained from UniProt database (accession numbers: Q13627 for DYRK1A and Q9Y463 for DYRK1B)[52]. The DYRK1A sequence comprising the kinase domain residues 125-493 was aligned with the kinase domain of DYRK1B including the residues 78-451 of the designed construct. The secondary structure annotation corresponds to the crystal structure of DYRK1A (2WO6[53]). Residues depicted in white and highlighted by red boxes are identical between the two sequences. Residues shown in red and highlighted by blue boxes are similar. The secondary structure elements are shown above the aligned sequences. Alpha helices are represented by spirals and beta strands by arrows. The clustalW2 online software was used to compute the pairwise sequence alignment[54]. The figure was made by using ESPript[55].

1.4 Kinase inhibitors

Since kinases are an important in processes such as cell cycle control and signaling pathways, they are an attractive target for drug development and inhibitor design[56]. Small molecular weight inhibitors (molecular weight range 200-600 Da) are able to effectively inhibit the kinases and prevent the development of diseases. One of the best examples among the kinase inhibitors is the Imatinib/Gleevec (Novartis, Switzerland) used in the therapy of patients with chronic myelogenous leukemia (CML) caused by formation of the so-called Philadelphia chromosome[57] (i.e. chromosomal defect leading to formation of BCR-Abl oncogene). Gleevec became a revolutionary drug, first, because it was a rationally designed inhibitor and, second, it is able to selectively inhibit the BCR-Abl kinase and effectively treat CML[58,59].

Inhibitors of protein kinases can be categorized into several types based on the interaction between kinase and inhibitor[60]:

1. Type I kinase inhibitors. ATP-competitive, inhibitors can bind through hydrogen bonds with the residues of the hinge region. Inhibitors bind to the ATP-pocket at the active conformation of the kinase, i.e DFG-in form.
2. Type II kinase inhibitors, non-ATP-competitive inhibitors, are able to bind to the ATP-pocket through residues of hinge region and hydrophobic interactions. Inhibitors bind to a DFG-out form targeting the inactive kinase.
3. Type III inhibitors, allosteric inhibitors, are able to bind to a binding site outside of ATP-pocket.
4. Type IV inhibitors, are able covalently bind to the active site of kinase domain, usually, through a cysteine residue.

Inhibitors can also be classified based on the source of origin, for example natural or synthetic.

Close attention has been given to the problem of development of a highly selective inhibition for kinases whose malfunction is a key factor in a pathogenesis of diseases. In order to distinguish a key structural feature responsible for the selectivity, a comprehensive analysis of kinase inhibition is required[61]. E. Åberg *et al.* studied the key residues which determine the inhibitor selectivity for the AGC kinase group (include PKA, PKC etc)[62]. E. Åberg *et al.* described that for the ATP-pocket binding, the important residue is the gatekeeper, the presence of a cysteine residue at or near the ATP-pocket (may serve as a target for formation of covalent bond with inhibitors)

and the second residue in the glycine-rich loop which is usually an aromatic residue and may influence on the hydrophobic interaction with inhibitor. The inhibitors for the kinase of interest may be designed with respect to the residues listed above.

Ambit Bioscience Company (USA) have performed a profile for 72 known kinase inhibitors (at concentration of 10 μM) against 442 kinases to determine the dissociation constant Kd and provided an overview over the kinase selectivity[63]. The profiling demonstrated that the known inhibitors can bind to distinct related kinases. This makes it possible to change an application for particular inhibitors. Statistic handling in this research showed that among the selective inhibitors the fraction of type II inhibitors is higher compared to the fraction of type I inhibitors. However, it is not a fixed rule: some type I inhibitor shown higher selectivity across the kinome and some type II inhibitor demonstrated weak selectivity.

In summary, the selectivity of kinases is a complicated field and vast numbers of factors are involved in rational inhibitor design. Development and design of selective inhibitors remains an urgent field in scientific and pharmaceutical research.

1.4.1 DYRK inhibitors

The DYRK1B inhibitor RO5454948 (**Figure 5, a**) has been shown to induce apoptosis of quiescent pancreatic cancer cells which are normally resistant to the conventional cancer chemotherapeutics[64]. RO5454948 was identified by Roche generic kinase inhibitor library. Ewton D.Z. *et al*. have demonstrated that in Panc1 (a pancreatic cancer cell line) with an amplified DYRK1B, the treatment of the cell by RO545494 leads to a decreasing of the fraction of the cancer cells in the G0 stage by around 60%. This was examined by flow cytometry method[65]. Hu J. *et al.* have studied the inhibition of RO5454948 in ovarian cancer cells and demonstrated that Mirk/DYRK1B inhibition leads to an increasing of cyclin D levels and consequently induces the cell cycle[44].
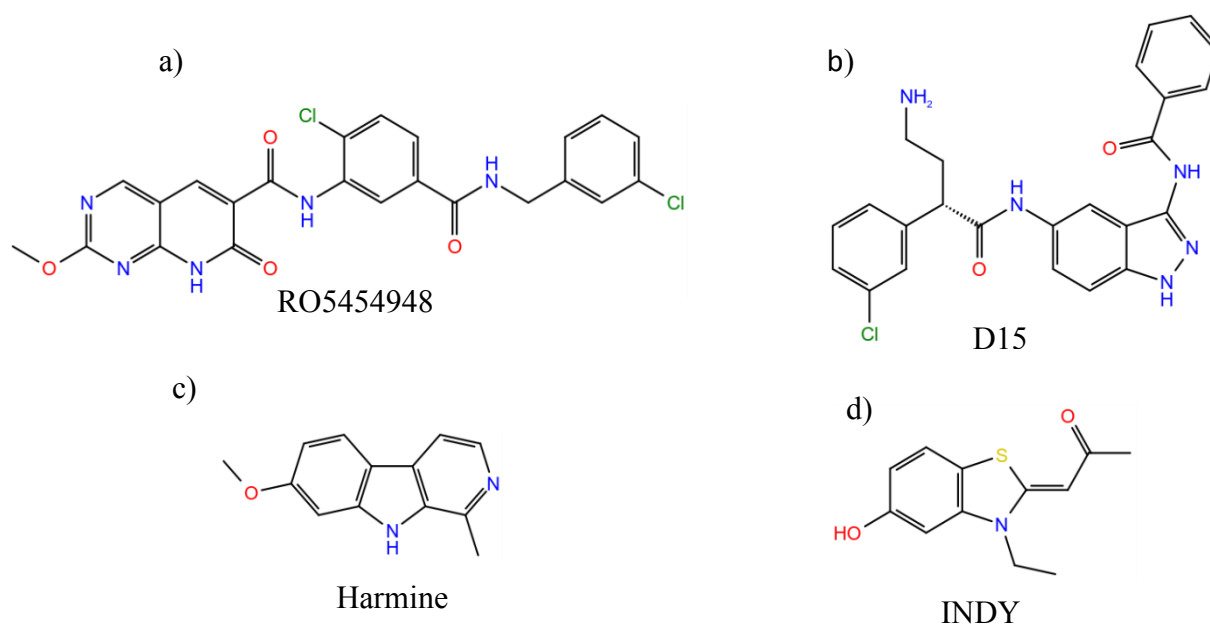
Figure 5.Chemical structure of some DYRKs inhibitors. a) RO5454948 is a known DYRK1B inhibitor[64]; b) D15 is a DYRK1A inhibitor; c) harmine is a DYRK1A/1B inhibitor[16], d) INDY is DYRK1A inhibitor[16]. The structures of inhibitors were drawn in Maestro suit (Schrodinger)[66].

Crystal structures in complex with inhibitors (**Figure 5, b-d**) have been solved for DYRK1A. The crystal structure of DYRK1A in complex with inhibitor INDY (3NAQ, **Figure 5, d**) has been published by Ogawa Y. *et al*.[16]. INDY is a type I inhibitor which binds with a Ki of 180 nM. This inhibitor binds to the hinge region and forms two hydrogen bonds. The first one is between the hydroxyl oxygen and backbone amide of Leu241 of the hinge and the second one is between the carbonyl oxygen and Lys188. Another structure by Ogawa Y. *et al*. is DYRK1A in complex with harmine (3NAR, **Figure 5, c**). Harmine binds to ATP-pocket (adenine region) via two hydrogen bonds: first one between the pyridine nitrogen and Lys188; second one between the methoxy group and backbone amide nitrogen of Leu241. Harmine has an IC_{50} of 350 nM. D15 inhibitor (2WO6, **Figure 5, b**) interacts with the hinge through a series of three hydrogen bonds between the backbone of Glu239, Met240 and Leu241. D15 also forms a salt bridge between a primary amide of inhibitor and carboxylate of Asp307[53].

1.4.2 PKC412

PKC412 (midostaurin, *N*-benzoyl-staurosporine), is an analog of the pan-kinase inhibitor staurosporine, an alkaloid isolated from *Streptomyces staurosoreus*[67]. PKC412 has a more selective inhibition profile compared to staurosporine and its main targets are the isoforms of protein kinase C (PKC)[68], VEGFR2[69] and FLT3[70]. PKC412 is currently under investigation as a treatment of acute myeloid leukemia[71,72]. The selectivity profile of PKC412 compared to the staurosporine is illustrated by the kinome interaction maps (**Figure 6**).

a)   b)
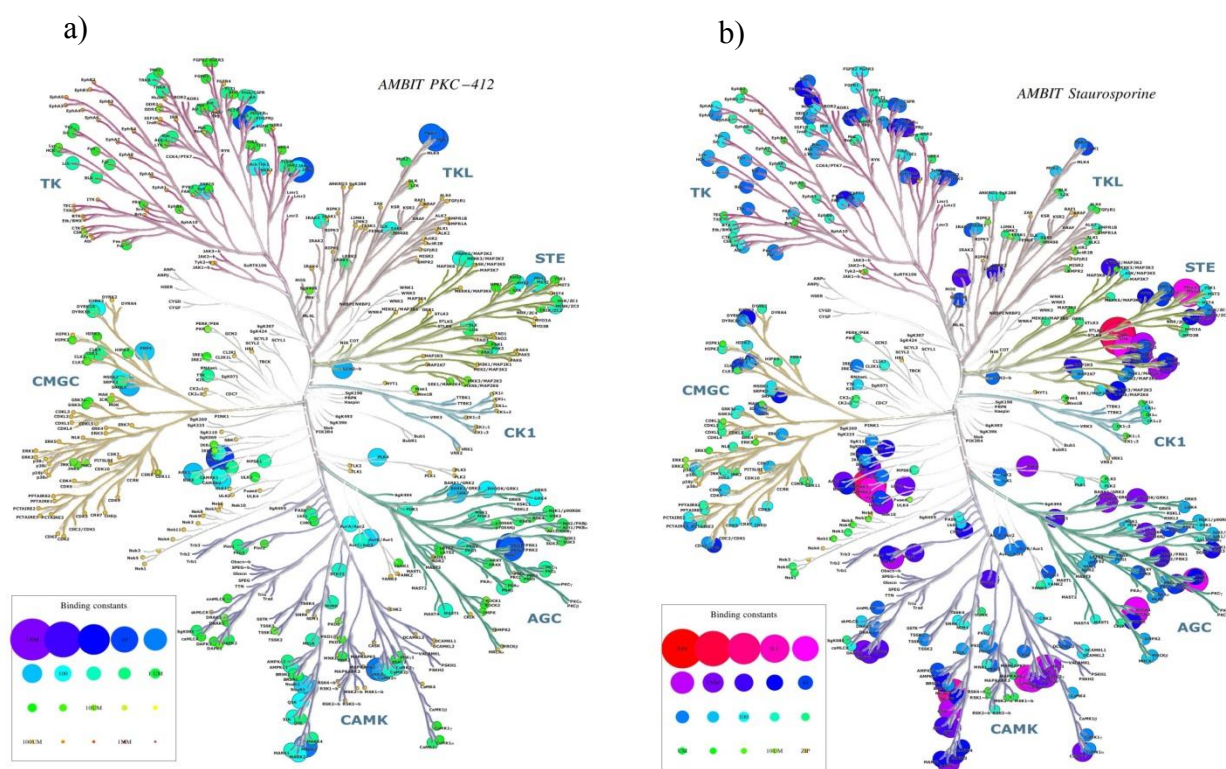
Figure 6. Kinome interaction map. a) PKC412, b) Staurosporine. The kinase maps were kindly provided by R.A. Engh, adapted from Manning *et al.*[4].

1.5 Enzyme Kinetics

Enzymes are able to dramatically increase the rate of chemical reactions in the cell[73]. First order enzyme kinetics may be described by simple conversion of substrate S to the product P catalyzed by enzyme E:

$$E + S \underset{k_{-1}}{\overset{k_1}{\rightleftarrows}} ES \overset{k_2}{\rightarrow} E + P$$
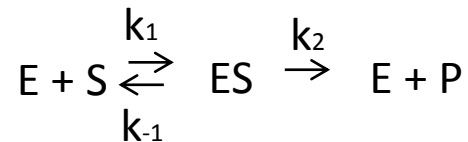
where enzyme E form a complex with the substrate S at the rate k_1, while the reverse reaction, the dissociation of the complex ES $\left(ES \rightarrow E + S \right)$ occurs at the rate k_{-1}. The second k_2 rate (denoted also as k_{cat}) describes the dissociation rate of ES complex and the product formation from the ES complex. The reverse reaction, forming the ES complex out of the product is assumed to be infinitesimally small for many enzymes[74].

The activity of enzymes is dependent on several factors like pH, salt, substrate and product concentration and temperature. Enzymes have in general a temperature and pH optimum where the activity is highest[75]. The enzyme activity can also be influenced by the presence of inhibitors. Inhibitors decrease the activity of enzymes and, as used in this thesis, kinase inhibitors are able to decrease an efficiency of the kinase catalytic activity and thus, lead to a decreasing or even partial blockage the downstream mediation of cellular processes[76].

In this master thesis, a set of inhibitors was tested by the Cook assay[77], a kinase activity assay that measures the NADH consumption while keeping the ATP concentration constant. In order to compare the inhibition efficiency for the tested inhibitors we need to determine the absolute inhibition constant Ki. Mathematically, the Ki value can be calculated using the Cheng-Prusoff equation[78] (1):

$$K_i = \frac{IC_{50}}{1 + \frac{[S]}{K_m}} \quad (1)$$

where IC_{50} is the concentration of inhibitor causing 50% reduction of catalytic activity of the kinase, $[S]$ is the substrate concentration, *i.e.* ATP concentration, K_m is a Michaelis-Menten constant that can approximate the affinity of substrate (ATP) to the enzyme. The K_m value is equal to the substrate concentration at which the enzyme activity is half of the maximum activity.

Leonor Michaelis and Maud Menten were the scientists who established the fundamental enzyme kinetics in 1913[79] presented the equation (2) which was further developed by Briggs and Haldane in 1925[80]:

$$Vo = \frac{Vmax\,[S]}{Km + [S]} \quad (2)$$

where the Vo is initial velocity of the catalytic reaction, Vmax is a maximum velocity, [S] is the substrate concentration and K_m is a Michaelis-Menten constant. The equation (2) is a mathematical representation of Michaelis-Menten curve depicted on the **Figure 7**:
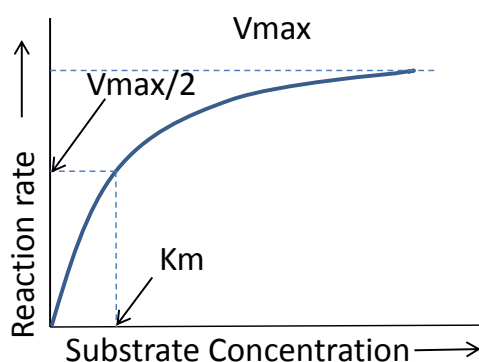
Figure 7. The Michaelis-Menten curve. The Michaelis-Menten kinetics shows that initial velocity at high substrate concentration cannot further increase and reaches a maximum velocity: Vmax. Km is the Michaelis-Menten constant, Vmax is the maximum velocity, Vmax/2 is a half of the maximum velocity, [S] is the substrate concentration.

The Michaelis-Menten equation requires a steady-stay condition, i.e. the period when the concentration of ES complex remains constant with time[81].

Originally the Michaelis-Menten equation was used to describe kinetics of first order reactions, meaning that only one substrate is used in the reaction. However, kinases are catalysts of a reaction involving two substrates[82]. As described by Alistair Rogers and Yves Gibon, there are three major classes of mechanisms of catalytic reaction with two substrates: random substrate binding, ordered substrate binding and the Ping-Pong mechanism[74]. For most kinases it is unknown which mechanism they follow but for some kinases a mechanism was described. For example, Szafranska, A.E. *et al.* have described the kinetic mechanism of p38 MAP kinase α, a kinase belonging to the same CMGC group as the DYRK family. The author found out that p38 MAP kinase α exploits a partial rapid-equilibrium random order ternary-complex mechanism[83].

Despite on the complexity bisubstrate catalytic reaction the Michaelis–Menten equation typically remains valid for these complex reactions[81]

2 MATERIALS AND METHODS

2.1 Buffers and solutions

The buffers and solutions used in this thesis are listed in the **Table 1**. Buffer C and Buffer G were filtered by 0.45 µl membrane filter prior to gel filtration.

Table 1. Buffers and solutions used for cloning, expression and purification of DYRK1B and its mutants.

Solution/buffer	Contents
Amp	100 mg/ml Ampicillin in MilliQ water
Cam	34 mg/ml Chloramphenicol in 100% ethanol
Kan	50 mg/ml Kanamycin in MilliQ water
IPTG	1 M IPTG
LB-agar	1% (w/v) Bacto Tryptone, 0.5% (w/v) Yeast extract, 1% (w/v) NaCl, 1.5% (w/v) Agar-agar in MilliQ water
LB media	1% (w/v) Bacto Tryptone, 0.5% (w/v) Yeast extract, 1% (w/v) NaCl in MilliQ water
SOC media	2% (w/v) Bacto Tryptone, 0.5% Yeast extract, 10 mM NaCl, 1 mM $MgCl_2$, 2.5 mM KCl, 10 mM $MgSO_4$, 0.4 % (w/v) Glucose in MilliQ water
TB media	1.2% (w/v) Peptone, 2.4% (w/v) Yeast extract, 72 mM K_2HPO_4, 17 mM KH_2PO_4, 0.4% (v/v) Glycerol
2YT media	1.6% (w/v) Peptone, 1% (w/v) Yeast extract, 86 mM NaCl in MilliQ water
TAE buffer	40 mM Tris, 20 mM Acetic acid, 1 mM EDTA in MilliQ water
TRIS-Glycine buffer	0.25 M Trizma Base, 1.95 M Glycine, 1% (w/v) SDS in MilliQ water
Buffer A	50 mM Na_2HPO_4 pH 8.0, 500 mM NaCl in MilliQ water
Buffer B	50 mM Na_2HPO_4 pH 8.0, 300 mM NaCl, 500 mM Imidazole in MilliQ water
Buffer C	50 mM Tris-HCl pH 7.5, 200 mM NaCl, 2 mM β-ME in MilliQ water
Buffer D	50 mM MOPS pH 6.8, 50 mM KCl, 2 mM β-ME in MilliQ H_2O
Buffer E	50 mM HEPES pH 8.0, 50 mM KCl, 250 mM NaCl in MilliQH_2O
Buffer F	50 mM HEPES pH 8.0, 50 mM KCl, 250 mM NaCl, 500 mM Imidazole in MilliQH_2O
Buffer G	50 mM HEPES pH 8.0, 50 mM KCl, 250 mM NaCl, 2 mM β-ME in MilliQH_2O

2.2 Cloning of DYRK1B wt

The sequence of NM_004714 cDNA clone of DYRK1B (OriGene[84]) was used to design the DNA construct suitable for protein expression. The full length protein comprises 629 amino acids[27,30]. The length and the boundaries of the construct are based on the published crystal structure of the DYRK1A (3NAR[16]) protein including kinase domain and showing the highest level of sequence identity (85%) with DYRK1B. The full length amino acid sequence of DYRK1B and the chosen protein construct (residues 78-451, where 111-431 is the kinase domain) for cloning are shown in **Figure 8.**

```
          10         20         30         40         50         60
   MAVPPGHGPF SGFPGPQEHT QVLPDVRLLP RRLPLAFRDA TSAPLRKLSV DLIKTYKHIN

          70         78         90        100        110        120
   EVYYAKKKRR AQQAPPQDSS NKKEKKVLNH GYDDDNHDYI VRSGERWLER YEIDSLIGKG

         130        140        150        160        170        180
   SFGQVVKAYD HQTQELVAIK IIKNKKAFLN QAQIELRLLE LMNQHDTEMK YYIVHLKRHF

         190        200        210        220        230        240
   MFRNHLCLVF ELLSYNLYDL LRNTHFRGVS LNLTRKLAQQ LCTALLFLAT PELSIIHCDL

         250        260        270        280        290        300
   KPENILLCNP KRSAIKIVDF GSSCQLGQRI YQYIQSRFYR SPEVLLGTPY DLAIDMWSLG

         310        320        330        340        350        360
   CILVEMHTGE PLFSGSNEVD QMNRIVEVLG IPPAAMLDQA PKARKYFERL PGGGWTLRRT

         370        380        390        400        410        420
   KELRKDYQGP GTRRLQEVLG VQTGGPGGRR AGEPGHSPAD YLRFQDLVLR MLEYEPAARI

         430        440        451        460        470        480
   SPLGALQHGF FRRTADEATN TGPAGSSAST SPAPLDTCPS SSTASSISSS GGSSGSSSDN

         490        500        510        520        530        540
   RTYRYSNRYC GGPGPPITDC EMNSPQVPPS QPLRPWAGGD VPHKTHQAPA SASSLPGTGA

         550        560        570        580        590        600
   QLPPQPRYLG RPPSPTSPPP PELMDVSLVG GPADCSPPHP APAPQHPAAS ALRTRMTGGR

         610        620
   PPLPPPDDPA TLGPHLGLRG VPQSTAASS
```

Figure 8. Amino acid sequence of DYRK1B. DYRK1B amino acid sequence was downloaded from Uniprot database: code Q9Y463[85]. The UniProt database format is used to illustrate the amino acid sequence of DYRK1B. The kinase domain composed of amino acids from 111 to 431 (bold sequence). The amino acid sequence 78-451 (green) was chosen for cloning. The construct was designed together with the kind help of Dr. Espen Åberg. The plasmid and vector maps are shown in the appendix.

28

Gateway cloning strategy together with TOPO® cloning was employed to create the expression clone of DYRK1B. The following steps are included in the TOPO® and Gateway cloning strategies[86,87]:

1. Amplification of blunt-end PCR product (selection of DNA template, primer design, PCR catalyzed by Phusion polymerase, agarose gel electrophoresis and extraction of blunt-end PCR product)

2. Construction of a Gateway entry clone by TOPO® cloning (reaction set-up, transformation in competent cells, analysis of colonies, plasmid isolation and purification, sequencing of selected clones)

3. Gateway cloning (LR recombination reaction, transformation, analysis of colonies, amplification and purification).

2.2.1 Cloning of PCR product encoding the DYRK1B kinase domain

In the first step of creating the expression construct of the DYRK1B kinase domain a PCR product suitable for TOPO® cloning was created. The TOPO® cloning reaction creates a construct that acts as the entry clone for the following Gateway cloning reaction. The pENTR Directional TOPO® cloning kit was purchased from Invitrogen (Life Technologies). A detailed description of the TOPO® cloning strategy can be found in the user manual for pENTR/D/TOPO cloning kit[88].

The TOPO® cloning method exploits a topoisomerase which was originally discovered in the *Vaccinia virus*[89]. This enzyme has a high affinity for duplex DNA and it binds to the specific site CCCTT. After binding to DNA at the specific site the topoisomerase cleaves the phosphodiester backbone in one strand of the double-stranded DNA and covalently binds to this strand with a tyrosine residue via 3' phosphate. The second remaining strand, also called an overhang, has the sequence GTGG (specific for the pENTR Directional TOPO® cloning kit), which can anneal to the sequence CACC at the 5' end of PCR product. Therefore, one of the parameters in the primer design is that the forward primer must begin from the sequence CACC to ensure perfect annealing to the TOPO® vector and in addition to ensure the correct orientation of the PCR product within the TOPO® vector. The forward primer also contains a sequence encoding a TEV recognition site for tag-cleavage and 6 triplets coding for amino acids 78-83 at the N-terminal end of DYRK1B. According to the user manual of TOPO® cloning kit the reverse primer does not contain any sequence which is complementary to the overhang sequence GTGG[88]. This is a necessary requirement for a correct orientation of PCR product of interest. The reverse primer is

complementary to the nucleotide sequence encoding the last 8 amino acid residue at the C-terminal end of designed construct and includes the stop codon TGA (**Figure 9**). The primers were designed by Dr. Espen Åberg in Vector NTI® Express Designer Software[90].

a) FW 5'**CACC**GAAAACCTGTATTTTCAGGGAGCTTCA*GATTCGAGCAACAAGAAG* 3'

b) RV 5'**TCA***CGAGGTGGAGGCACTGCTGC* 3'

Figure 9. Primers for DYRK1B construct. a) Forward primer for the DYRK1B construct. Nucleotide sequence in bold is required for the annealing with the overhang of the TOPO® vector, underlined sequence encodes for the TEV recognition site, sequence in italic is complementary to the first amino acid residues. b) Reverse primer for the DYRK1B construct. The reverse primer is complementary to the last 8 amino acid residues of the DYRK1B construct (italic). Stop codon is shown in bold.

The primers for the DYRK1B construct were purchased from SigmaAldrich, and as a template the pDONR223-DYRK1B (Addgene plasmid 23761[91] containing full length DYRK1B clone) was used for the PCR. The Addgene plasmid 23761 was amplified in DH5α *E. coli* (transformation was performed according to the protocol[92]) and purified by QIAprep spin Miniprep kit[93] (QIAGEN). The concentration of the amplified DNA plasmid was measured by Nanodrop.

The primers were dissolved in MilliQ water to a concentration of 100 pmol/µl. The reaction mixture, composed of 200 pg of DNA template, 0.5 µM of forward and reverse primers, 200 µM of dNTPs and 1xHF buffer, was assembled on ice. The reaction was filled up with nuclease-free water to 20 µl. 0.04 U/µl of Phusion Polymerase (BioLabs) was added to the reaction mixture at the last step prior to the thermal cycling according to the protocol of the Phusion Polymerase[94].

Dyad DNA Engine (BIO-RAD) thermal cycler was employed to run the following steps summarized in **Table 2**. Gradient setting was used to cover a broader range of annealing temperatures.

Table 2. Thermocycling conditions for cloning by the Phusion Polymerase. Four temperatures 50 ℃, 55.5 ℃, 66 ℃, 70 ℃ were chosen in the settings of the thermocycler program.

Cycle	Temp, ℃	Time	Step
1	98	30"	initial denaturation
	98	10"	denaturation
30	50-70	30"	annealing
	72	45"	extension
1	72	10"	Final extension
1	4	hold	hold

The amplified PCR product was separated by agarose gel electrophoresis to check the size and the integrity of the designed PCR product. Agarose was dissolved by heating in 1xTAE buffer to a final concentration of 0.7% (v/w). RedSafe nucleic acid staining solution (ChemBio) was added to the melted agarose after it had cooled down to about 60℃. The final concentration of RedSafe was 0.05% (v/v). The RedSafe /agarose solution was poured into the gel cassette with a comb to prepare a gel with 10 wells. The comb was removed after the gel had solidified. The gel was placed in a chamber for electrophoresis filled with 1xTAE buffer. The PCR product was mixed with 6x Gel loading Dye Blue (BioLabs) and loaded into the agarose gel. 6 µl of 1kb DNA ladder (BioLab) was used as a marker to analyze the size of PCR product. A PowerPac Bacis machine (BIO-RAD) was used for the electrophoresis at a constant voltage of 90V for 30 min. After electrophoresis the agarose gel was examined in Gel Doc (BIO-RAD) with UV lights. The band with expected size was cut from the agarose gel and the PCR product was extracted using QIAquick Gel Extraction kit from QIAGEN according to the kit protocol[95]. The concentration of extracted PCR product was measured by Nanodrop.

2.2.2 TOPO® cloning

The TOPO® cloning reaction (as described above) combines the pENTR vector with the gene of interest. The pENTR contains an ttL1 and an attL2 site. The presence of the attL1 and attL2 sites makes the recombination reaction of the entry clone with a Gateway destination vector (as pDEST17) possible. The TOPO® cloning reaction was done by mixing the purified PCR product and the TOPO® cloning vector in a ratio 2:1 (volume ratio) together with 1µl of salt solution and nuclease free water provided by kit (**Table 3)**. The TOPO® cloning mixture was kept at room temperature for approximately 5 min.

Table 3. TOPO® cloning reaction mixture

Reagent	Volume
Fresh PCR product	1 µl
Salt solution	1 µl
Sterile water	3.5 µl
TOPO® vector	0.5 µl
Final volume	**6 µl**

2 µl of TOPO® cloning reaction was added to One Shot® Top10 chemically competent *E. coli.* (Life Technologies). Transformation was performed according to the transformation protocol[96] (Life Technologies). 200µl of each transformation were spread on prewarmed LB plate containing 50 µg/ml kanamycin. Plates were incubated overnight at 37 ℃. Two colonies were picked from the plate and cultivated in 4 ml of LB media containing 50 µg/ml kanamycin. Plasmids were isolated and purified by QIAprep spin Miniprep kit[93] (QIAGEN).

The plasmids were sequenced with the Big.Dye Terminator v3.1 sequencing kit to verify the correctness of the entry vector. The two sequencing reaction per isolated plasmid (one with M13 forward primer, another with M13 reverse) were done to check the 5' and 3' ends of construct and to cover the whole length of DYRK1B kinase construct. Sequencing reaction were performed according to the protocol of Big.Dye Terminator v3.1 sequencing kit[97].

2.2.3 Gateway cloning

The Gateway cloning strategy is based on the feature of the *Bacteriophage lambda* which is able to integrate into the *E. coli* chromosome[98]. In order to create the expression clone, Gateway cloning system exploits the recombination reaction between the attL sites in entry clone and attR sites in the destination vectors. The scheme of recombination reaction between entry and destination vectors is depicted in **Figure 10.**
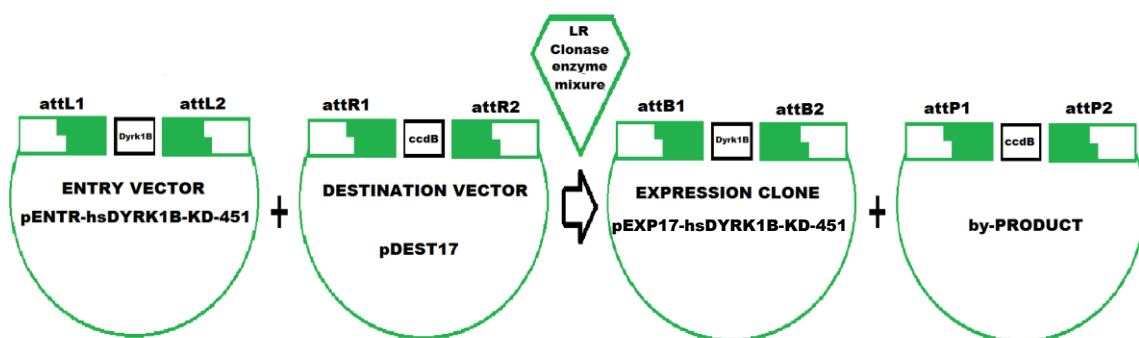
Figure 10. The DYRK1B gene is flanked by attL1 and attL2 recombination sites in the entry vector pENTR-hsDYRK1B-KD-451. The destination vector possesses the ccdB gene flanked by attR1 and attR2 sites. These sites are the binding sites for proteins comprising LR Clonase enzyme mixture which mediates the recombination reaction. Recombination occurs between recombination sites and as result creates the expression clone pEXP-hsDYRK1B-KD-451 and a by-product. The figure is modified from the Gateway technology user guide (Life technology)[99].

The expression vector pEXP17-hsDYRK1B-KD-451 possesses the T7 promoter. T7 promoter is necessary to transcribe the gene during expression in *E. coli*. The expression construct has an N-terminal 6XHis tag which allows purification of the protein of interest with immobilized metal ion affinity chromatography (IMAC) columns. An ampicillin resistance gene is present in the vector which is required for antibiotic specific selection in *E. coli*, thus, ampicillin has to be added to the media during transformation, growth and induction of bacteria.

The recombination reaction between entry and destination vector was performed in a 1.5 ml Eppendorf tube at room temperature. As it is described in the user manual of the Gateway Technology kit[99] (Life Technologies), the reaction mixture was composed of 200 ng pENTR-hsDYRK1B-KD-451, 300 ng pDEST17 vector, 5x LR clonase reaction buffer and TE buffer (pH 8.0) which was added to 16 µl. Four µl of LR clonase enzyme mixture was added to the mixture and the reaction was incubated for 1 hour at room temperature. Afterwards, 2 µl of 2 µg/µl proteinase K was added into reaction mixture and incubated for additional 10 min at 37℃. The pEXP17-hsDYRK1B-KD-451 expression clone was transformed into DH5α competent *E. coli*. Transformation was performed according to the transformation protocol of DH5α competent *E. coli* provided by user manual of Gateway Technology kit (Life Technologies)[92]. 100 µl of the transformation mixture was spread on a prewarmed LB agar plate containing 100 µg/ml ampicillin and incubated overnight at 37℃. Two colonies were picked for propagation in mini cultures containing 4 ml of LB media with the same amount of antibiotic as described above. The mini cultures were incubated at 37℃ overnight with 250 rpm shaking and the plasmids were isolated and purified by QIAprep spin Miniprep kit[93] (QIAGEN).

2.3 Site-directed mutagenesis DYRK1B

Three point mutations L192M, Q164K and C238R were chosen to study different properties of DYRK1B with respect to role of these residues in activity, binding of small molecular inhibitors and crystallization. The L192M mutant changes the ATP binding site of DYRK1B to mimic the binding site in DYRK1A. The Q164K was chosen to improve crystallization ability of DYRK1B since this lysine residue forms intermolecular salt bridges in the crystal packing in DYRK1A crystal structures[16]. The C238R mutation aimed to study the influence of the HCD motif with a possible disulfide bridge formation and to compare it to the more conserved HRD motif in the catalytic loop found in the majority of the kinases in the kinome. The expression plasmid pEXP17-hsDYRK1B-KD-451 was used as a template for site-directed mutagenesis. The

primers for mutagenesis were designed with the help of the QuikChange Primer Design online software[100]. The designed primers were ordered from SigmaAldrich. The forward and reverse primers for each of the three point mutations are presented in **Table 4.** Codons depicted in red bold encode the substituted amino acid. The nucleotides underlined in red bold are the mutated ones.

Table 4. Primers for site-directed mutagenesis.

Point mutation	Fwd/Rv	Nucleotide sequence
L192M	Fwd	5'-CCTGTGCCTGGTATTTGAG**ATG**CTGTCCTACAACCTGTACG-3'
	Rv	5'-CGTACAGGTTGTAGGACAG**CAT**CTCAAATACCAGGCACAGG-3'
Q164K	Fwd	5'-GCTGGAGCTGATGAAC**AAG**CATGACACGGAGATGA-3'
	Rv	5'-TCATCTCCGTGTCATG**CTT**GTTCATCAGCTCCAGC-3'
C238R	Fwd	5'-GCTCAGCATCATTCAC**CGC**GACCTCAAGCCCGAAAACATCTTGC-3'
	Rv	5'- GCAAGATGTTTTCGGGCTTGAGGTC**GCG**GTGAATGATGCTGAGC-3'

A similar strategy as described in the Quik-Change II site-directed mutagenesis protocol (Agilent Technologies) was used to produce the DYRK1B mutants[101]. The strategy of the site-directed mutagenesis is depicted on the **Figure 11**.

The PfuTurbo™ DNA Polymerase (Agilent Technologies) was employed for the site-directed mutagenesis[102]. The pEXP17-hsDYRK1B-KD-451 plasmid was used as a template. Reaction mixture was prepared according to the following scheme: 5 µl of 10x reaction buffer, 50 ng of template plasmid pEXP17-hsDYRK1B-KD-451, 1 µl 10 mM dNTPs, 1 µl 100-200 ng/µl reverse and forward primer. The mixture was filled up with nuclease-free water to 50 µl. 1 µl 2.5 U/µl PfuTurbo™ polymerase was added last and gently mixed[102].
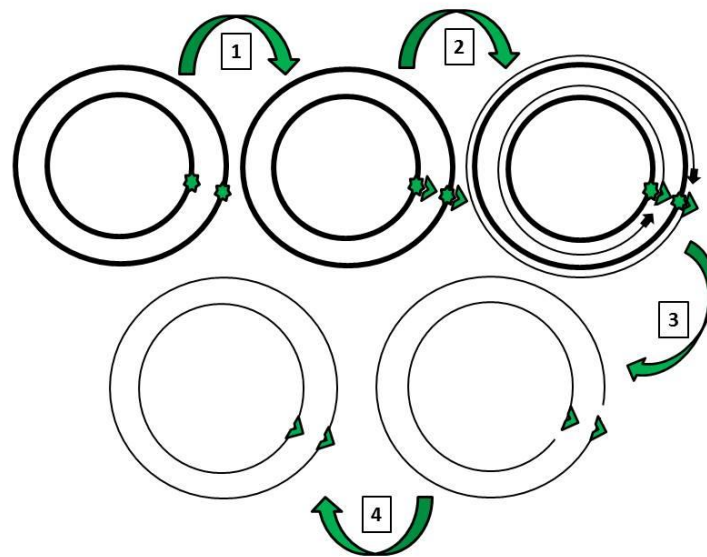
Figure 11. Strategy of the site-directed mutagenesis by QuikChange II site-directed mutagenesis. The star ✿ marks the site for the point mutation in the plasmid. ▲ are the primers possessing the mutated codon. 1. Denaturation of the plasmid which is followed by annealing of specific primers. The process is executed by a temperature cycler. 2. Pfu Turbo™ DNA polymerase replicates the parental plasmid and incorporates the primers containing the desired mutation leading to a nicked plasmid. 3. DpnI digests the parental plasmid without the mutation. 4. Transformation of plasmid into competent cells where the bacteria ligate the nicked plasmids and amplify it. The figure is modified from QuikChange™ site-directed mutagenesis protocol (Agilent Technologies)[101].

The PCR tubes with the reaction mixture were placed in the Dyad DNA Engine (BIO-RAD) thermal cycler. The thermal cycling conditions for the mutagenesis reaction are listed in **Table 5.**

Table 5. Thermal cycling condition for The PfuTurbo™ DNA Polymerase

Cycle	Temp, ℃	Time	Step
1	95	30"	initial denaturation
16	95	30"	denaturation
	55	1'	annealing
	68	1'/kb	extension
1	4	hold	hold

Afterwards, 1 µl 10 U/µl DpnI (BioLabs) was added to reaction mixture and incubated at 37 ℃ for 1 hour to digest parental plasmid. The plasmids containing the point mutation was transformed into XL10 Gold ultracompetent *E. coli* (Agilent Technologies). The transformation of the plasmids possessing the mutations was performed according to the transformation protocol[103].

250 µl of each transformation reaction was plated on LB-agar plate containing 100 µg/ml ampicillin. Plates were incubated at 37 ℃ o/n. Two colonies from each plate were inoculated in 4 ml of LB-media containing the same amount of ampicillin and incubated at 37 ℃ o/n with shaking at 220 rpm. 2 ml of the mini culture were used to isolate and purify the plasmid by QIAprep spin Miniprep kit (QIAGEN). The concentration of the plasmid was measured by Nanodrop. Each plasmid was analyzed by sequencing. Sequencing reaction was composed according the protocol of the Big.Dye Terminator v3.1 sequencing kit[97].

2.4 Expression of DYRK1B wt and mutants

2.4.1 Transformation into expression strain

BL21-CodonPlus(DE3)-RIL *E. coli* strain[104] (Agilent Technologies) was used for the expression of DYRK1B wt, DYRK1B Q164K, DYRK1B L192M and DYRK1B C238R. 1 µl of the plasmid was transferred into 50 µl of competent cells and incubated for 20 min on ice. BL21 *E. coli* competent cells were heat-shocked in water bath at 42 ℃ for 45 sec followed by incubation on ice for 5 min. 500 µl of LB media containing 100 mM of glucose was added to the BL21 cells and the cells were incubated at 37 ℃ for 1 hour with shaking at 220 rpm. In order to produce the starter culture for expression 250 µl LB media with BL21 cells were resuspended in 50 ml 2YT media containing 100 µg/ml of ampicillin and 34 µg/ml of chloramphenicol for selection. The starter culture was incubated in sterile flasks at 37 ℃ o/n with shaking at 220 rpm.

2.4.2 Expression of DYRK1B wt and mutants

For expression of the DYRK1B wt and the mutants a starter culture was prepared as described above. For large scale expression 2-4 L of TB (or 2YT) media were used for each of the constructs. 25 ml of starter culture was inoculated into 1 L of TB (or 2YT) media containing 100 µg/ml of ampicillin and 34 µg/ml of chloramphenicol. The 2.5 L sterile baffled Erlenmeyer flasks with the expression media were incubated at 37 ℃ to grow the bacteria. The optical density of the cultures was measured at a wavelength of 600 nm in a spectrometer to observe the growth rate of the bacteria. The cultures were incubated at 37 ℃ until the OD_{600nm} reached 1.6-1.8. (Cultures grown in 2YT media were induce at an OD_{600nm} of ~0.7) The cultures were than induced by 1 mM IPTG and incubated at 17.8 ℃ o/n with shaking.

2.5 Cell disruption

The cell pellets from the 2-4 L TB media were resuspended in approximately 50-70 ml lysis buffer and transferred into a 100 ml glass beaker. The beaker with the resuspended cells was immediately placed in an ice/water mixture where it was kept during cell disruption. Cell disruption was performed by sonication with following settings: 5 sec pulse on, 4 sec pulse off, 50% of amplitude and maximal temperature cut of 8℃ to avoid overheating of the sample. The cells were sonicated by the Vibra-Cell sonicator (Sonics) for 15 min (total time 27 min). After sonication, the disrupted cells were transferred in centrifuge tubes, and spun down at 20000 rpm for 45 min at 4℃. The supernatant was collected and pellets discarded. The supernatant was further used in following protein purification steps.

2.6 Protein purification

The first step of the protein purification was an affinity chromatography purification by HisTrap HP 5 ml column[105] (GE HealthCare). The next step was a TEV cleavage of the HisTag by TEV (*Tobacco Etch Virus*) protease. The TEV cleavage followed a second affinity chromatography via HisTrap HP 1ml to purify the target protein from the TEV protease, the HisTag peptide, uncut protein and other contaminant proteins. At last step gel filtration (size exclusion chromatography) was executed in order to produce the most pure protein as possible and also to change the buffer of the protein to one suitable for crystallization and/or the kinetic assays[106].

2.6.1 Affinity chromatography and TEV cleavage

Affinity chromatography was executed by HisTrap HP 5 ml columns in first step of purification protocol. HisTrap columns are packed with Ni Sepharose HP (High Performance) beads that facilitates to formation of chelate complexes between Ni^{2+}-ions and (His)6-tag protein of interest[105].

Routinely, HisTrap chromatography consists of consecutive steps as column equilibration, sample application including washing of unbound proteins, and, finally, sample elution. Äkta prime plus Fast Protein Liquid Chromatography (FPLC) system (GE Healthcare) and software Unicorn 5.0 (GE Healthcare) was used to perform and analyze the affinity chromatography.

HisTrap HP 5 ml column was connected to a peristaltic pump Pharmacia LKB (model Pump P-1) and washed by 3 CV by MilliQ water which was followed by column equilibration by 5 CV of binding buffer. Afterwards, the supernatant with the target protein, which has been obtained in the cell disruption step described previously, was applied by the pump into the column. The column was connect to the Äkta prime plus FPLC system and washed by 5 CV of binding buffer with a flow rate of 1 ml/min. The flowthrough was collected in fractions of 5 ml. The column was washed with 5% elution buffer, and the (His)6-DYRK1B wt and the mutants were eluted by an imidazole gradient (5-100% elution buffer corresponds to 10-500 mM of imidazole) with a gradient length of 8-10 CV. 1 ml fraction size was set during running of gradient to collect the eluted protein. Based on the chromatogram fractions were chosen to be analyzed by SDS-PAGE.

In order to cut the (His)6-tag a TEV-protease cleavage step was employed. After the SDS-PAGE the fraction containing the target protein were pooled and mixed with 500 µl of 2 mg/ml TEV. The mixture was transferred to a SnakeSkin Dialysis Tubing with 10kDa molecular weight cut-off membrane (Termo Scientific). The membrane tube was carefully closed by clips and placed into dialysis buffer with magnetic stirrer o/n at 4°C. After dialysis the sample was poured out from the dialysis membrane and placed on ice, meanwhile, a HisTrap HP 1 ml column was washed and equilibrated as described for the HisTrap HP 5 ml columns. Depending on the volume 15 of 20 ml of loading tube were connected to the Äkta prime plus system and sample was loaded into the tube by a syringe. The sample was then further injected from the loading tube onto the column with a flow rate of 1 ml/min. The flowthrough was collected in 5 ml fractions. The proteins were eluted by an imidazole gradient (5-100% elution buffer corresponds to 10-500 mM of imidazole) with a gradient length of 35-50 CV. The fraction size during the gradient was 1 ml to collect the eluting proteins. Based on the chromatogram fractions were chosen to be prepared as samples for the SDS-PAGE. After the SDS-PADE fractions with the target protein were pooled and concentrated for gel filtration chromatography.

2.6.2 Gel filtration

HiLoad™ 16/60 Superdex™ 200 column[106] (GE Healthcare) and the Äkta basic FPLC system were employed for gel filtration. The gel filtration was performed with a flow rate of 1 ml/min at 4°C. The gel filtration column was washed by 1 CV of MilliQ and, after that, equilibrated by 1 CV of gel filtration buffer. With the help of syringe, the sample was loaded into a 5 ml loading tube connected to Äkta basic FPLC system. The sample was injected through 5 ml tube onto the column and eluted by 1.2 CV of gel filtration buffer. The eluted protein was collected in 2 ml

fractions. SDS-PAGE samples were selected based on the chromatogram. After the SDS-PAGE the fractions containing the protein of interest were pooled and the concentration of the protein was measured by Nanodrop.

2.7 SDS-PAGE

The protein was analyzed by Sodium Dodecyl Sulphate-Polyacrylamide Gel Electrophoresis (SDS-PAGE) to verify the size, enrichment and the purity of the purified protein. A SDS-PAGE was run after each step of the protein purification. 10-, 12- and 15-well Mini-PROTEIN® TGX™ gels (BIO- RAD) were used for SDS-PAGE. Sample preparation included the following steps: choice of protein fraction based on the chromatogram, mixing of 15 µl of each fraction together with 5 µl of 4x NuPAGE LDS sample buffer (Life Technologies), and, finally, all samples were boiled at 95℃ for 5 min to denature the protein. After denaturing the sample were ready to be loaded in the well of the gel. The Mini-PROTEIN$^{®}$ TGX™ gel was vertically oriented in a holder and place between two electrodes in an electrophoresis cell. Inner and outer cambers of the electrophoresis cell were filled with Tris-Glycine running buffer.

10 µl of Mark12 protein ladder (Life Technologies) was used as standard to compare the molecular weight and loaded into the first well. 15-20 µl of protein prepared as described above were loaded in the wells of the Mini gel. The electrophoresis cell was attached to a PowerPac Basic power supply (BIO-RAD) and the SDS-PAGE was run at 200 V, 90 mA for 35 min. The voltage was kept constant throughout the run. After the electrophoresis was completed the gel was rinsed by 100 ml of MilliQ water and boiled for 1-1.5 min. SimplyBlue™ SafeStain (Invitrogen) was added to the gel in the volume of 20 ml to cover the gel. The gel was boiled with SimplyBlue™ SafeStain for 1-1.5 min and placed on an orbital shaker for 1 hour. Afterwards, SimplyBlue™ SafeStain was discarded, and gel was rinse by MilliQ water and kept at room temperature with gentle shaking.

2.8 Nanodrop

The concentration of proteins used in this thesis was measured by the Nanodrop 2000c spectrophotometer (Thermo Science)[107]. 2 µl of buffer was used as a blank and 2 µl of protein solution was used for measurement of its concentration. The extinction coefficient and molecular weight of the proteins used in this thesis were calculated by the on-line tool Protparam at the ExPasy webpage[100] **(Table 6).**

**Table 6. Extinction coefficient and molecular weight of proteins DYRK1B wt and its mutants.**

Protein	Extinction coefficient, $\Delta\varepsilon$	Molecular weight (Da)
DYRK1B wt	40 340	42 583.8
DYRK1B L192M	40 340	42 601.8
DYRK1B Q164K	40 340	42 601.9

2.9 Thermoflour Assay for solubility and stability screen

The thermoflour assay can be used as a stability and solubility optimization screens of proteins[108]. The principle of the thermoflour assay with a typical melting curve is depicted in **Figure 12**. The assay is based on the monitoring of the melting of protein in the presence of fluorescent dye. A gradual increase of the temperature leads to unfolding of the protein and the hydrophobic regions/core gets exposed. In this thesis Sypro orange was used as a fluorescent dye. The Sypro orange dye binds to internal hydrophobic regions of unfolded protein and this change the fluorescence signal which can be monitored. At high temperature the protein undergoes aggregation leading to a dissociation of the dye and a decrease of the fluorescence signal. The melting temperature is calculated from the slope of the melting curve. It is the point where 50% of the protein is denatured. The melting point of a protein can be influenced by different buffers, salts, ligands etc. This is used in the thermal shift experiment where the melting point is measured in the presence/absence of a ligand of interest or in the presence of different buffers. Higher melting temperature compared to the apo-protein indicates a stabilization effect that the ligand has to the protein which is connected to binding of the ligand. Lower temperature indicates a destabilization effect[109]. This method can also be used to screen for an optimize pH or buffer

condition[110]. Buffers that stabilize the protein most will have the highest melting points. The thermofluor method was used to determine optimal buffer condition for DYRK1B.
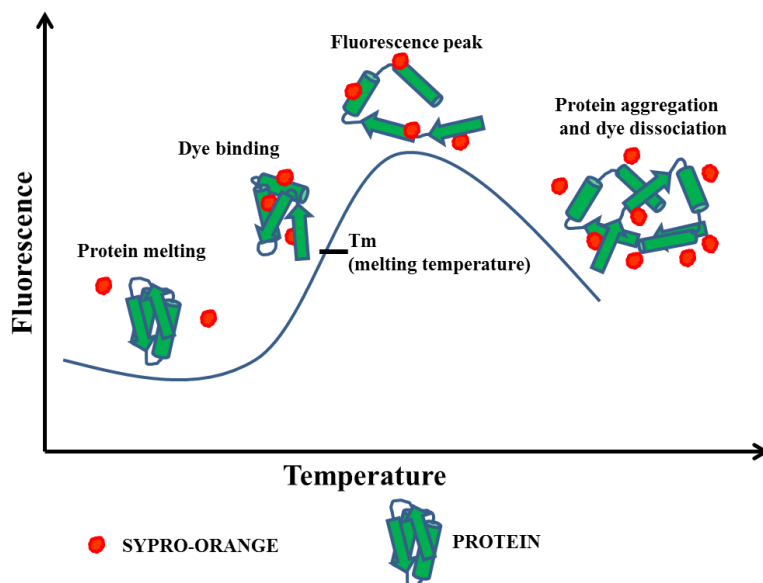
Figure 12. Melting curve of a protein in the thermofluor assay. The figure was modified from the Argonne national laboratory web-site[111].

The Solubility and Stability buffer screens 1 for DYRK1B buffer optimization was design based on the available buffers, experimental data and features of DYRK1B. Concentrations of buffers and salts were calculated according to the protocol of the commercially available Solubility & Stability screen (Hampton Research)[112]. The Stability and Solubility buffer screen 2 was designed based on the results of first screen to obtain higher melting temperatures of DYRK1B. Both buffer screens were dispensed by the liquid handling system Alchemist 2.6.2 (Rigaku, Inc.) The reagents of the Stability and Solubility buffer screen 1 and 2 are listed in the appendix. The thermoflour assay includes the preparation of a kinase-Sypro orange dye solution by adding 1.2 µl of Sypro Orange dye (Sigma Aldrich) to 1.2 ml of DYRK1B wt in buffer A with the final kinase concentration kinase of 0.15 mg/ml. Afterwards, 10 µl of DYRK1B-Sypro orange dye solution was added to each well of a 48-well PCR microplate. On the next step, 10 µl of each condition of Stability and Solubility screen 1 or 2 were mixed with the DYRK1B-Sypro orange dye solution in the microplate. To determine the melting point of DYRK1B wt each condition from the screen was tested in duplex. The microplate was sealed with transparent sealing film. The thermoflour assay was performed by a temperature gradient from 10°C to 90°C (with increments of 0.3°C) in a MJ Mini personal thermal cycler (BIO-RAD). The data was analyzed by Opticon Monitor 3 software.

2.10 Enzyme kinetics

The activity of DYRK1B wt and its mutants as well as the inhibitor potency were measured by the ATP-regenerative and NADH-consuming assay described by Cook et $al.$[77] The method was modified for DYRK kinases. In the Cook assay, DYRKtide is exploited as the substrate for DYRK kinases. The peptide RRRFRPASPLRGPPK (DYRKtide) contains a serine as a specific phosphorylation sites and is recognized by DYRK. The kinase activity assay was measured in a Molecular Device SpectraMax M2e plate reader at room temperature. The assay mixture contains the following ingredients: 100 mM MOPS (pH 6.8), 10 mM KCl, 10 mM $MgCl_2$, 1 mM phosphoenolpyruvate (PEP), 1 mM DYRKtide, 1 mM β-ME, 15 units/ml lactate dehydrogenase, 10 units/ml pyruvate kinase and 10,7 mM NADH. The Cook assay reaction was composed by adding 75 µl of assay mixture, 10 µl of DYRK kinase (concentration range 5-20 µM), 10 µL of 2560 or 1280 µM ATP with total volume 95 µl. For the K_m determination a serial of ATP concentration from 50 mM to 4 µM was used. The enzymatic velocity measured in the Cook assay is the consumption of NADH and in the loss of absorption at 340 nm. Therefore the velocity has a negative slope. As a standard for testing the inhibitors the concentrations of the kinase and ATP were adjusted to obtain an initial velocity of around -10 AU/sec. The measurements were done in triplex and each individual measurement over a time period of 300 sec. In the case of the K_m determination shorter time periods were chosen, in particular for the higher ATP concentration, to obtain the initial velocity while the curve was still linear. For the screening, all inhibitors were tested at a concentration of 20 µM in the reaction mixture. In order to identify IC_{50} values a serial dilution of inhibitor concentrations were used in the range between 20 µM and 4 nM.

2.11 Microscale thermophoresis

Thermophoresis is a phenomenon describing the ability of molecules to move along a temperature gradient, which first was described in 1856 by Carl Ludwig[113]. Particularly in solutions molecules have the tendency to move away from the high temperature region with a dependency of the hydration shell and the solvation entropy of the molecules[114]. The depletion of molecules in the region of the elevated temperature compared to the initial thermal conditions (ΔT) can be quantified by the Soret coefficient S_T described by following equation[115] (3)

$$C_{hot}/C_{cold} = \exp(-S_T \Delta T) \quad (3)$$

This principle was utilized to develop the microscale thermophoresis (MST) by NanoTemper Technologies GmbH (Germany). In the instrument Monolith NT.115 the NanoTemper technology employs fluorescence in combination with infrared-laser optics for local heating of the sample in a small capillary. The biomolecules are labeled by fluorescence dyes and the fluorescent signal is recorded before turning the laser on followed by the fast temperature dependent changes in fluorescent intensity when the laser is switch on, and finally the signal returns to the starting point in a back diffusion after switching off the laser[116]. The binding of a ligand to a biomolecule changes its hydration shell and affects the thermophoretic movement. This principle is used to determine binding affinities with high accuracy[117].

The interaction of DYRK1B wt with ATP was tested by MST. For detailed Kd analysis 16 capillaries each with different ATP concentrations were employed in MST. DYRK1B in the concentration of 14 μM in buffer D was used for the MST. DYRK1B was labeled with the Monolith NT Labeling kit (Cat No. L001). A 2-fold dilution series of ATP was prepared and an equal amount of DYRK1B was added to each ATP concentration. Each sample was loaded into a MonolithTM hydrophilic capillary through capillary action and then analyzed with the Monolith NT.115 instrument.

2.12 Crystallization trials of DYRK1B and DYRK1A

Crystallization trials of DYRK1A and DYRK1B in gel filtration buffer were performed by vapor diffusion method[118]. After gel filtration the DYRK kinase was concentrated in an Amicon® Ultra-4 centrifugal filter (Merck Millipore) in order to reach the concentration of ~ 7-8 mg/ml (DYRK1A) or ~11-13 mg/ml (DYRK1B) (measured by Nanodrop). The apo-protein, and protein in the complex with inhibitor were used for the crystallization trials. Routinely, 100 μl of high concentrated DYRK kinase was gently mixed with 4 μl of 10 mM inhibitor in DMSO or water (final concentration of the inhibitor in the crystallization trials was 400 μM). The commercially available crystallization screen JCSG-plus™ (Molecular Dimensions)[119], Wizard I and II (Emerald Bio)[120] and the in house screen KCSG were used to screen for crystallization conditions. The screening was set up by Phoenix protein crystallization robot (Art Robbins Instruments) in 96-wells sitting drop plates in ratio of 200 nl protein solution and 200 nl of crystallization condition[121]. Crystallization trials were performed at room temperature and at 4℃. The hits from the screen were selected for further optimization. The conditions from the screen were optimized by designing 24-well screens with gradients of precipitants and salts and dispensed by Alchemist 2.6.2 (Rigaku, Inc.). The crystallization trials were set up by hanging drop method in 24-well

crystallization plates with the ratio of 2+2 μl and 2+4 μl of protein solution to reservoir solution containing optimized crystallization conditions.

In the case of DYRK1A an Additive Screen (Hampton Research) was employed[122]. A 96-deep well block was dispensed by Alchemist 2.6.2 with 900 μl of a crystallization condition found in the JCSG-plus™ screen and in each of the well of deep well block 100 μl of each additive solution was added and mixed. The 96-well sitting drop plate with new Additive Screen was set up by Phoenix protein crystallization robot with the same 200 nl +200 nl ratio of protein solution to crystallization condition. The plates were placed at 4℃ and room temperature and the drops were examined every second day. The conditions with the additives which gave the best crystals were further selected to be set up in crystallization trials with 24-well hanging drop plates.

Crystals were flash frozen with different cryoprotectants in liquid nitrogen in either 30% ethylene glycol, paratone, 30% glycerol, 30% PEG400 or 40% PEG3350. The crystals were sent to BESSY II at the Helmholtz Zentrum Berlin (Germany) for X-ray data collection. Diffraction data was integrated by XDSAPP program[123] and the crystal structure was solved together with Dr. Ulli Rothweiler by molecular replacement with MolRep[124,125] of the CCP4 software package[126,127]. The structure was refined in the Refmac5[128] and Phenix[129].
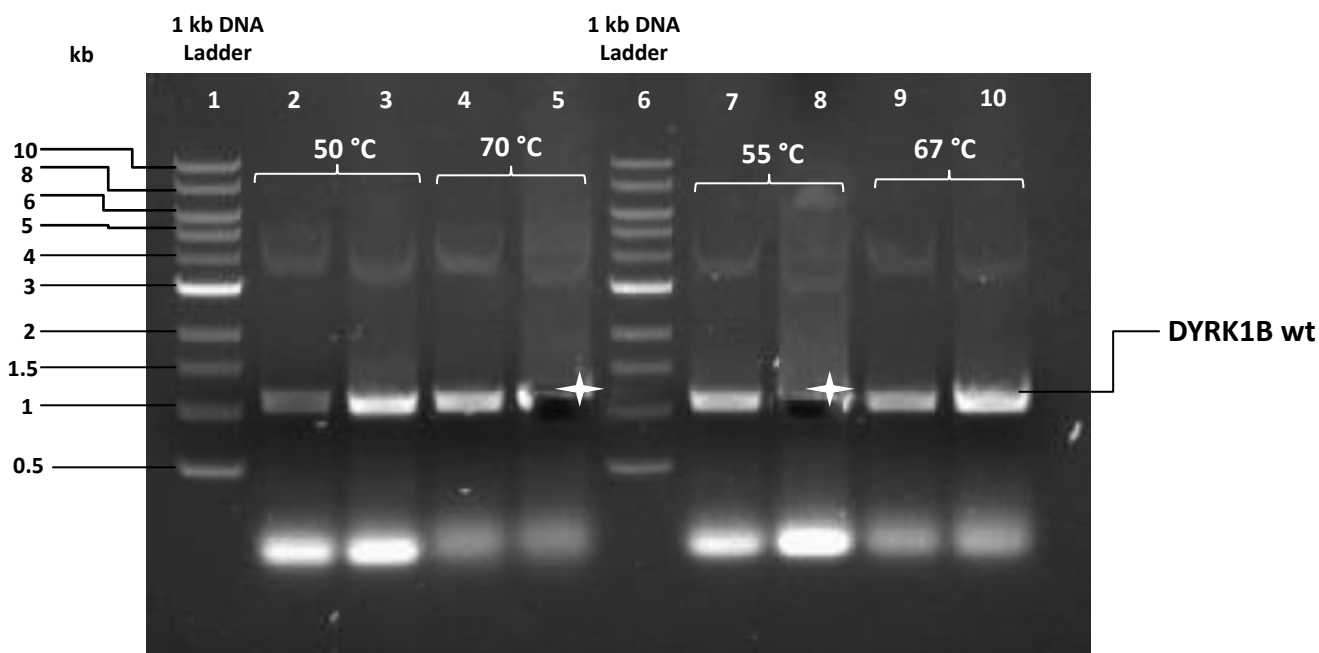
3 RESULTS

3.1 Cloning and mutagenesis

The human *DYRK1B* gene was originally cloned and characterized by Leder S. *et al.*[30]. The *DYRK1B* gene encoding full length protein that was used in this thesis was the Addgene plasmid 23761[130] in the vector pDONR223-DYRK1B.

The original expression clone of the DYRK1B containing amino acid sequence 78-442 was mostly expressed in inclusion bodies and had low yield and solubility. Therefore, it was decided to create a longer construct by adding several amino acids at the C-terminal end to improve the solubility of DYRK1B. The Gateway cloning strategy (Life Technologies) together with directional TOPO® cloning (Life Technologies) were used to produce expression clone pEXP17-hsDYRK1B-KD-451 comprising residues 78-451. The template DNA from plasmid pDONR223-DYRK1B was amplified in DH5α *E. coli*, isolated and purified by QIAprep spin Miniprep kit (QIAGEN). The concentration of amplified DNA template was 276 ng/µl measured by absorbance at 260 nm on a Nanodrop spectrophotometer. To obtain the blunt-end PCR product containing desired DYRK1B gene, Phusion polymerase was employed and PCR was performed as described in the method section of this thesis.

Electrophoresis on a 0.7% agarose gel was used to separate the PCR product. The successful amplification of DYRK1B construct which has the length of 1153 bp is shown in **Figure 13.** The PCR product was extracted from the 0.7% agarose gel by QIAquick Gel Extraction kit (QIAGEN). The concentration of the purified PCR products was measured by Nanodrop. The concentration of PCR-I product (lane 5, annealing temperature 70℃) and PCR-II product (lane 8, annealing temperature 55℃) were 11.3 ng/µl and 10.3 ng/µl, respectively. Two TOPO® cloning reactions, one with each PCR-I product and PCR-II product, were performed to produce the entry clone as described in the methods chapter.

Figure 13. The results of PCR amplification separated by electrophoresis on a 0.7% agarose gel. Four different annealing temperatures were employed during amplification process. Each temperature was run in duplicate. Lanes 1 and 6 are the 1 kb DNA Ladder; Lanes 2 and 3 had 50℃ annealing temperature; 4 and 5 had 70℃; 7 and 8 had 55℃, 9 and 10 had 67℃. The thick bands between 1 kb and 1.5 kb are the successfully amplified DYRK1B wt PCR products obtained using the pDONR223-DYRK1B plasmid as a template. Bands in lanes 5 and 8 marked with a star were selected to proceed with cloning and cut out from the gel. (In the figure shown here these bands are already cut out).

pENTR-DYRK1B-451-I and pENTR-DYRK1B-451-II were transformed into One Shot® Top10 chemically competent *E. coli*. The plate with the transformed construct containing PCR product from the annealing temperature at 70℃ did not give any colonies, thus, the first entry vector pENTR-DYRK1B-I was used to continue the cloning. Three colonies from the plate with pENTR-DYRK1B-I plasmid were selected to be amplified. Plasmids were isolated and purified by QIAprep spin Miniprep kit (QIAGEN). Three plasmids were sequenced with M13 forward and reverse primer using the Big.Dye Terminator v3.1 sequencing kit. The results of sequencing showed that one plasmid had the correct insert with the correct N- and C-terminal ends. The concentration of the correct pENTR-DYRK1B-451-I vector was 158.7 ng/μl. In the next step, the recombination reaction as described in the methods section was performed to produce the expression clone: pEXP17-hsDYRK1B-KD-451.

The recombined vector was transformed into One Shot® Top10 competent *E. coli* (Life Technologies). Two colonies were selected for amplification followed by purification and sequencing with T7 forward and reverse primers. Results of the sequencing showed that one colony was a positive clone. This plasmid was used for large scale expression of DYRK1B wt and it was used as the template for the site-directed mutagenesis.

Site-directed mutagenesis was performed using a strategy similar to the QuikChange II site-directed mutagenesis protocol (Agilent Technologies). The wild-type pEXP17-hsDYRK1B-KD-451 plasmid was used as a template. Pfu Turbo DNA polymerase was used together with the specific primers, described in the section 2.3 p.34, to produce the desired mutants. After the PCR amplification the parental plasmids were digested by DpnI endonuclease followed by transformation of the new mutated plasmid into XL10 Gold ultracompetent *E. coli* (Agilent Technologies). Two colonies from each transformation were selected to be amplified in mini cultures. Plasmids with point-mutations were purified by QIAprep spin Miniprep kit (QIAGEN) and sequenced by Big.Dye Terminator v3.1 sequencing kit to verify the mutations. The three point-mutations were successfully confirmed by the sequencing results represented in **Figure 14**.
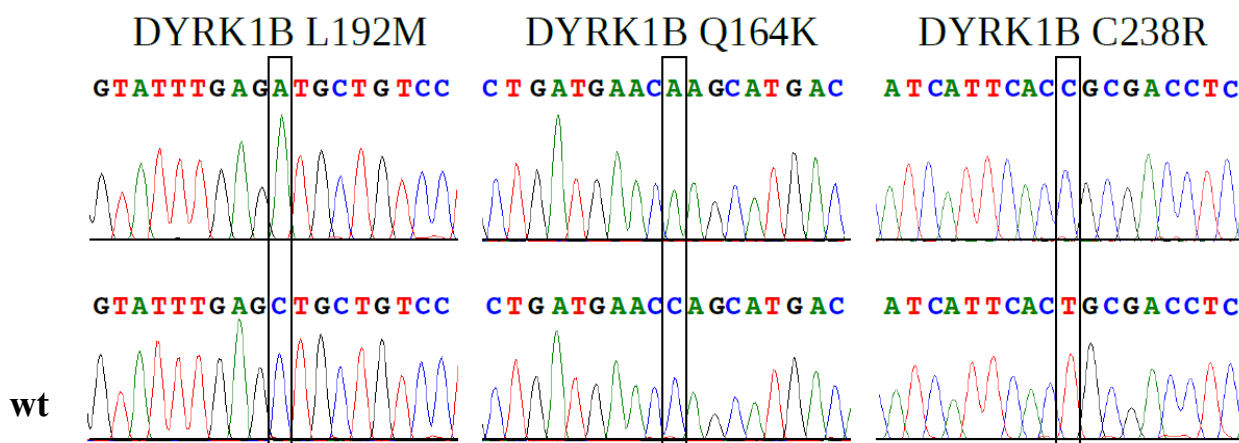
Figure 14. Results of sequencing DYRK1B L192M, DYRK1B Q164K and DYRK1B C238R mutants. The sequencing chromatogram of DYRK1B wt is represented in the lower row. Sequencing chromatograms of DYRK1B L192M, DYRK1B Q164K and DYRK1B C238R are depicted on the upper row. The mutated nucleotides are highlighted by vertical black box.

3.2 Purification of DYRK1B wt in original phosphate buffer

The purification protocol of the DYRK1B wt was established based on the protocol of the close homolog DYRK1A. The kinase domain of DYRK1A was successfully expressed as a soluble protein with a good yield of more than 20 mg per liter. Since the two proteins DYRK1A and DYRK1B are so similar the same expression and purification protocol was used.

The pEXP17-hsDYRK1B-KD-451 plasmid was transformed into BL21-CodonPlus(DE3)-RIL *E. coli* strain (Agilent Technologies) and expressed in 4 L of TB media. Buffer A (Table 1, p.27) was used as binding buffer to resuspend the pellets containing the cells with DYRK1B wt

protein. After sonication followed by separation of soluble fraction of the cell lysate by centrifugation, the first step of purification was performed by HisTrap HP 5 ml column (GE Healthcare). Routinely, the column was washed, equilibrated and the supernatant was loaded into the column by a peristaltic pump. The flow rate of 1 ml/min and pressure limit 0.5 MPa was employed during the purification. DYYRK1B wt was eluted on a gradient of 5-100 % (25 -500 mM Imidazole) elution buffer B (Table 1, p.27) in 8 CV. The peak corresponding to DYRK1B wt had a average value of 200 mAU. DYRK1B wt elutes at aproximatly 50-70% of elution buffer B (250-350 mM imidazole), **Figure 15, a**. The fractions 19, 20, 22, 24, 26, 28, 30, 32, 35, 37 and 38 were analysed by SDS-PAGE (**Figure 15**, **b**). The results of SDS-PAGE shown that fractions 30-38 contains the DYRK1B wt. Based on the chromatogram and results of SDS-PAGE, the fractions 32-40 were pooled to conduct the TEV-cleavage by dialysis in buffer C o/n.

In order to separate TEV protease, the (His)6-tag peptide, and contaminants from the DYRK1B wt protein, a second affinity chromatography by HisTrap HP 1 ml column was used (**Figure 16, a**). Flow rate was set to 1 ml/ min and max pressure was 0.5 MPa. Unbound materials are depicted as a flowthrough in the chtomatogram. DYRK1B was eluted by gradient of buffer 0 - 100% (0-500 mM Imidazole). Fractions 2, 10, 11, 12, 14, 15, 18, 19 and 20 were selected for SDS-PAGE. Based on the results of SDS-PAGE (**Figure 16, b**) the main peak of around 250 mAU and a concentration of 25% of Buffer B corespended to cleaved DYRK1B wt. The (His)6 - tag was successfully cleaved by the TEV protease. The TEV cleavage was confirmed by the difference in size of uncleaved band (uc on the **Figure 16, b**) and cleaved fractions (10, 11 and 12). Fractions 10, 11 and 12 were pooled and futher used for gel filtration (size exclusion chromatography).

A HiLoad™ 16/60 Superdex™ 200 column was employed for final purification to obtain pure protein suitable for kinetic assays and crystallization trails. The sample was eluted with a flow rate of 1 ml/min during 1.2 CV. The fractions were collected to 2 ml. The results of chromatography is represented in the **Figure 17, a**. The fractions 33-41 were selected for SDS-PAGE (**Figure 17**, **b**). The peak in the chromatogram around 60 mAU corresponded to DYRK1B wt. The fractions 36-41 were pooled and the final concentration was 0.04 mg/ml in 12 ml measured by absorbance at 280 nm on the Nanodrop which is a final yield of 0.6 mg protein (0.15 mg of protein per liter) based on the molar absorbance coefficient (Table 6, p.40). The estimated purity of DYRK1B wt was around 98%. The band from SDS-PAGE after gel filtration was cut out and sent to Mass Spectrometry. The results of the Mass Spectrometry confirmed that the purified protein is DYRK1B and that it is phosphorylated at the tyrosine in the activation loop Y273.

a)

b)
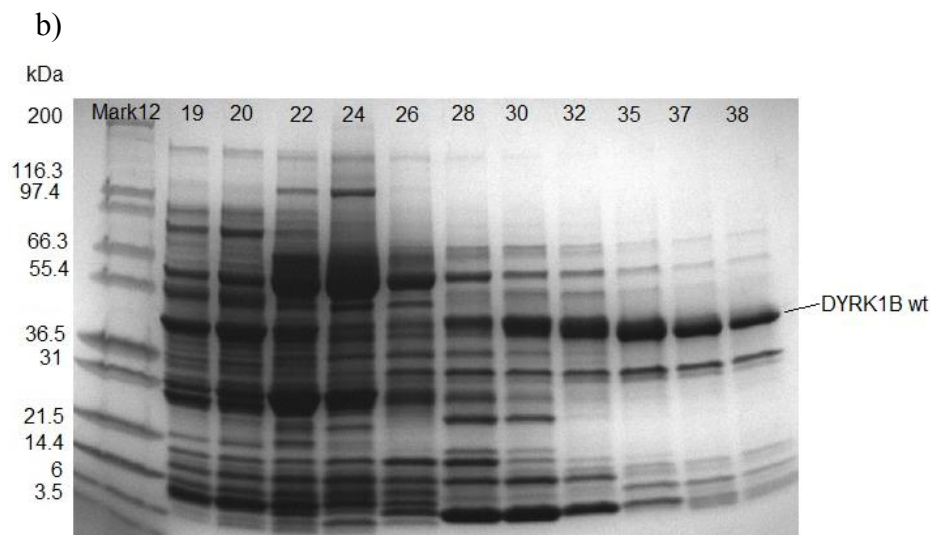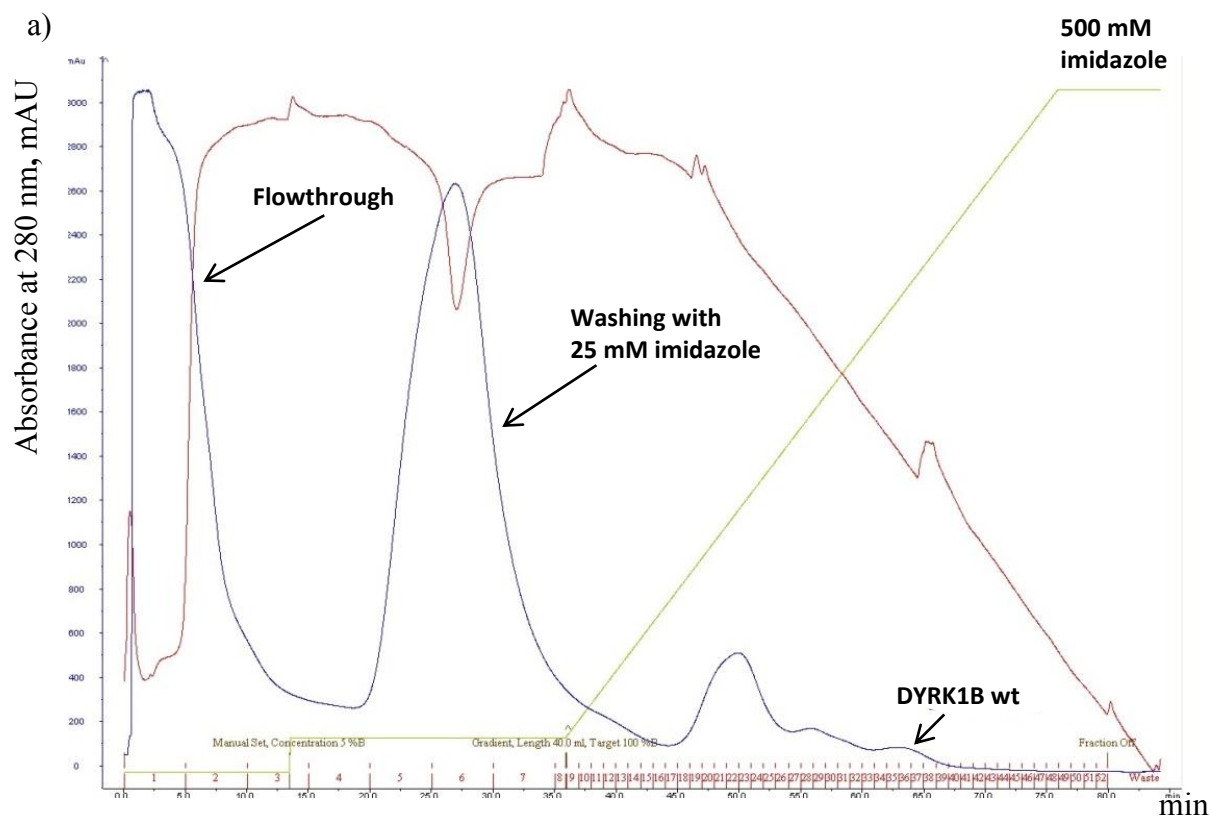
Figure 15. Purification of (His)6 -DYRK1B wt. a) The chromatogram shows the affinity purification of DYRK1B wt by HisTrap HP 5ml column. The blue line is the absorbance at 280 nm, the green line is percentage of elution buffer B (0%-100% corresponds to 0-500 mM imidazole). The red line is the conductivity. Different peaks in the chromatogram are depicted by arrows. The sample was loaded by a peristaltic pump prior to the purification with Äkta prime thus the chromatogram begins with the column wash step. b) SDS page of the selected fractions of the chromatogram. Mark12 in lane 1 was used as marker; the numbers above the lanes represent the fractions. Fractions 30-38 contain DYRK1B wt. The bands located between 55.4 and 36.5 kDa corresponded to DYRK1B wt.
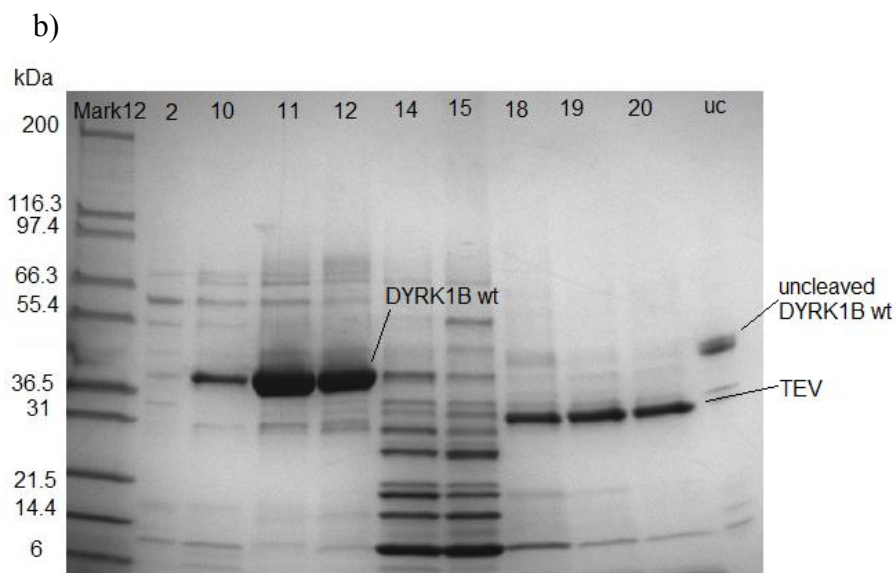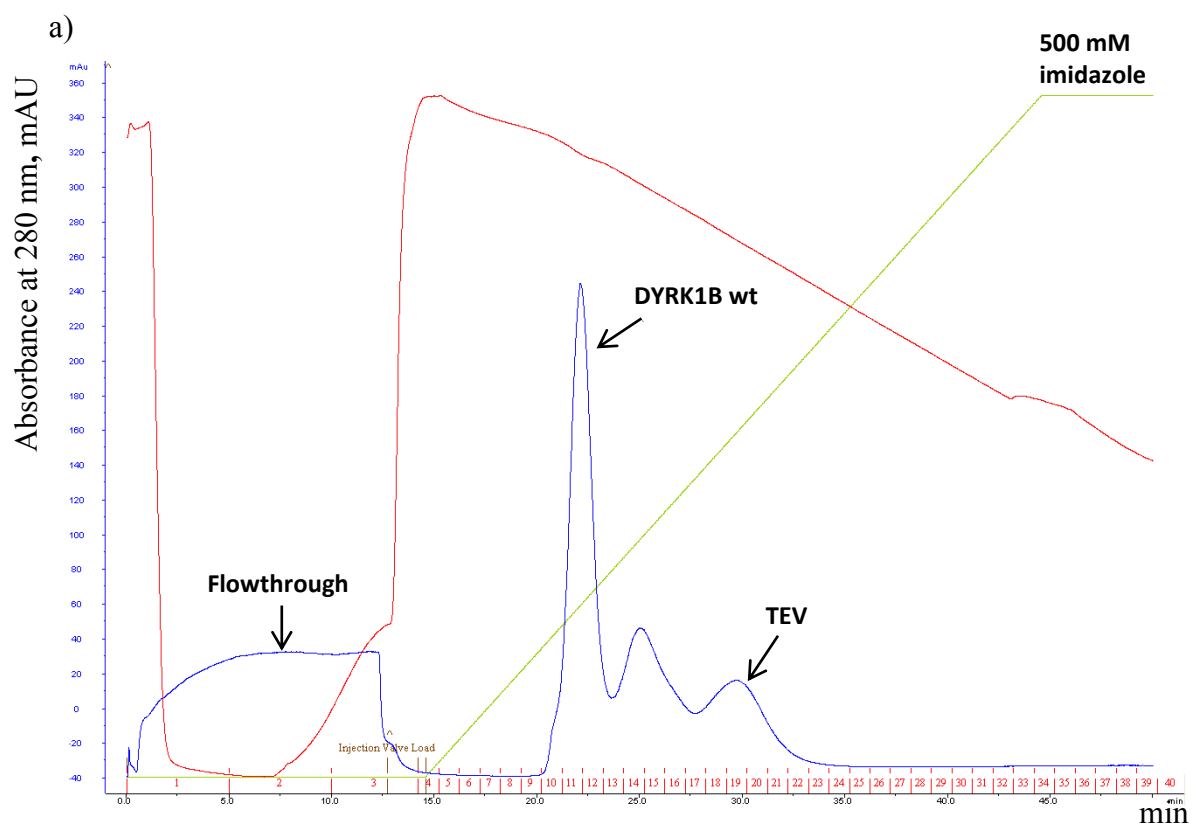
Figure 16. Purification of DYRK1B wt after TEV-cleavage. a) The chromatogram shows the affinity purification of DYRK1B wt by HisTrap HP 1ml column.The blue line is the absorbance at 280 nm, the green line is percentage of elution buffer B (0%- 100% corresponds to 0-500 mM imidazole). Different peaks in the chromatogram are depicted by arrows. The red line is the conductometry. DYRK1Bwt elutes at an imidazole concentration of approximately 125 mM. b) SDS page of the selected fractions of the chromatogram. Mark12 in lane 1 was used as marker, the numbers above the lanes represent the fractions, uc (uncleaved) is a sample form the first HisTrap and contains DYRK1B with a uncleaved (His)6-tag. Fractions 10-12 contain DYRK1B wt.

a)

b)
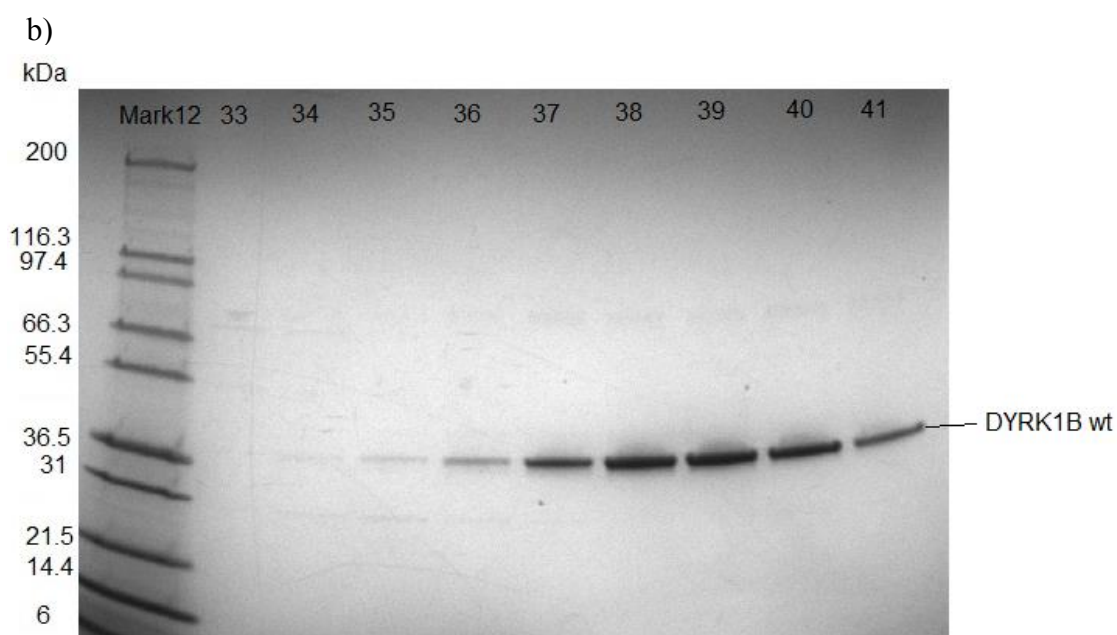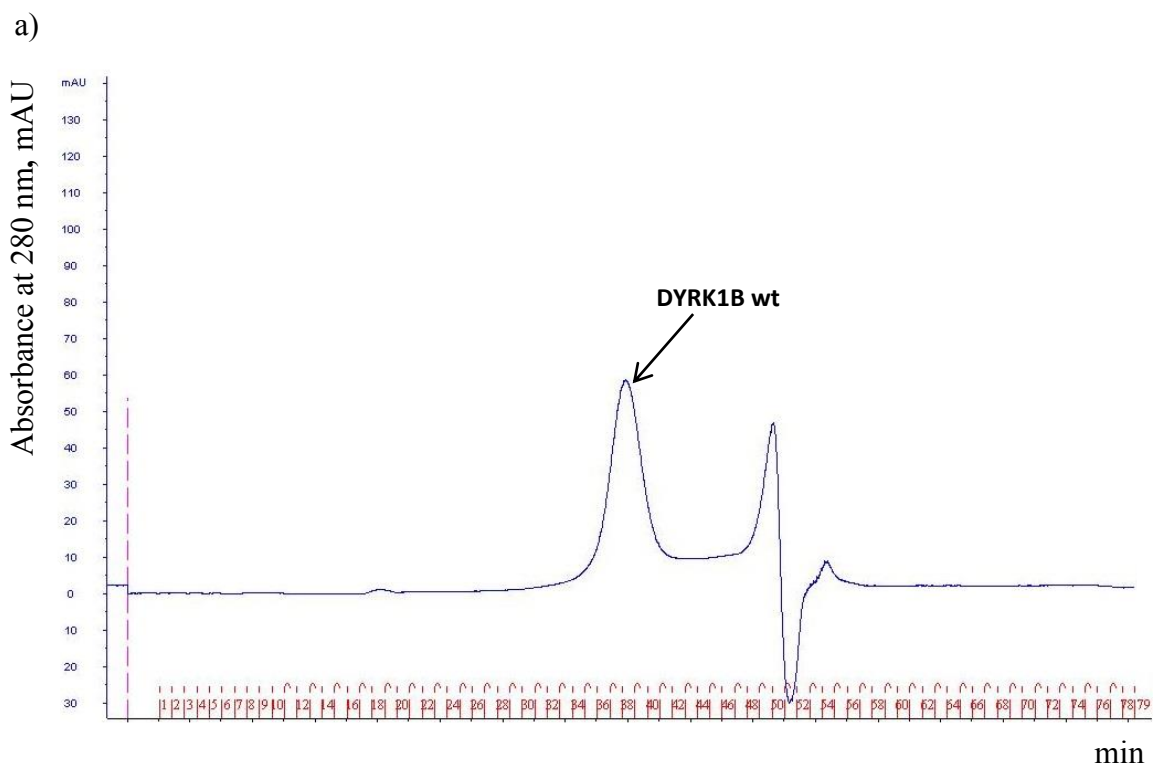
Figure 17. Gel filtration of DYRK1B wt. a) Gel filtration (size-exclusion chromatography) was performed by HiLoad™ 16/60 Superdex™ 200 column. Flow rate was 1 ml/min. Fraction size was 2 ml. Different peaks in the chromatogram are depicted by arrow. The Blue line is the absorbance at 280 nm. b) SDS page of the selected fractions of the chromatogram. Mark12 in lane 1 was used as marker, the numbers above the lanes represent the fractions. Fractions 35-41 contain DYRK1B wt.

## 3.3 Thermofluor Assay for Solubility and Stability Screen

The initial protocol, which employed phosphate buffer for the lysing of cells and affinity chromatography, showed that the protein had low solubility and the yield was low. The expression however was high, so the protein was mostly expressed in inclusion bodies. A fraction of protein in phosphate buffer did not bind to the column, probably, because it formed soluble aggregates in this buffer. The protein could be concentrated only to 6 mg/ml in gel filtration buffer (buffer D). The crystallization trials with commercial screens showed however that the vast majority of the drops stayed clear for more than 2 weeks after the crystallization setup. This fact indicates that a higher concentration has to be used for the crystallization of protein. Since it was impossible to concentrate the protein more than 6 mg/ml in the gel filtration buffer, and because the protein precipitated, it was decided to change the buffers for the purification. Thermoflour assay was employed to screen for an optimal buffer. The first screen was comprised of 96 conditions including five different buffers with a pH range between 5.5 and 8.5, a combination of three different salts, and CHAPS as a detergent. The second screen was designed based on the result of first one in order to establish the concentration of KCl which will give the highest melting point.

Results of the Stability and Solubility screen 1 are represented in the **Figure 18**. The best condition was MES pH 6.5 which improved the melting temperature compared with phosphate by 10 degrees. In case of the HEPES pH 7.5 buffer, it was observed that the Tm of the protein in conditions containing KCl (light blue columns) gave increased melting temperatures compared to conditions with alternative alkali salts like LiCl (orange columns) or NaCl (green columns). In other cases it was also detected that the presence of KCl in the buffer stabilizes the protein better than NaCl or LiCl. In general no extra addition of salt (dark blue columns) was best, but it should be kept in mind that all samples contained 250 mM NaCl from the 1:1 mixing with the buffer the protein was purified with in the first place (50 mM Na_2HPO_4 pH 8.0, 500 mM NaCl). The first step in the purification of DYRK1B is via the HisTrap columns, therefore, a pH above 7.5 for an optimal interaction of the (His)6-tag with the column and high salt concentrations to avoid unspecific interactions was desired. Thus, it was decided to design a second screen, where we could determine the exact concentration of KCl that is beneficial for the stability.
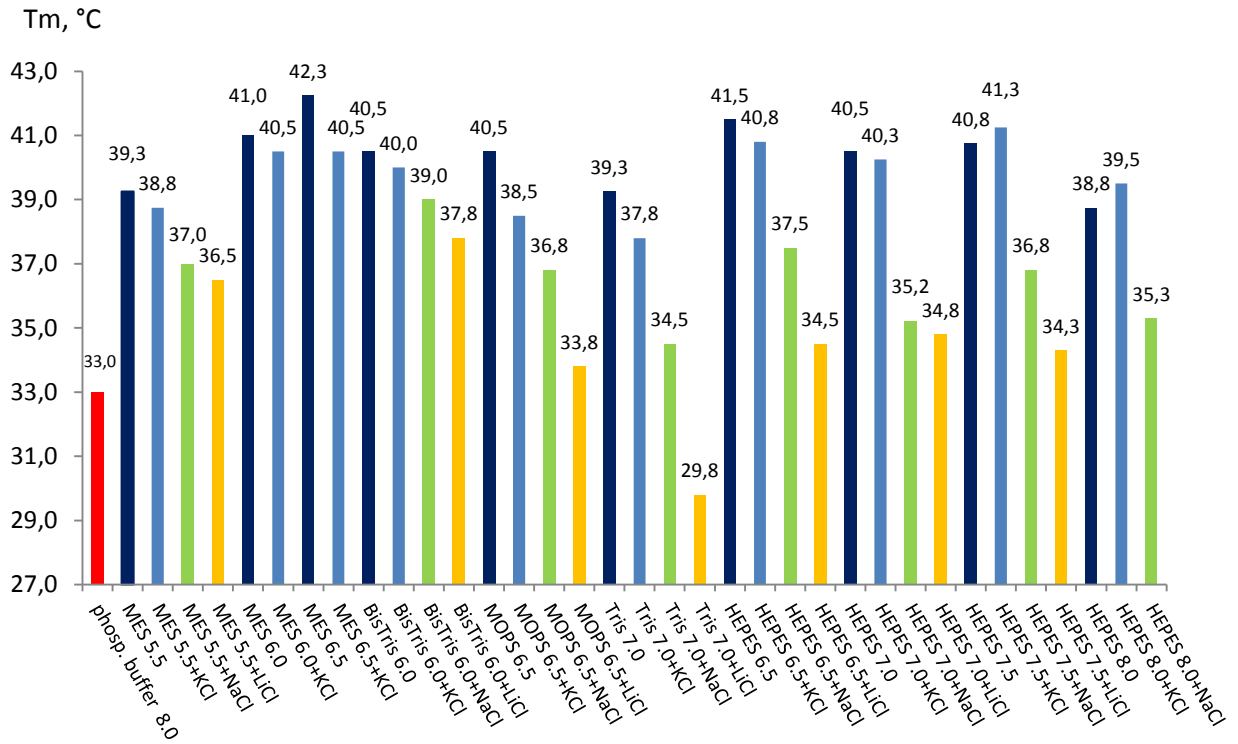
Figure 18. Results of Stabilization and Solubility buffer screen 1. Red column is the starting condition with protein in phosphate buffer (50 mM Na$_2$HPO$_4$ pH 8.0, 500 mM NaCl). All samples contain 250 mM NaCl from the starting condition. 50 mM buffer without additional salts (dark blue), 50 mM buffer and 400 mM KCl (light blue), 50 mM buffer and 400 mM NaCl (green), 50 mM buffer and 400 mM LiCl (orange). Tm is the melting temperature of the protein. The graph shows a representative fraction of the 96 tested conditions to illustrate the type of alkali salts dependence of the stability of the protein.

Stability and Solubility screen 2 was composed of 49 conditions (Appendix) including the buffers (50 mM) which gave the best scores in the first run and four different concentrations of KCl: 50, 10, 150 and 200 mM. The MES pH 6.0, pH 6.5 and MOPS pH 6.5 buffers showed no sensitivity to the KCl concentration. The Tris buffer pH 7.0 showed a decrease in stability with higher KCl concentrations. The best hits of Screen 2 were the HEPES buffers pH 7.5 and pH 8.0 which showed an increase in stability with higher KCl concentrations compared to the buffer without KCl. The results are summarized in the **Figure 19**. The biggest improvement was seen for the HEPES buffer at pH 8.0 where the addition of 50 mM KCl improved the melting temperature by 6.7 degree from 38.8 to 45.5 compared to the KCl free buffer which was better than the MES buffer identified in the first screen (**Figure 18**).
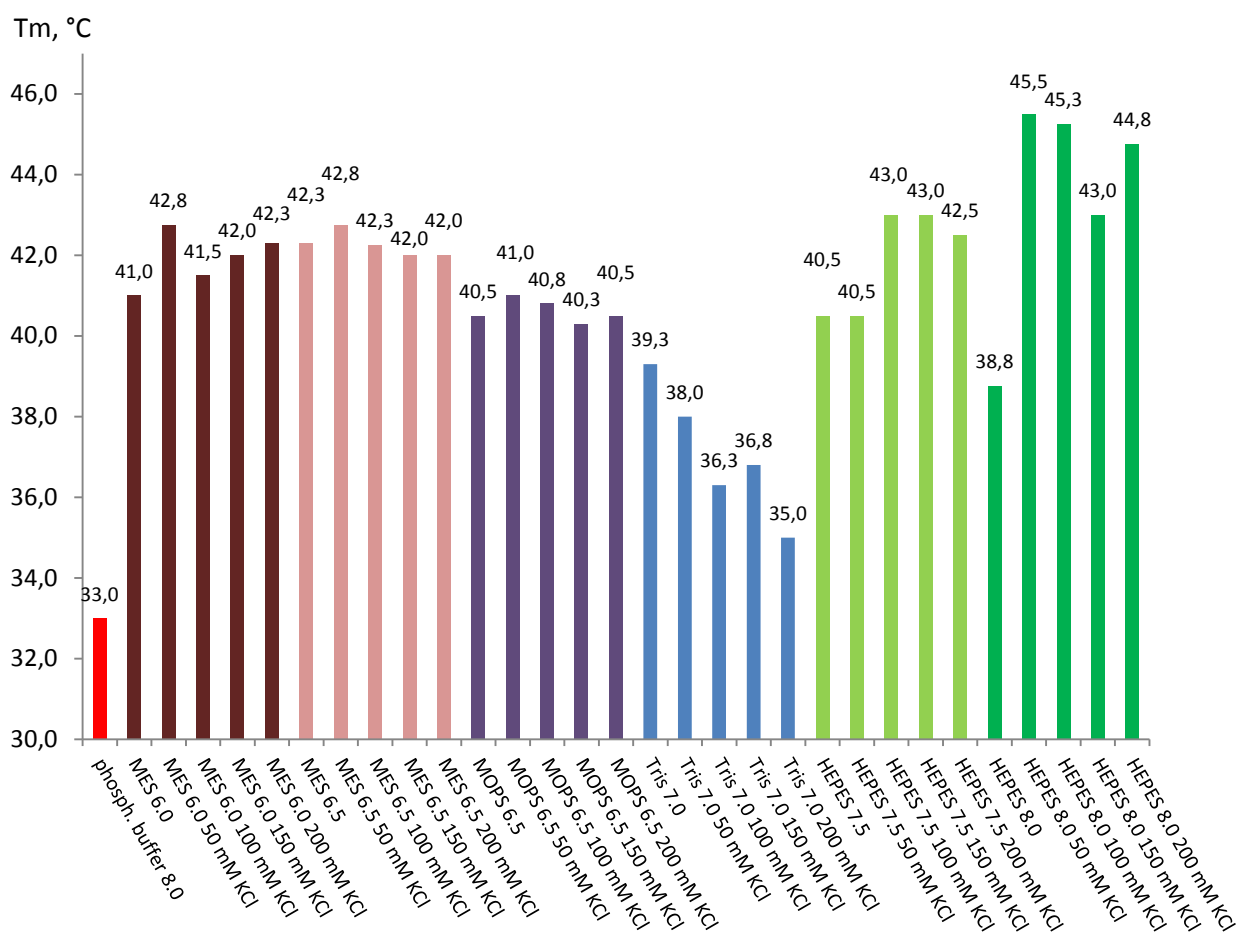
Figure 19. Results of the Stability and Solubility Screen 2 by thermoflour assay. The graph shows a representative fraction of the 49 condition in Stability and Solubility screen 2. The red column indicates the starting condition with the phosphate buffer (50 mM Na$_2$HPO$_4$ pH 8.0, 500 mM NaCl). All samples contain 250 mM NaCl from the starting condition. The best stabilization effect by KCl is seen for HEPES buffer (dark green columns). The values of the KCl-free buffer conditions from Stability and Solubility screen 1 were added to the graph to illustrate the effect of KCl on the stability of DYRK1B.

The results of Thermofluor of Stability and Solubility Screen 2 shown also that the addition KCl salt to MES pH 6.5 did not increasing the melting point of DYRK1B. In contrast, HEPES buffer pH 8.0 with different KCl concentrations increased the melting point by about 12.5℃ compared to the original phosphate buffer (**Figure 20**). DYRK1B wt is significantly more stable in every tested buffer than the buffer used so far for the purification. Since the first step of the purification is affinity chromatography which requires the (His)6-tag to be charged the HEPES buffer at pH 8 was finally chosen over the equally good MES buffer at pH 6.5.
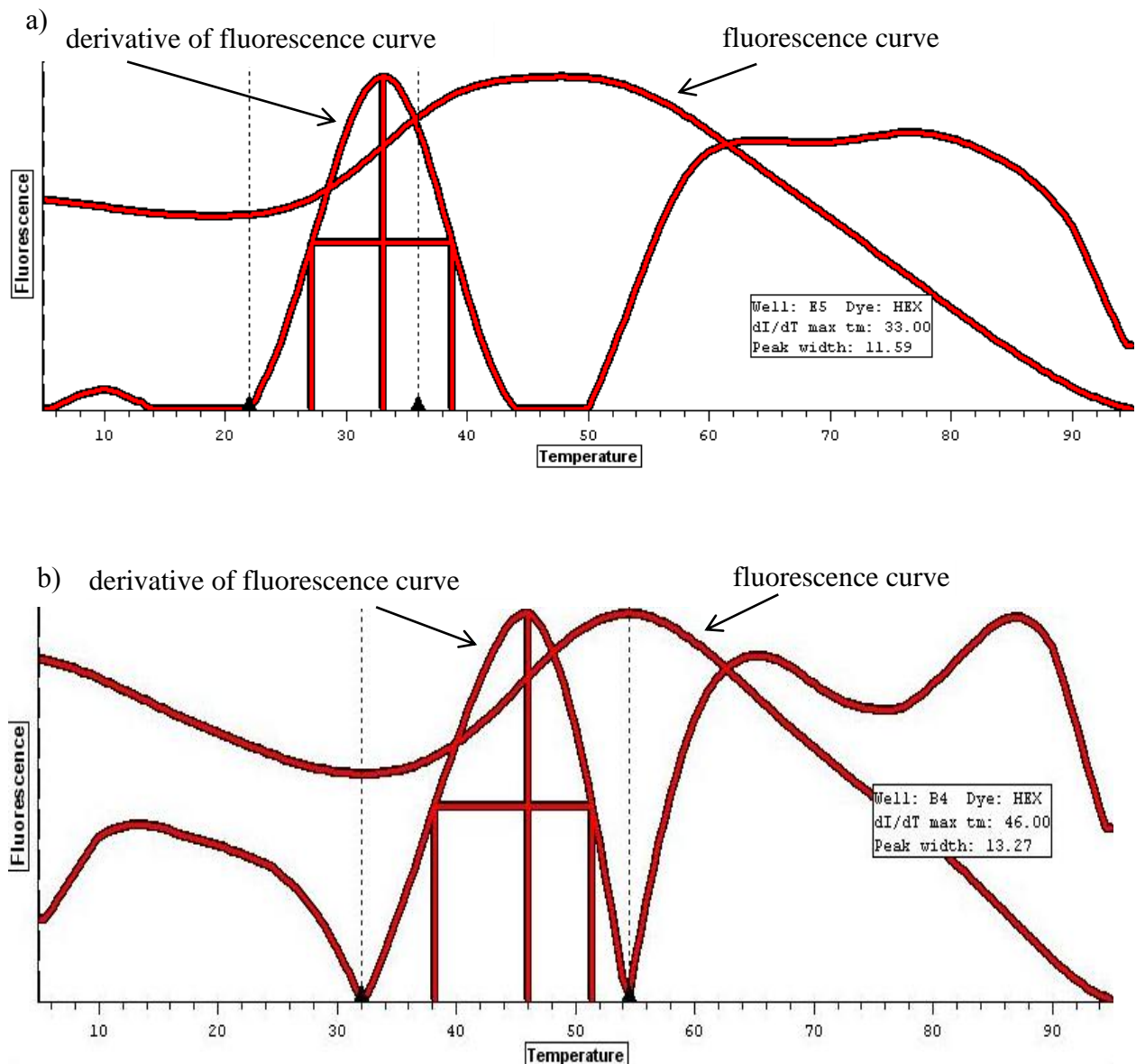
Figure 20. Comparison of thermoflour assay results of phosphate buffer pH 8.0 and HEPES buffer pH 8.0 with 50 mM KCl of Screen 2. Fluorescence on the Y-axis. Temperature in ℃ on the X-axis. a) Melting point of protein in Phosphate buffer pH 8.0 is 33℃. b) Melting point of DYRK1B wt in condition containing 50 mM HEPES buffer pH 8.0 and 50 mM KCl is 46℃. The figures were taken from program Opticon Monitor 3.

3.4 Purification of DYRK1B Q164K using HEPES buffer

The DYRK1B Q164K mutant was designed and produced for crystallization trials. DYRK1B Q164K was initially purified using the same protocol as for DYRK1B wt employing phosphate buffer. The use of phosphate buffer for purification of DYRK1B Q164K presented the same issues as for DYRK1B wt: low yield and solubility, weak binding to the HisTrap column and expression in inclusion bodies. The result of the Stability and Solubility screen 1 and 2 by thermofluor assay shows that the highest melting temperature for DYRK1B wt was a buffer containing 50 mM HEPES pH 8, 50 mM KCL and 250 mM NaCl. Large scale purification of DYRK1B Q164K was therefore tested in the new buffer because we were interested to produce this mutant at high yield, purity and solubility for crystallization trails.

Following the procedure described in the methods section, DYRK1B Q164K was purified in a similar way to DYRK1B wt with phosphate buffer, and for comparison with the HEPES buffer. The chromatogram of DYRK1B Q164K (**Figure 21, a**) and the following SDS-PAGE (**Figure 21, c**) represents the results of the affinity chromatography performed by HisTrap HP 5 ml column in phosphate buffer. To show the positive impact of HEPES buffer and for direct comparison to the phosphate the chromatogram (**Figure 21, b**) and SDS-PAGE (**Figure 21, d**) of DYRK1B Q164K are shown for the purification in HEPES buffer.

In the case of phosphate buffer, the flow-through and fractions 5, 15, 16, 18, 19, 21, 23, 24, 25 and 26 were selected to be analyzed by SDS-PAGE. The result of SDS-PAGE shows that DYRK1B Q164K is present in the fractions 21-26. The peak on the chromatogram with absorption of around 200 mAU corresponds to the DYRK1B Q164K. DYRK1B Q164K was eluted at around 60% of Buffer B (300 mM imidazole).

In the case of HEPES buffer, flow through and fractions 6, 19, 20, 22, 24, 25, 26, 27, 28 and 29 were selected for SDS-PAGE. The result of SDS-PAGE shows that fractions 19-28 contain the DYRK1B Q164K. These fractions correspond to a peak about 825 mAU in chromatogram which is significantly higher compared to the one with phosphate buffer. The maximum of DYRK1B Q164K was eluted by 55 % of buffer G (275 mM imidazole). Although it is poorly visible on the SDS-PAGE (**Figure 21, d**), the flow-through does not contain DYRK1B Q164K indicating a good binding of the protein to the column, and later experiments confirms that the protein in HEPES buffer binds better to the column compared with the phosphate buffer.

The comparison of the two chromatograms allows the conclusion that HEPES buffer has positive impact on the solubility, binding and yield of DYRK1B Q164K compared to phosphate buffer, which is in agreement with the thermofluor data.

In the case of the purification with phosphate buffer, fraction 22-30 were pooled together with TEV protease and dialyzed in buffer C to cleave the (His)6-tag o/n. In the case of HEPES buffer, fractions 22-34 were selected for TEV cleavage in buffer H o/n.

The second affinity chromatography step was carried out after TEV cleavage similar to the protocol for DYRK1B wt. The chromatogram of DYRK1B Q164K in phosphate buffer is depicted in the **Figure 22, a**. Fractions 6, 10, 17, 18, 19, 20, 21, 22, 24 26 were selected for SDS-PAGE (**Figure 22, c**). In the case with phosphate buffer, based on the SDS-PAGE the peak with the value around 280 mAU corresponds to the DYRK1B Q164K. The maximum of protein was eluted at 20% of elution buffer B (100 mM imidazole).

The chromatogram of DYRK1B Q164K in HEPES buffer is represented in the **Figure 22, b**. The fractions 2, 9, 10, 11, 12, 13, 14, 15, 18 and 20 were selected for SDS-PAGE (**Figure 22, d**). Based on the results of SDS-PAGE the main peak with a value of around 725 mAU corresponds to the DYRK1B Q164K. Protein was mostly eluted at 16 % of buffer F (80 mM imidazole). In both cases TEV cleavage was successful which is confirmed the size difference of cleaved and uncleaved samples on the SDS-PAGE (uc in the **Figure 22, c** and **d**).

In the last step of the purification, a gel filtration was performed using a HiLoad™ 16/60 Superdex™ 200 column. Buffer D was used as a gel filtration buffer in the protocol prior to the buffer optimization. The chromatogram of the gel filtration with buffer D is shown in **Figure 23, a.** Fractions 21, 27, 32, 34, 36, 37, 38, 40, 44 and 49 were selected for SDS-PAGE. The result of the SDS-page (**Figure 23, c**) shows that fractions 34-40 contain DYRK1B Q164K, therefore, the peak in the chromatogram with the value of 20 mAU corresponds to the DYRK1B Q164K mutant. The fractions 34-39 were pooled and the final concentration was 0.04 mg/ml in 12 ml measured by Nanodrop which is a final yield of 0.6 mg protein (0.15 mg of the protein per liter of media).
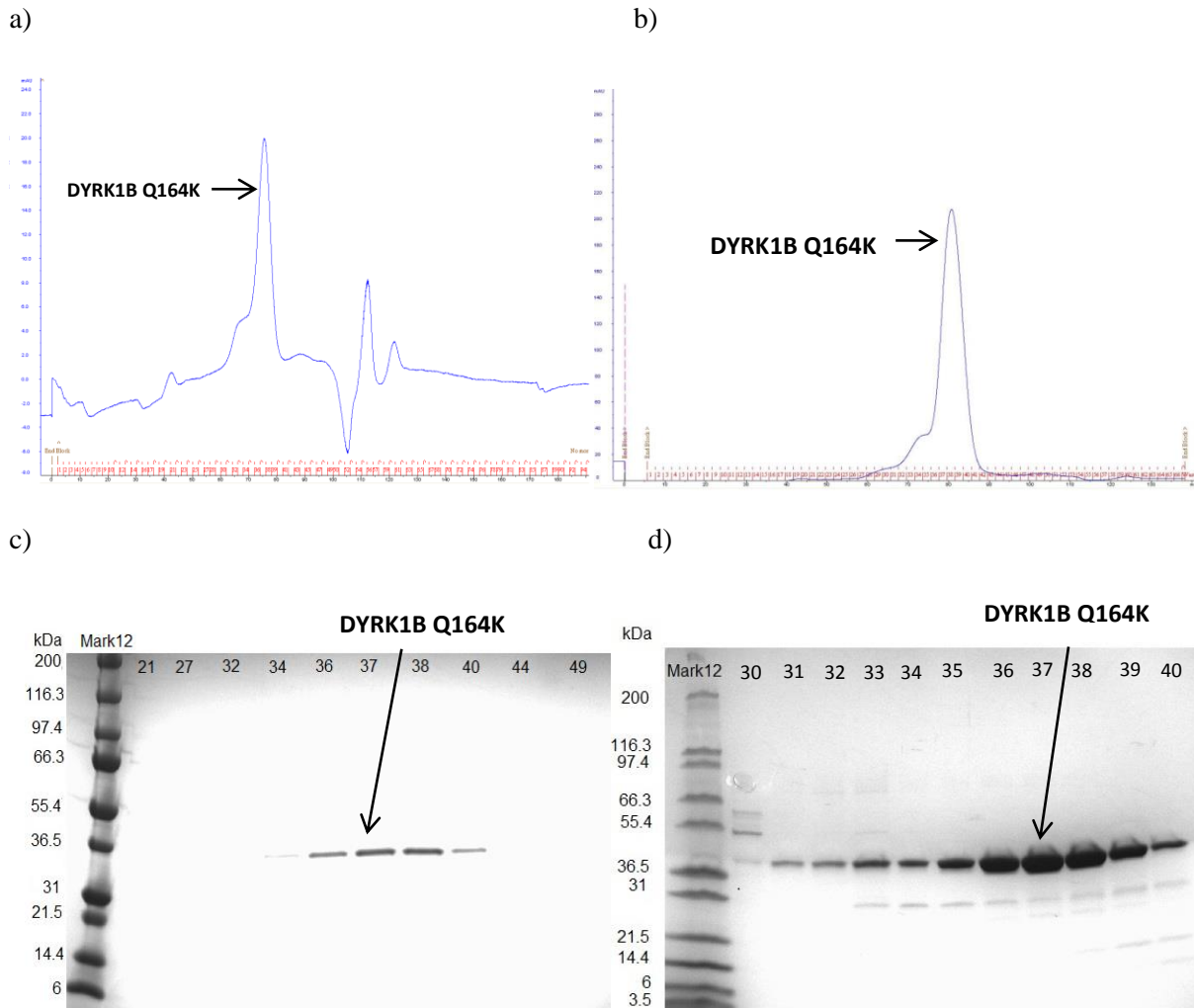
After buffer optimization, the gel filtration was performed using the buffer G as a gel filtration buffer. The chromatogram of the gel filtration is represented in the **Figure 23, b**. Fractions 30, 31, 33, 34, 35, 36, 37, 38, 39 and 40 were selected for SDS-PAGE. The results of SDS-PAGE are shown in the **Figure 23, d**. Fractions 30-40 contain DYRK1B Q164K. The peak in the chromatogram with the value of around 206 mAU corresponds to DYRK1B Q164K. The fractions 31-40 were pooled and final concentration was 0.43 mg/ml in 20 ml measured by Nanodrop which is a final yield of 8.6 mg protein (2.15 mg of the protein per liter of media).

Thus, buffer change from phosphate buffer to the HEPES buffer improved the yield of DYRK1B Q164K by more than 10 fold.

a)   b)

c)   d)
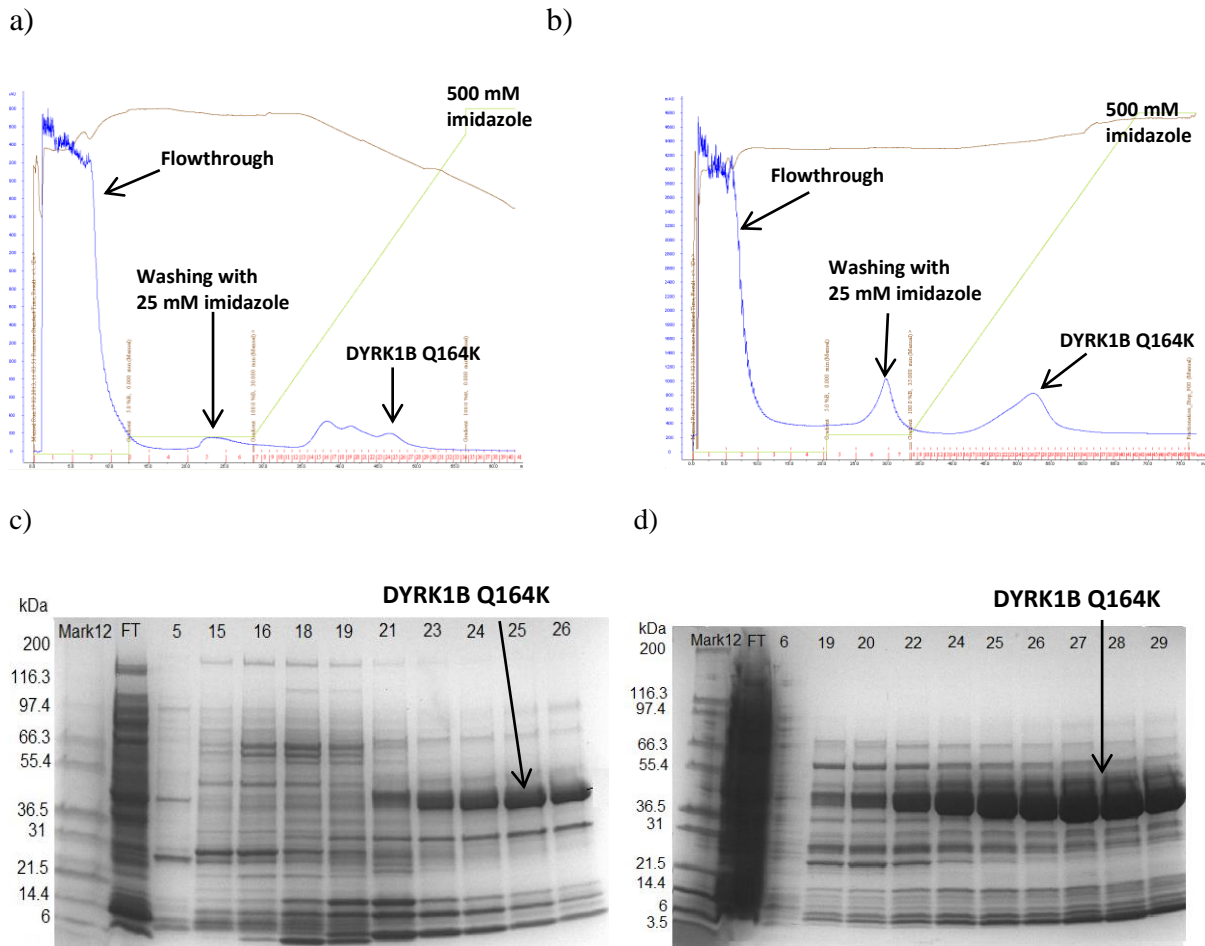
Figure 21. Purification of (His)6 - DYRK1B Q164K. a) The chromatogram shows the affinity purification of DYRK1B Q164K by HisTrap HP 5ml using phosphate buffer. b) The chromatogram shows the affinity purification of DYRK1B Q164K by HisTrap HP 5ml using HEPES buffer. The blue line is the absorbance at 280 nm, the green line is percentage of elution buffer B (0%-100% corresponds to 0-500 mM imidazole). Absorbance in mAU is shown on the Y-axis, min (blue) is shown under the X-axis. The number of fraction is shown above the X-axis. The red line is the conductivity. Different peaks in the chromatogram are depicted by arrows. The sample was loaded by a peristaltic pump prior to the purification with Äkta prime thus the chromatogram begins with the column wash step. b) SDS page of the selected fractions of DYRK1B Q164K in phosphate buffer. Fractions 21-26 contain DYRK1B Q164K. c) SDS page of the selected fractions of DYRK1B Q164K in phosphate buffer. Fractions 19-29 contain DYRK1B Q164K. Mark12 in lane 1 was used as marker; the numbers above the lanes represent the fractions. The bands located between 55.4 and 36.5 kDa corresponded to DYRK1B Q164K.
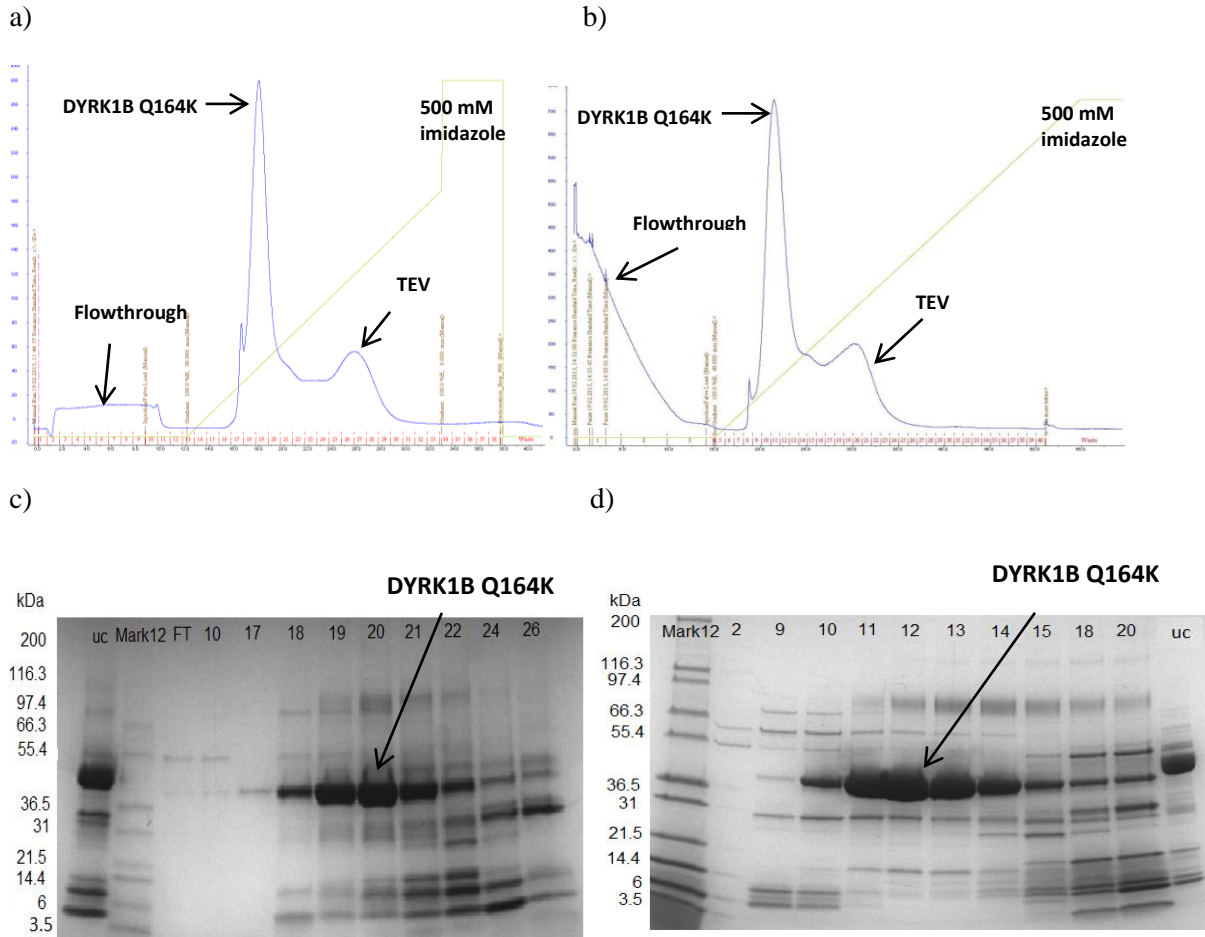
Figure 22. Purification of DYRK1B Q164K after TEV-cleavage. a) The chromatogram shows the affinity purification of DYRK1B Q164K by HisTrap HP 1ml column using phosphate buffer. b) The chromatogram shows the affinity purification of DYRK1B Q164K by HisTrap HP 1ml column using HEPES buffer. The blue line is the absorbance at 280 nm, the green line is percentage of elution buffer (0%-100% corresponds to 0-500 mM imidazole). Absorbance in mAU is shown on the Y-axis, min (blue) is shown under the X-axis. The number of fraction is shown above the X-axis. The red line is the conductivity. Different peaks in the chromatogram are depicted by arrows. The sample was loaded by a peristaltic pump prior to the purification with Äkta prime thus the chromatogram begins with the column wash step. b) SDS page of the selected fractions of DYRK1B Q164K in phosphate buffer. Fractions 18-22 contain DYRK1B Q164K. c) SDS page of the selected fractions of DYRK1B Q164K in HEPES buffer. Fractions 10-15 contain DYRK1B Q164K. Mark12 in lane 1 was used as marker; the numbers above the lanes represent the fractions. The bands located between 55.4 and 36.5 kDa corresponded to DYRK1B Q164K.

a)

DYRK1B Q164K →

b)

DYRK1B Q164K →

c)

DYRK1B Q164K

kDa Mark12   21 27 32 34 36 37 38 40 44 49
200
116.3
97.4
66.3
55.4
36.5
31
21.5
14.4
6

d)

DYRK1B Q164K

kDa
       Mark12 30 31 32 33 34 35 36 37 38 39 40
200
116.3
97.4
66.3
55.4
36.5
31
21.5
14.4
6
3.5

Figure 23. Gel filtration(size-exclusion chromatography) of DYRK1B Q164K. a) The chromatogram shows the purification of DYRK1B Q164K by HiLoad™ 16/60 Superdex™ 200 column using buffer D (before the buffer optimization). b) The chromatogram shows the purification of DYRK1B Q164K by HiLoad™ 16/60 Superdex™ 200 column using buffer G (optimized buffer). Flow rate was 1 ml/min. Fraction size was 2 ml. DYRK1B Q164K peak in the chromatogram are depicted by arrow. The Blue line is the absorbance at 280 nm. b) SDS page of the selected DYRK1B Q164K fractions of the chromatogram in the buffer D. Fractions 34-40 contain DYRK1B Q164K. c) SDS page of the selected DYRK1B Q164K fractions of the chromatogram in the buffer G. Fractions 31-40 contain DYRK1B Q164K. Mark12 in lane 1 was used as marker, the numbers above the lanes represent the fractions, Fraction 35-41 contain DYRK1B Q164K.

3.5 Purification of DYRK1B L192M

The transformation, expression and purification protocol of DYRK1B L192M mutants was similar to those described for DYRK1B wt and DYRK1B Q164K. DYRK1B L192M mutant was expressed in 2l of TB media. Äkta prime plus FPLC system was employed to perform the affinity chromatography with HisTrap HP 5ml column. Buffer E was used as a binding buffer and protein was eluted by gradient of elution buffer G with the length of 8 CV and target concentration of buffer F 500 mM imidazole. The chromatogram of DYRK1B L192M purification is represented in **Figure 24, a**. Flow through and fractions 14, 16, 17, 18, 20, 22, 25, 26, 27, 28, 29, 30 and 32 were selected for SDS-PAGE. The result of SDS-PAGE gel is shown in the **Figure 24, b**. Fractions 25-32 contain DYRK1B L192M. DYRK1B L192M had a peak with the value of 250 mAU and eluted at 65 % of buffer F corresponding to the 325 mM of imidazole. Based on the chromatogram and SDS-page the fractions 25-34 were pooled, mixed with TEV protease dialyzed in the buffer G o/n. The TEV cleavage was followed by a second affinity chromatography step using a HisTrap HP 1 ml column. The chromatogram is shown in **Figure 25**, a. Buffer E and buffer F were used as binding and elution buffers, respectively. Flow through and fractions 12, 13, 14, 15, 16, 17, 18, 19, 20 and 21 were run on SDS-PAGE, represented in **Figure 25, b**. The peak on the chromatogram around 146 mAU and 34% of buffer F (170 mM imidazole) corresponds to the DYRK1B L192M confirmed by SDS-PAGE. The TEV cleavage was successfully executed since the bands from uncleaved fraction (uc on the SDS-PAGE figure) and band with cleaved DYRK1B L192M have different sizes that can be clearly seen on the SDS-PAGE figure. Fractions 11-15 were pooled together to continue the purification of the kinase by gel filtration. Gel filtration was the last step in purification protocol of DYRK1B L192M. The gel filtration was performed as previously described for DYRK1B wt and Q164K mutant. β-ME has a short half-life of 8.5 h[131] and has to be added fresh to the gel filtration buffer. However, the fresh β-ME was not added to the gel filtration buffer G while performing the last purification step of L192M. The chromatogram of gel filtration of DYRK1B L192M is shown in the **Figure 26, a**. There are three peaks in the chromatogram. The SDS-PAGE (**Figure 26, b)** shows that the first peak does not contain L192M mutant, but two other peaks contain the L192M mutant. Comparison with a molecular weight standard for the gel filtration column identifies these two peaks as a monomer and dimer of DYRK1B. This was further verified by mass spectrometry were samples from both peaks were identified as DYRK1B. The fractions 34-44 were pooled and the final concentration was 0.06 mg/ml in 22 ml measured by Nanodrop which is a final yield of 1.32 mg protein.
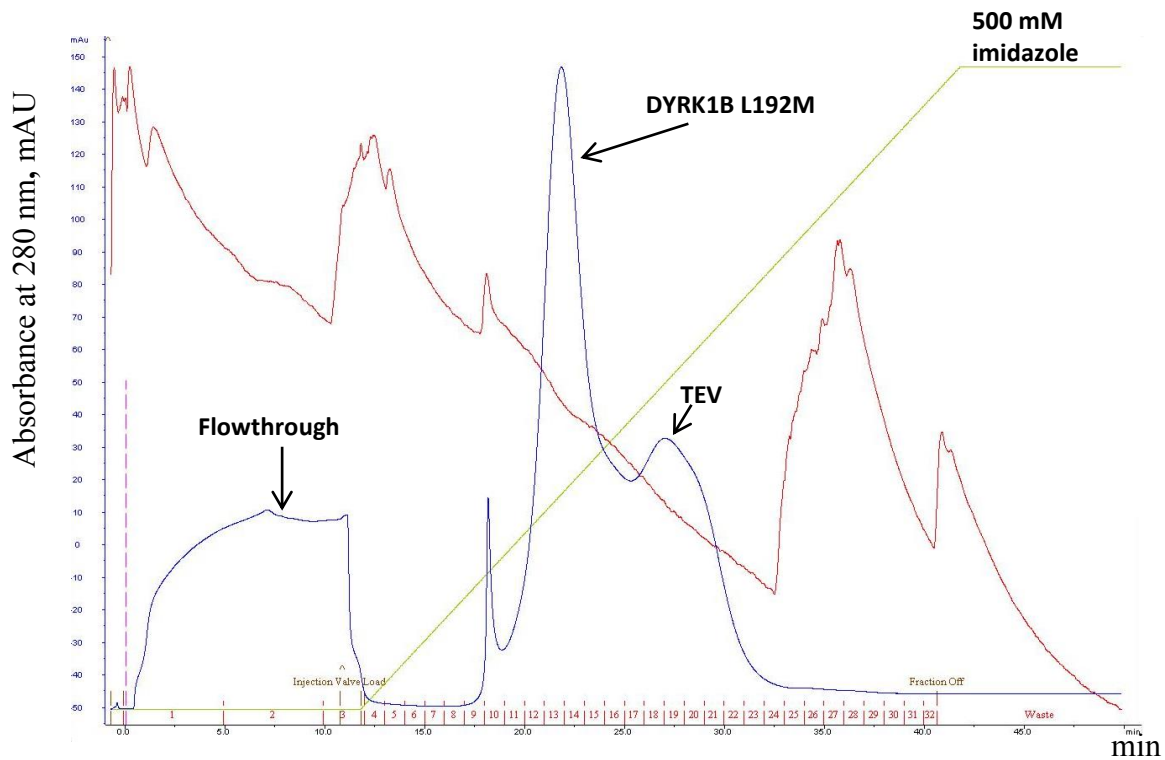
a)
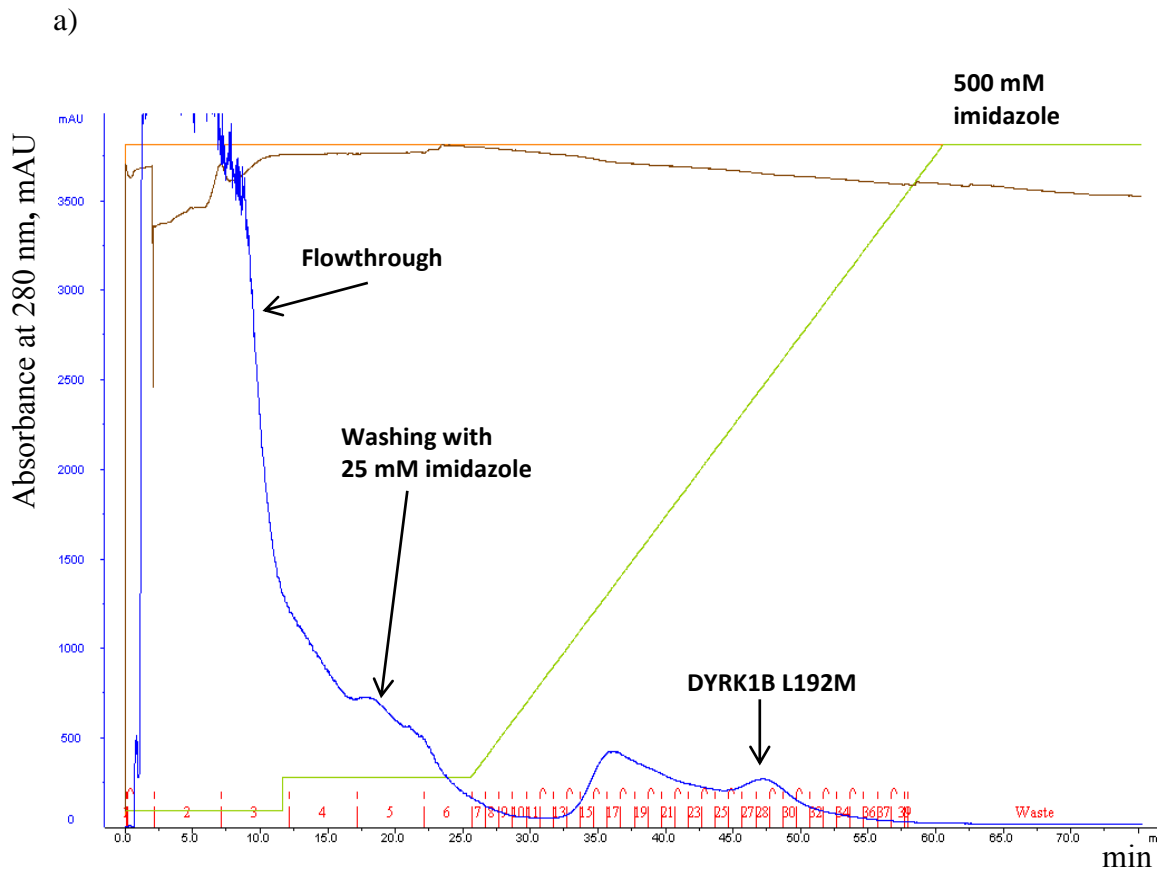
b)
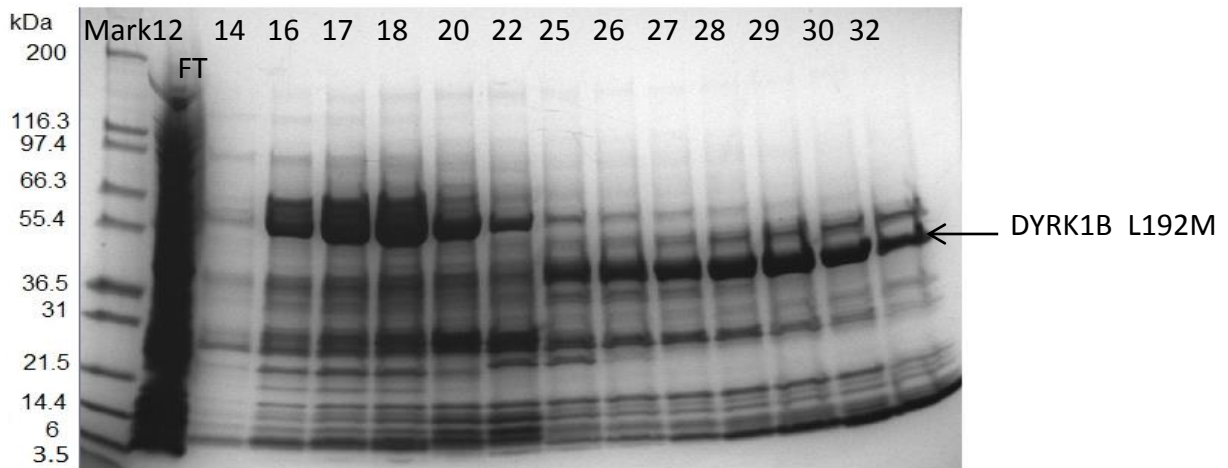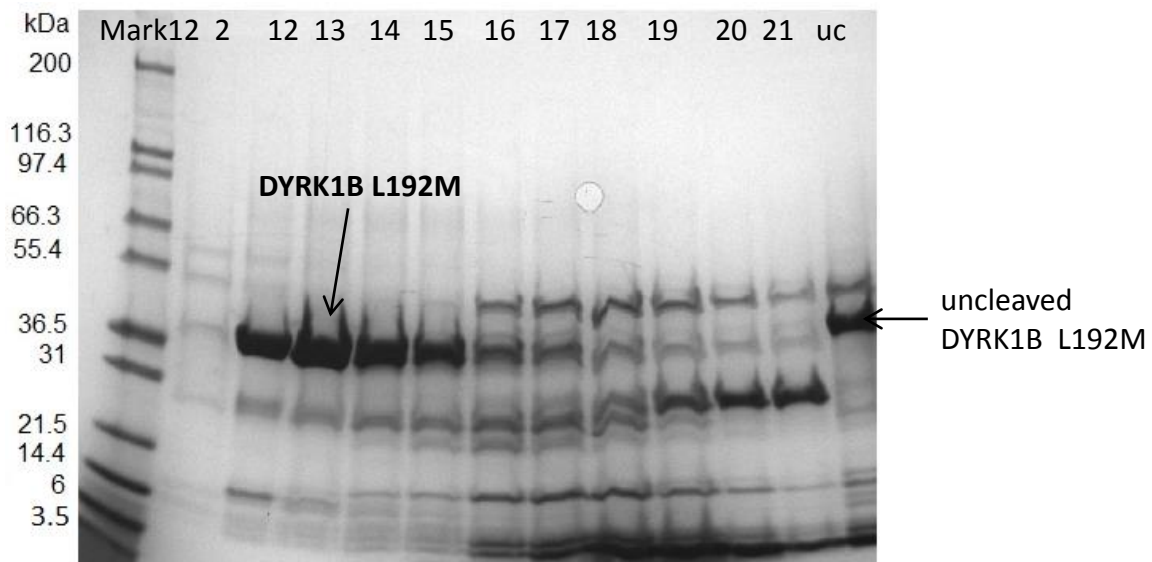

Figure 24. Purification of (His)6 -DYRK1B L192M. a) The chromatogram shows the affinity purification of DYRK1B L192M by HisTrap HP 5ml column. The blue line is the absorbance at 280 nm, the green line is percentage of elution buffer F (0%-100% corresponds to 0-500 mM imidazole). The red line is the conductivity. Different peaks in the chromatogram are depicted by arrows. The sample was loaded by a peristaltic pump prior to the purification with Äkta prime thus the chromatogram begins with the column wash step. b) SDS page of the selected fractions of the chromatogram. Mark12 in lane 1 was used as marker; the numbers above the lanes represent the fractions. Fractions 30-38 contain DYRK1B L192M. The bands located between 55.4 and 36.5 kDa corresponded to DYRK1B L192M.

a)

b)

Figure 25. Purification of DYRK1B L192M after TEV-cleavage. a) The chromatogram shows the affinity purification of DYRK1B L192M by HisTrap HP 1ml column. The blue line is the absorbance at 280 nm, the green line is percentage of elution buffer F (0%-100% corresponds to 0-500 mM imidazole). Different peaks in the chromatogram are depicted by arrows. The red line is the conductometry. DYRK1B L192M elutes at imidazole concentration of approximately 170 mM. b) SDS page of the selected fractions of the chromatogram. Mark12 in lane 1 was used as marker, the numbers above the lanes represent the fractions, uc (uncleaved) is a sample form the first HisTrap and contains DYRK1B with a uncleaved (His)6-tag. Fractions 12-15 contain DYRK1B L192M.

a)
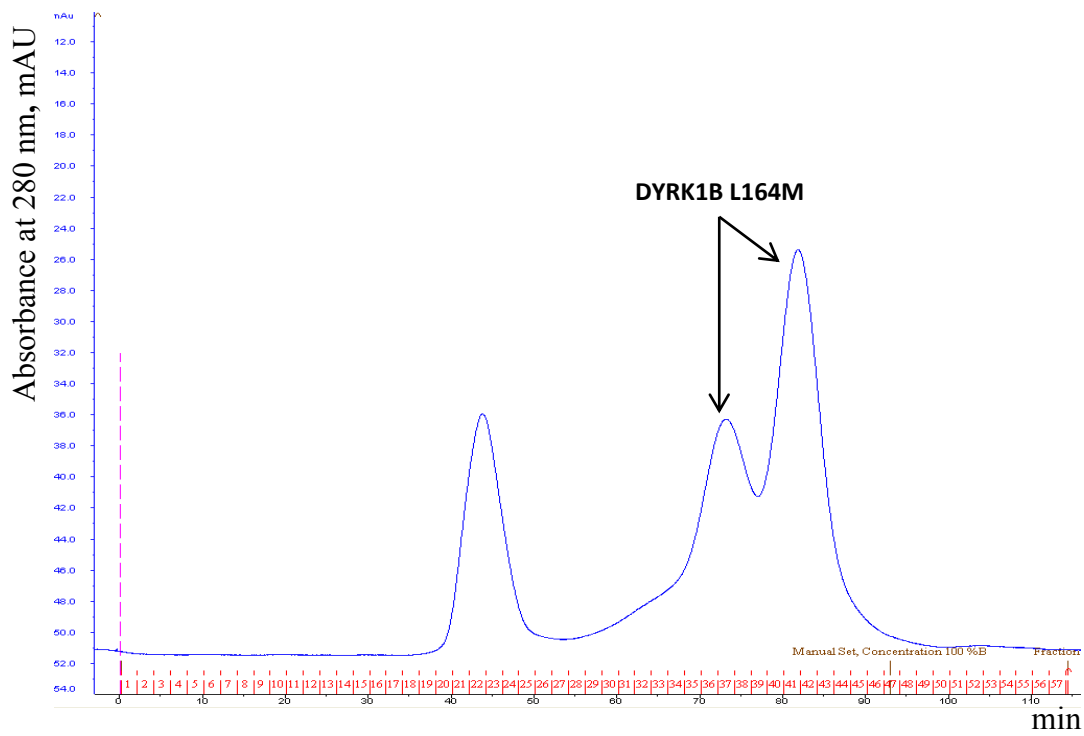
b)
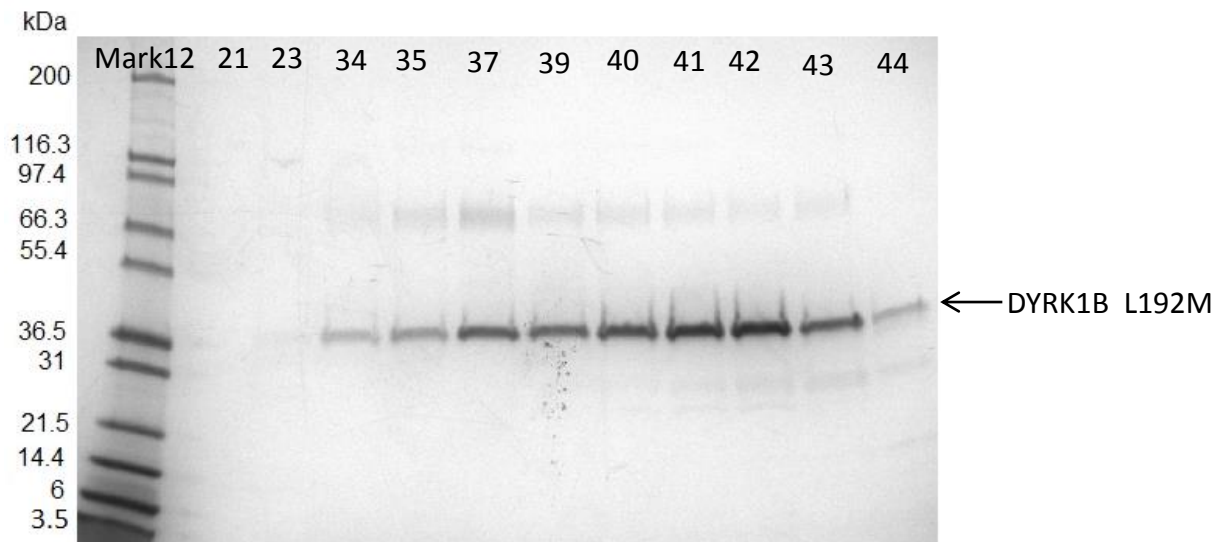
Figure 26. Gel filtration of DYRK1B L192M. a) Gel filtration (size-exclusion chromatography) was performed by HiLoad™ 16/60 Superdex™ 200 column. Flow rate was 1 ml/min. Fraction size was 2 ml. DYRK1B L192M peakes in the chromatogram are depicted by arrow. The blue line is the absorbance at 280 nm. b) SDS page of the selected fractions of the chromatogram. Mark12 in lane 1 was used as marker, the numbers above the lanes represent the fractions. Fraction 32-44 contain DYRK1B L192M.

3.6 DYRK1B C238R purification

DYRK1Q C238R possesses the mutation in the catalytic motif HCD. The transformation of the plasmid was performed following the protocol of DYRK1B wt. Buffer A was used as a binding buffer and buffer B was used as elution buffer because expression of C238R mutant was done before buffer optimization. The C238R mutant was expressed in 2 L of TB media. HisTrap HP 5 ml column was used for affinity chromatography. The chromatogram of the first purification step is shown on the **Figure 27, a**. Fractions 1, 5, 20, 25, 28, 30, 32, 34, 35, 37 and 40 were selected for SDS-PAGE. Based on the SDS PAGE picture the fractions 28-40 contain C238R mutant (**Figure 27, b**). DYRK1B C238R peak in the chromatogram corresponds to the value of 65 mAU and 66% of elution buffer B (330 mM imidazole). Fractions 30-40 were pooled together. Unfortunately the low yield of protein after purification made it impossible to further purify this mutant. The band was cut out from the gel and sent to the mass spectrometry facilities for verification.

Mass spectrometry indicates that majority of protein is not phosphorylated at YQY motif. The kinase was tested for an activity by the Cook assay. The C238R mutant was not active. However, the amount of the kinase might have been too low and the presence of imidazole in the elution buffer the kinase was in might have also inhibited its activity.

a)
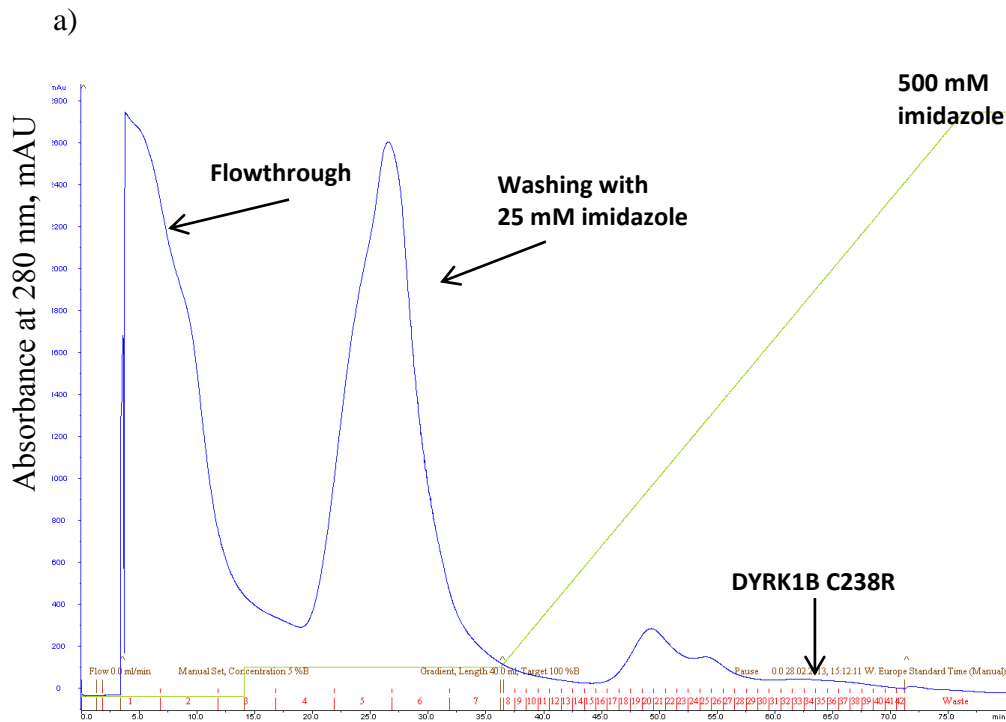
b)
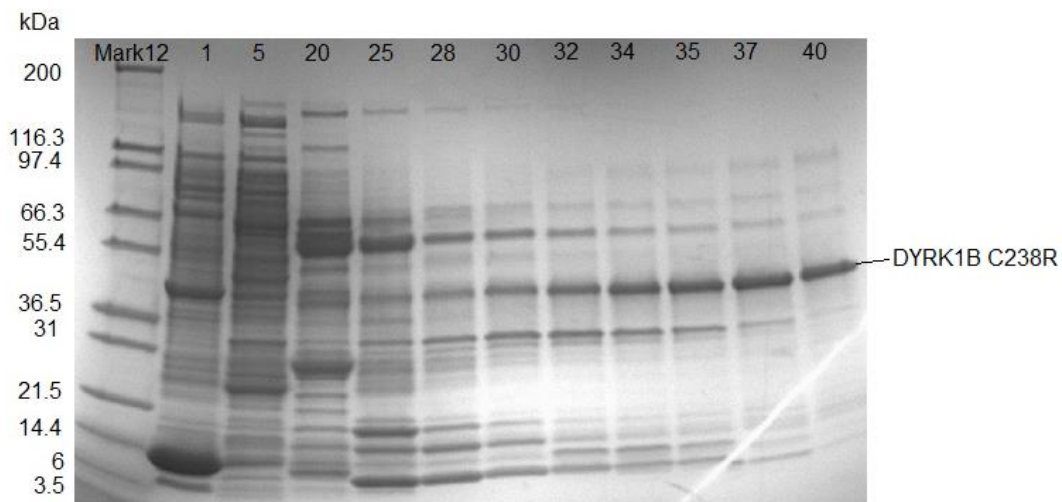
Figure 27. Purification of (His)6 -DYRK1B C238R. a) The chromatogram shows the affinity purification of DYRK1B C238R by HisTrap HP 5ml column. The blue line is the absorbance at 280 nm, the green line is percentage of elution buffer B (0%-100% corresponds to 0-500 mM imidazole). The red line is the conductivity. Different peaks in the chromatogram are depicted by arrows. The sample was loaded by a peristaltic pump prior to the purification with Äkta prime thus the chromatogram begins with the column wash step. b) SDS page of the selected fractions of the chromatogram. Mark12 in lane 1 was used as marker; the numbers above the lanes represent the fractions. Fractions 32-40 contain DYRk1B C238R. The bands located between 55.4 and 36.5 kDa corresponded to DYRK1B C238R.

3.7 Inhibitor screen by the Cook assay

Harmine and 49 inhibitors provided by a private pharmaceutical company were tested for DYRK1A and DYRK1B wt. The inhibitor screen was performed by an activity-based ATP-regenerative NADH-consuming assay (Cook assay[77]). Routinely, a "quick" screen for the best inhibitors was performed by testing the inhibitors at concentration of 20 µM in the reaction mixture with 256 µM of ATP. In the screen the inhibitors were compared according to the remaining activity of the kinases. The remaining activity was calculated in percentage by dividing the value of the negative slope of the kinase with inhibitor by the negative slope of kinase without inhibitor. The results of the inhibitor screen for the 50 inhibitors sorted by their rank for DYRK1A wt and DYRK1B wt are summarized in **Table 7** (a bar chart of the 50 inhibitors sorted by remaining activity of DYRK1B is shown in the Appendix).

Table 7. Comparison of inhibitors for DYRK1A wt, DYRK1B wt. *Data for DYRK1A were kindly provided by Dr. Ulli Rothweiler.

DYRK1A wt*			Dyrk1B wt		
Rank	Inhibitor number	Remaining activity, %	Rank	Inhibitor number	Remaining activity, %
1	harmine	0	1	Inh 47	6.0
2	Inh 07	0	2	harmine	12.4
3	Inh 14	0	3	Inh 04	13.9
4	Inh 31	1.6	4	Inh 41	17.0
5	Inh 12	2.9	5	Inh 27	19.9
6	Inh 47	9.3	6	Inh 45	20.1
7	Inh 32	9.9	7	Inh 31	21.9
8	Inh 45	13.9	8	Inh 07	25.2
9	Inh 04	14.9	9	Inh 12	25.8
10	Inh 02	16.2	10	Inh 48	25.9
11	Inh 09	19.6	11	Inh 14	30.6
12	Inh 08	20.3	12	Inh 08	33.9
13	Inh 27	23.8	13	Inh 02	36.2
14	Inh 41	24.6	14	Inh 25	38.2
15	Inh 42	31.3	15	Inh 32	40.2
16	Inh 03	34.2	16	Inh 33	42.3
17	Inh 30	34.5	17	Inh 26	48.7
18	Inh 21	34.5	18	Inh 42	49.5
19	Inh 33	37.5	19	Inh 39	51.9
20	Inh 25	41.9	20	Inh 49	52.6
21	Inh 22	42.9	21	Inh 22	56.5
22	Inh 01	45.5	22	Inh 03	59.9
23	Inh 48	46.9	23	Inh 15	60.8
24	Inh 35	52.0	24	Inh 44	61.3
25	Inh 50	52.1	25	Inh 50	67.3
26	Inh 39	55.0	26	Inh 09	68.4
27	Inh 29	57.0	27	Inh 36	68.7
28	Inh 49	57.7	28	Inh 13	69.4
29	Inh 24	61.9	29	Inh 11	73.1
30	Inh 10	64.5	30	Inh 43	74.7
31	Inh 17	65.6	31	Inh 01	76.3
32	Inh 13	66.1	32	Inh 23	75.1
33	Inh 36	66.3	33	Inh 40	79.0
34	Inh 44	67.2	34	Inh 20	81.1
35	Inh 26	70.4	35	Inh 37	81.3
36	Inh 28	73.2	36	Inh 35	81.9
37	Inh 11	74.9	37	Inh 38	83,3
38	Inh 43	75.2	38	Inh 06	85.5
39	Inh 20	76.2	39	Inh 34	88.1
40	Inh 06	76.9	40	Inh 30	88.2
41	Inh 18	79.1	41	Inh 05	89.7
42	Inh 15	79.9	42	Inh 21	91.0
43	Inh 23	80.0	43	Inh 18	93.8
44	Inh 38	82.1	44	Inh 19	94.2
45	Inh 40	83.0	45	Inh 24	97.1
46	Inh 19	84.0	46	Inh 28	97.3
47	Inh 37	85.4	47	Inh 17	97.9
48	Inh 34	90.0	48	Inh 29	99.0
49	Inh 05	92.5	49	Inh 46	100.0
50	Inh 46	94.3	50	Inh 10	100.0

In order to investigate the effect of mutation in the hinge region to the binding with inhibitors the DYRK1B L192M mutant was tested with the 5 best inhibitors of DYRK1A wt and DYRK1B wt at the same assay conditions (**Table 8**).

Table 8. Result of testing the inhibitors for DYRK1B L192M.

DYRK1B L192M		
Rank	Inhibitor number	Remaining activity,%
1	harmine	3.6
2	Inh 7	6.4
3	Inh 47	8.4
4	Inh 31	10.3
5	Inh 14	14.6
6	Inh 4	14.6
7	Inh 12	15.0
8	Inh 27	15.3
9	Inh 41	30.3

The results comparing the effects of inhibitors on mutant of DYRK1B are summarized in **Table 9** and **Figure 28**. Most of the inhibitors (5 out of 9) inhibit DYRK1A wt better than DYRK1B wt with the L192M mutant in between. Two inhibitors follow no clear trend. Two inhibitors did not distinguish between the three DYRKs and showed the same inhibition towards the kinases.

Table 9. Comparison of remaining activity for DYRK1B wt and L192M mutant with DYRK1A wt. (Values in % of remaining activity).

Inhibitor number	Remaining activity of DYRK1A, %	Remaining activity of DYRK1B L192M, %	Remaining activity DYRK1B wt, %
Inhibitors better for DYRK1A wt			
Harmine	0	3.8	6
Inh 07	0	6.4	25.2
Inh 14	0	14.6	30.6
Inh 31	1.8	10.3	21
Inh 12	2.9	15.3	25.8
Inhibitors without any trends			
Inh 41	24.6	30.3	17
Inh 27	23.8	15.3	19.9
Inhibitor that does not distinguish between the DYRKs			
Inh 04	14.9	13.9	14.6
Inh 47	9.3	8.4	6.0
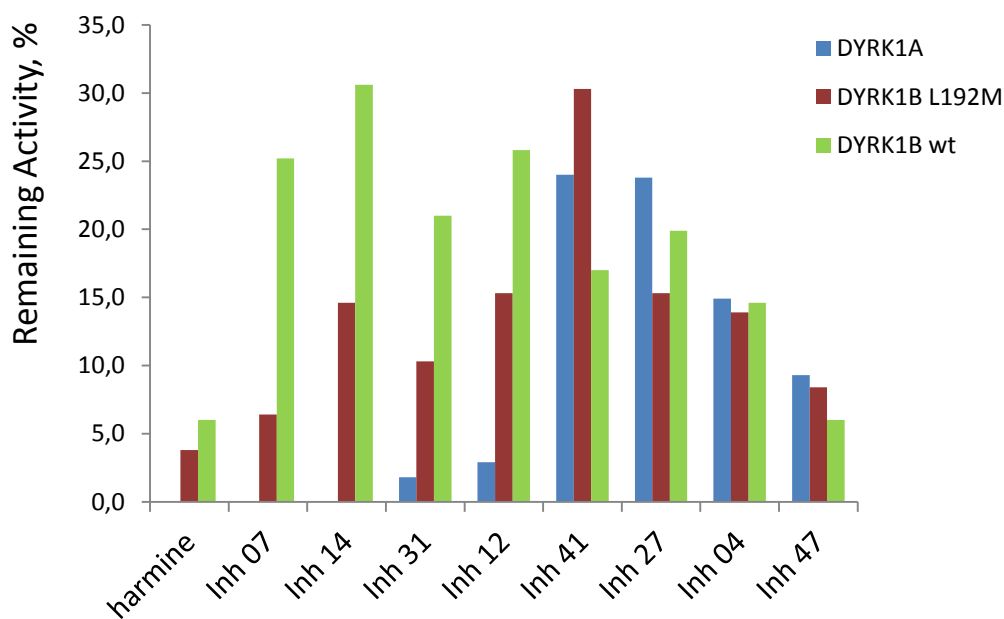
Figure 28. The comparison of remaining activity of inhibitors between DYRK1A (blue), DYRK1B wt (green) and DYRK1B L192M (red).

3.8 Enzyme kinetics of DYRK1B wt, DYRK1B L192M and DYRK1A.

The inhibitors tested are designed to be ATP-competitive. In order to calculate the Ki value (equation (1)) for the inhibitors we need to study enzyme kinetics and determine K_m value, i.e. Michaelis-Menten constant for ATP, for each kinase of interest. The K_m value describes how strongly the ATP binds to the kinases. To determine the K_m value, a serial of ATP concentrations were used in the Cook assay to measure the reaction velocity. The experiments were performed in triplicate with each dilution of ATP in the range from 50 mM to 4 µM. The data were analyzed by GraphPad software (**Figure 29)** and summarized in the **Table 10**.
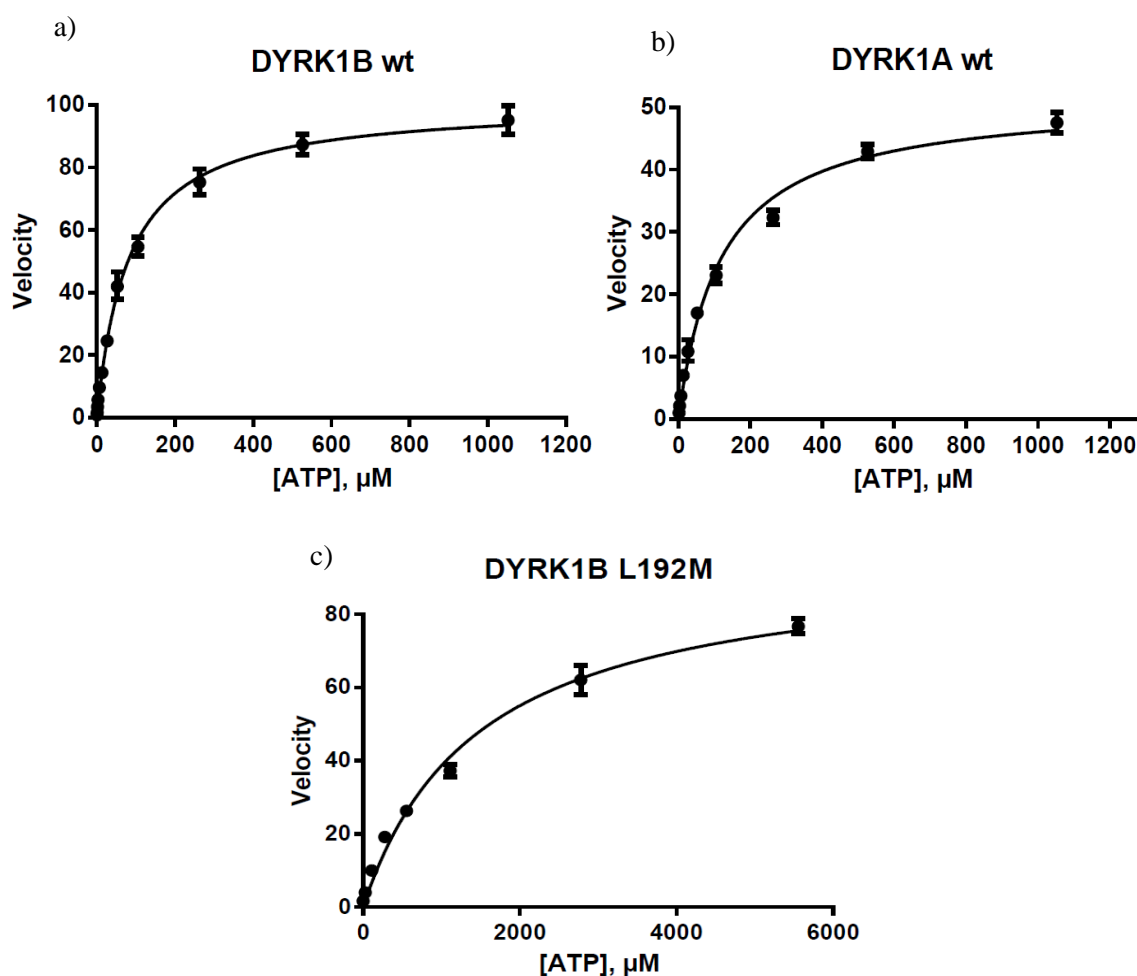
Figure 29. Michaelis-Menten plots. a) DYRK 1B wt, b) DYRK1A wt, c) DYRK1B L192M

Table 10. K_m values for DYRK A wt, DYRK1B wt and DYRK1B L192M

Kinase	K_m, µM	Vmax, AU/sec
DYRK1A wt	118.5 ± 7.8 µM	51.5 ± 1.0
DYRK1B wt	80.7 ± 2.7 µM	100.7 ± 0.9
DYRK1B L192M	1400 ± 300 µM	95.5 ± 3.4

The experimental data allow the conclusion that all three kinases have different affinities for ATP. To be exact, DYRK1B wt has highest affinity to ATP based on the lowest value of K_m compared to DYRK1A wt and DYRK1B L192M. DYRK1B L192M mutant has a significantly higher K_m value compared to the wt kinases. If correct, it may indicate that other factors in spite of the mutation in the hinge region have a greater influence to the binding affinity of ATP than the simple sequence alignment of DYRK1A and DYRK1B would have suggested.

3.9 Ki determination for kinase inhibitors.

The screening of inhibitors was performed to determine the strongest inhibitors from the set of 50 inhibitors at a fixed concentration. Based on the results of the screening, inhibitors which showed the lowest remaining activity were selected for a more precise determination of the inhibition potency. For this purpose the Cook assay was employed for some selected inhibitors in serial dilutions (concentration in a range from 20 µM to 4 nM) enabling IC_{50} value determination followed by a Ki calculation using the Cheng-Prusoff equation (1). Routinely, assay trials with all kinases were performed at ATP concentrations of 128 or 256 µM and kinase concentrations in a range between 0.05 and 0.2 µM in order to obtain a negative slope value of around -10 AU/s. Measurements were performed in triplicate for each of the inhibitor concentrations. It was decided to select Inh 04, Inh 07, Inh 14, Inh 47 and harmine for IC_{50} determination and Ki calculation (**Figure 30**).
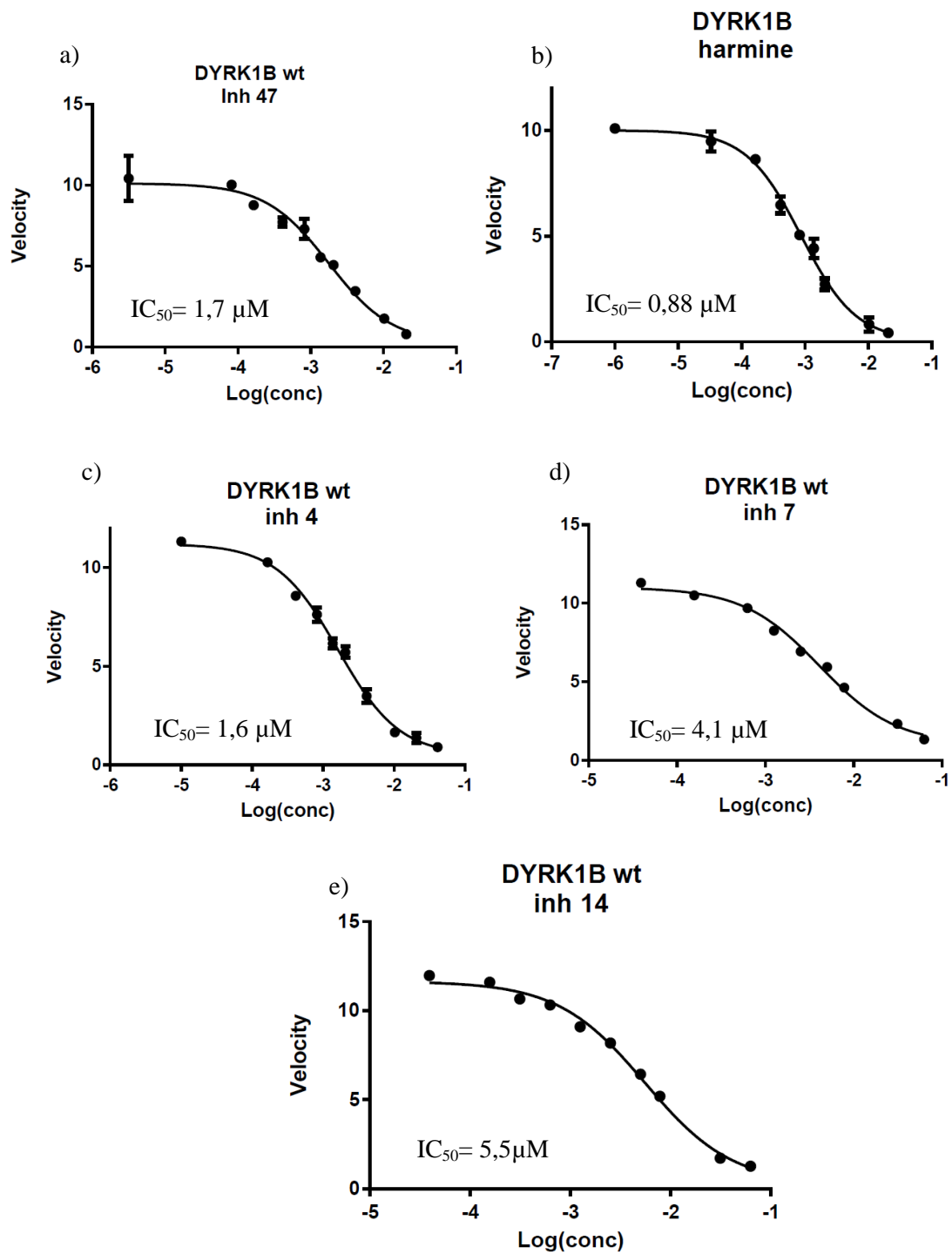
Figure 30. Dose-response curve of IC_{50} determination. DYRK1B wt. a) Inh 47, b) harmine, c) Inh 04, d) Inh 07, e) Inh 14.

In order to compare the effect of mutation on the binding with the inhibitor harmine was selected for DYRK1B L192M to determine the IC_{50} value (**Figure 31**).
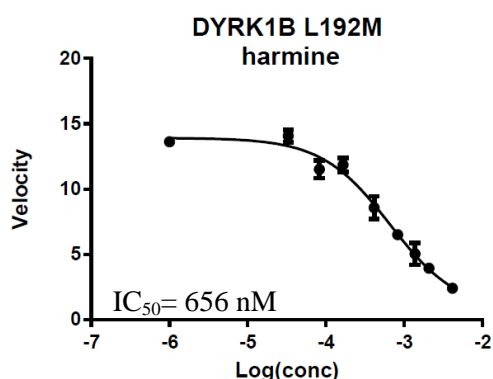
Figure 31. Dose-response curve of IC_{50} determination for DYRK1B L192M with harmine.

The inhibitor PKC412 was discovered from the crystallization trial for DYRK1A wt with commercially available inhibitors. The binding strength of PKC412 was determined for DYRK1A wt, DYRK1B wt and DYRK1B L192M mutant. The dose-response curves for PKC412 for all three targets are represented on the **Figure 32.**
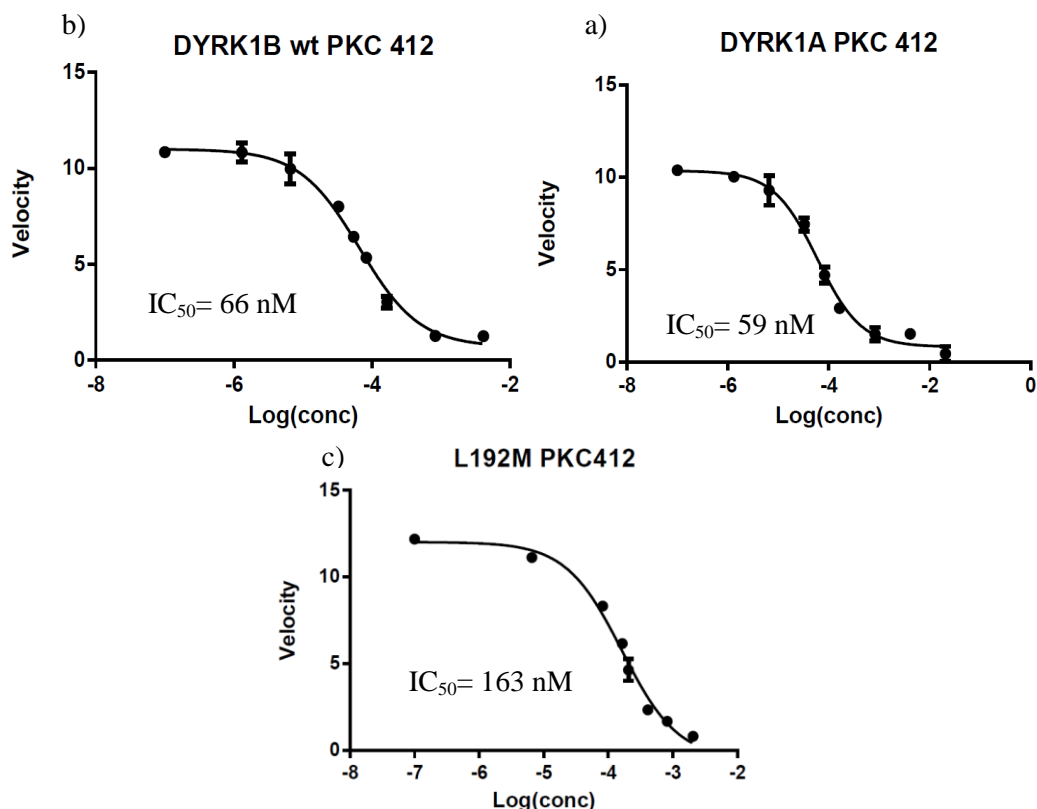
Figure 32. Dose-response curve for PKC412 inhibitor, a) DYRK1A wt, b) DYRK1B wt, c) DYRK1B L192M. Data for DYRK1A was kindly provided by Dr. Ulli Rothweiler.

The Ki value was calculating using the equation (1) using ATP concentrarion and K_m value. The IC_{50} value and calculated Ki for inhibitors and DYRKs were summurized in the **Table 11**.

Table 11. IC_{50} value and Ki for inhibitors and kinases DYRK1A wt, DYRK1B wt and L192M mutant.

Kinase	Inhibitor	ATP, µM	IC_{50}, nM	Ki, nM
DYRK1A wt	PKC412	128	59	28.4
DYRK1B wt	PKC412	128	66	25.4
DYRK1B L192M	PKC412	128	163	149.4
DYRK1B wt	harmine	128	876	337.2
DYRK1B L192M	harmine	128	656	601.1
DYRK1B wt	Inh 4	128	1624	624.6
DYRK1B wt	Inh 7	256	4108	978.1
DYRK1B wt	Inh 14	256	5549	1321.2
DYRK1B wt	Inh 47	128	1780	684.6

The Ki values are indicators for the potency of an inhibitor. A smaller value of Ki indicates a stronger inhibition. The Ki calculation shows that the best inhibitor for DYRK1B wt was the commercial inhibitor PKC412. On the second place is the inhibitor harmine. The inhibitors from the private pharmaceutical company, Inh 04 and 47, were the best from the set of 50 inhibitors, however, they are two times weaker than harmine and 25 times weaker than PKC412. The DYRK1B L192M has around 6 time higher Ki value for PKC412 compared to DYRK1B wt and DYRK1A wt. The comparison of the Ki value for harmine between the DYRK1B wt and DYRK1B L192M shows that the Ki value of DYRK1B L192M is also two times higher than for DYRK1B wt. If correct, this is mainly due to the significant higher K_m value for DYRK1B L192M compared to DYRK1A and DYRK1B wt. The IC_{50} values for the inhibitor harmine are with 876 nM (DYRK1B) and 656 nM (DYRK1B L192M) in the same magnitude with a slight advantage for DYRK1B L192M.

3.10 Microscale thermophoresis

The microscale thermophoresis was used to determine a Kd value of ATP towards the DYRK1B wt. 16 capillaries with the serial twofold dilutions of ATP, constant buffer concentration and concentration of DYRK1B were employed during the experiment. An affinity of 78 μM could be derived (**Figure 33**).
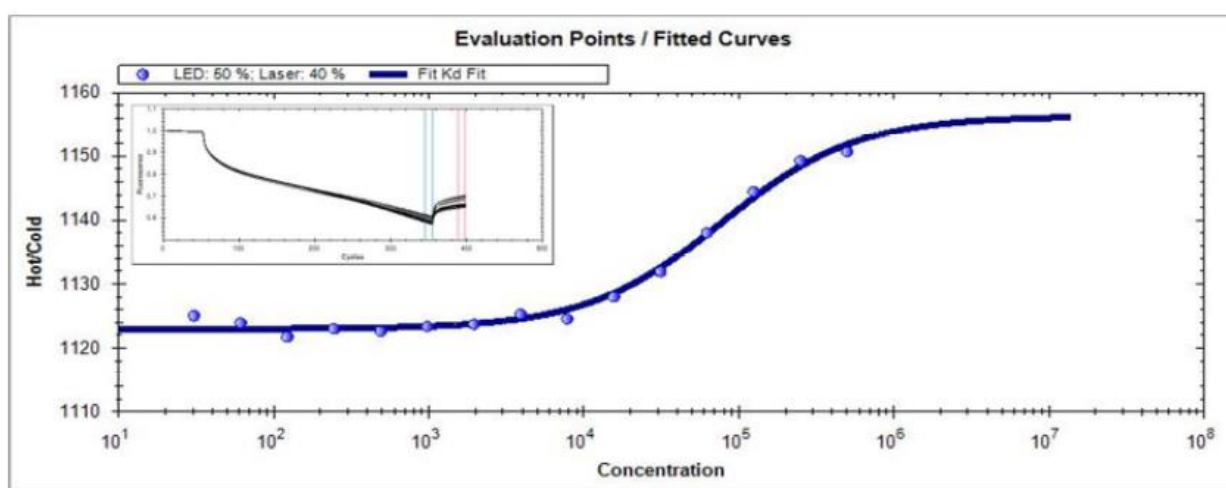
Figure 33. Microscale thermophoresis traces and back diffusion analysis of the interaction between DYRK1B wt and ATP.

3.11 Crystallization of DYRK1B wt and DYRK1B Q164K

DYRK1B wt and DYRK1B Q164K were obtained in large enough amounts to proceed with crystallization trials either as apo-proteins, or in complex with inhibitors selected from the inhibitor kinase activity screen: either commercially available inhibitors, or inhibitors from the company. The commercially available crystallization screens (e.g. JCSG plus, Wizard) were employed to screen for crystallization conditions at different concentrations of protein, temperatures and ratios of protein solution to reservoir solution. The promising hits from the crystallizations screen were chosen for further optimizations but, unfortunately, the control tests, (when the protein solution was excluded from the crystallization experiment), showed that the inhibitors themselves crystallized under these selected conditions, even at low concentration (around 400 μM), and therefore gave false positive hits. One condition from the in-house KCSG crystallization screen (comprising 2 M ammonium sulfate, 0.1 M sodium cacodylate pH 6.5 and 0.2 M sodium chloride) gave small plates of crystals. These crystals were sent to the synchrotron

76

for data collection but the first diffraction image contained only a few strong diffraction spots that indicate the crystallization of a small molecule, most probably the inhibitor. Unfortunately neither DYRK1B wt nor DYRK1B Q164K obtained for the crystallization trials crystallized - neither as an apo-protein nor in the complex with inhibitors (commercial available or from the kinase inhibitor screen).

3.12 Crystallization of DYRK1A

Repeating the published crystallization conditions for DYRK1A did not give crystals with the company's inhibitor. Therefore a JCSG-plus™ screen was used in a co-crystallization trial with DYRK1A and inhibitor 4. The screen gave a hit containing 0.2 M NaSCN and 20% PEG 3350. This condition was used for optimization with gradient of 16-25% PEG 3350 and 0.1-0.3 M KSCN or NaSCN. The condition with 16% PEG 3350 with 0.1 M KSCN gave the best hits and was chosen to run an additive screen, which gave hits with 0.1 M NaCl, 0.1 M KCl, 0.1 M LiCl and to minor extent with other salts of alkali halide.

The hits from additives were added to the crystallization screens. The trials were performed at room temperature and 4℃. However, it was observed that at room temperature the crystal grows larger, so it was decided to continue to crystallize the protein at the room temperature. The final crystallization condition for DYRK1A with PKC412 that gave the best crystal, was 100 mM KSCN, 50 mM LiCl, 10-16 % PEG3350. For the crystallization by hanging drop, the protein/inhibitor mixture was then mixed 1:1 with the crystallization solution. Octahedral crystals appeared within 5 days at the room temperature (**Figure 34**). The data collection showed that a suitable cryoprotectant was 30% ethylene glycol, while N-paratone did not cryoprotect the crystals and the crystals did not diffract.
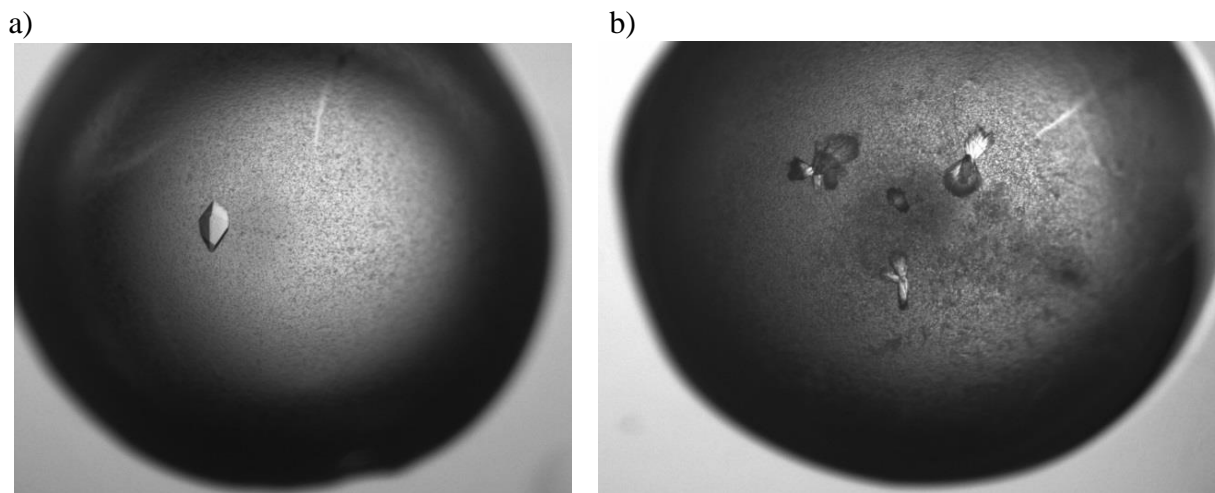
Figure 34. Crystal of DYRK1A in complex with PKC412. a) octahedral form of crystal, b) bundle of parallel twisted crystals.

First two diffraction images were taken at 90 degree apart to determine the space group and strategy of data collection (**Figure 35**). The crystal diffracted to 2.6 Å and the diffraction data was integrated by XDSapp to calculate the structural factors and convert them in a *.mtz file. The structure was solved by molecular replacement method in Molrep, refined by Refmac5 (CCP4 package) and Phenix. The crystallographic data and model statistics are summarized in the **Table 12**.
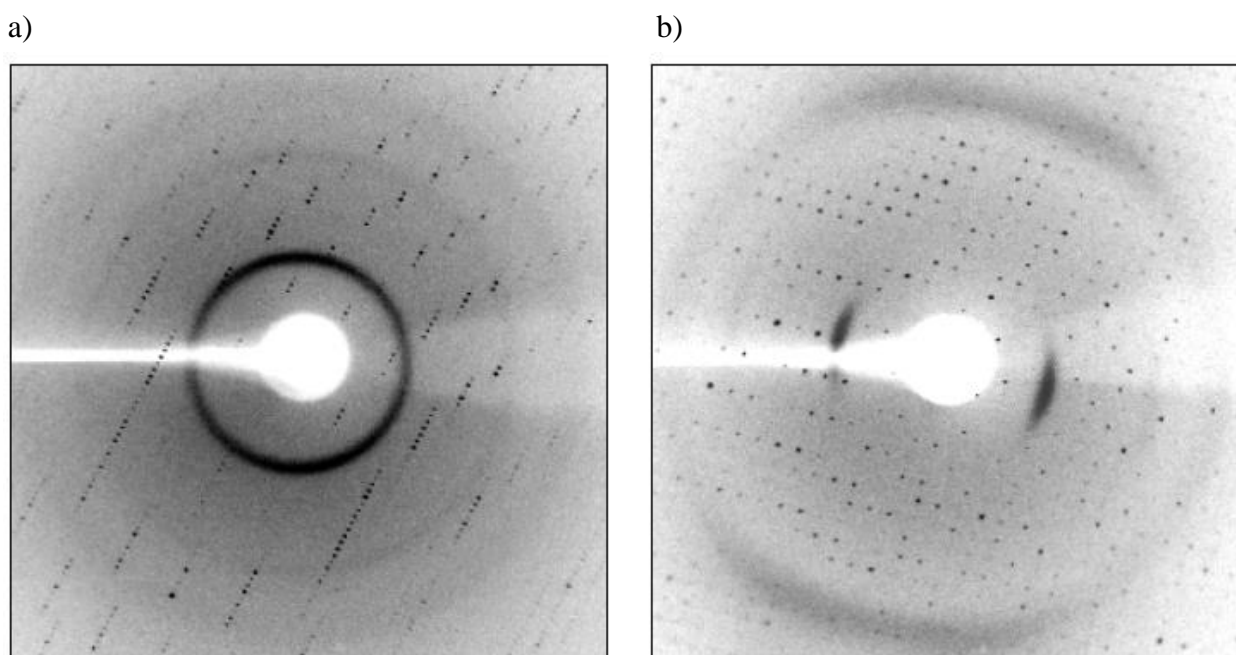
Figure 35. Diffraction images of DYRK1A in complex with the inhibitor PKC412. a) ω is 0°,1° oscillation, b) ω is 90°, 1° oscillation.

The crystal structure contains one DYRK1A tetramer as an asymmetric unit with the four individual DYRK1A molecules related to each other by three perpendicular twofold rotation axes, as it was previously described in the DYRK1A structures 3ANQ and 3ANR[16] (**Figure 36**).
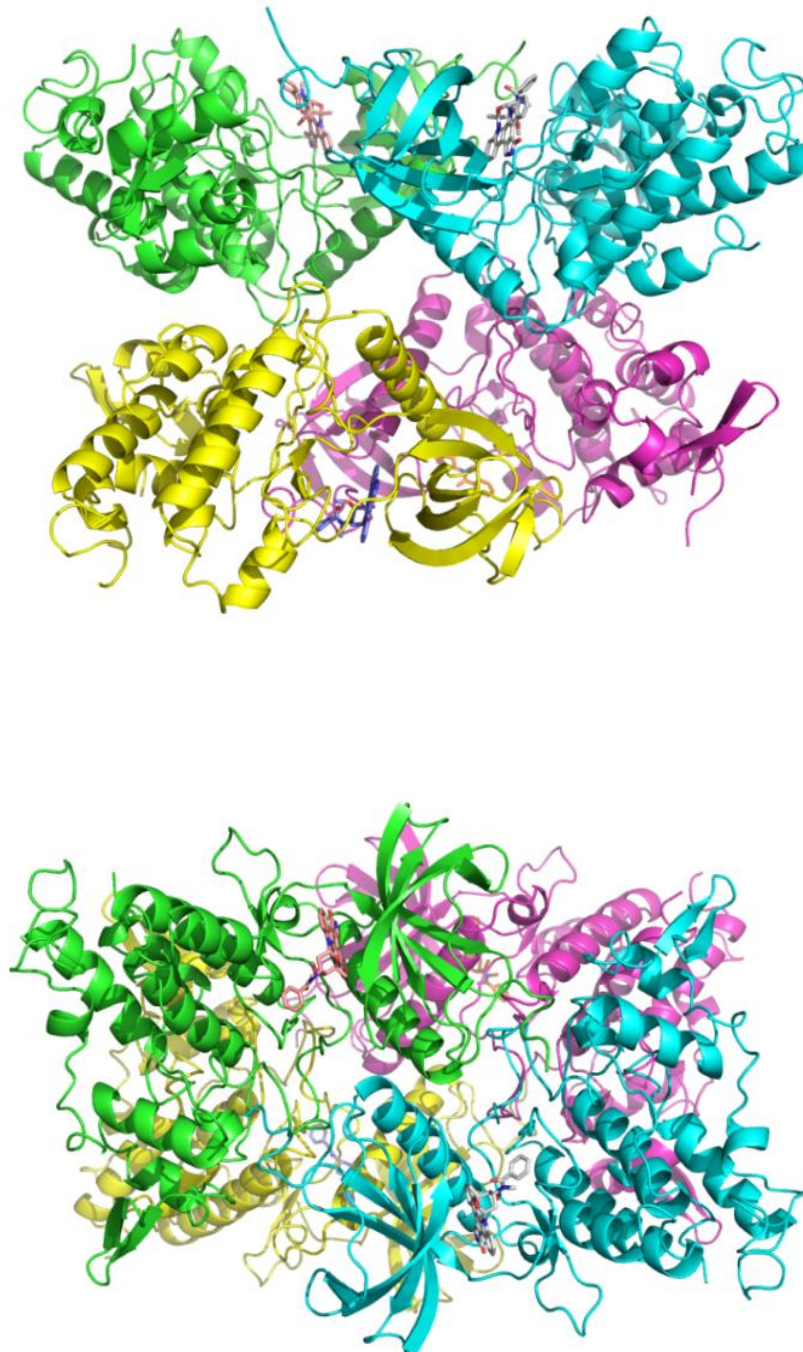
Figure 36. The asymmetric unit comprising of four individual DYRK1A molecules at 2.6 Å resolution

Table 12. Crystallographic data and model statistics.

DATA COLLECTION	
Synchrotron radiation	BESSY II 14.1
Detector	Pilatus 6M
Wavelength, Å	0.918409
Number of crystals used	1
Number of frames	360
Oscillation range / frame	$0.5°$
DIFFRACTION DATA	
Space group	$P2_12_12_1$ (19)
Unit cell parameters, Å	87.76, 87.90, 229.92
Protein molecules in asymmetric unit	4
Number of measurements	359740
Unique reflections	55625
Resolution Range, Å (final shell)	48.251-2.597 (2.664-2.597)
Completeness (final shell)	99.6 (98.6)
Mosaicity	$0.236°$
I/σ (final shell)	9.10 (1.89)
REFINEMENT	
Resolution limits, Å (final shell)	48.251-2.597 (2.664-2.597)
Number of used reflections	52841
Percentage observed	99.7 %
Percentage of free reflections	5.0 %
Number of protein atoms	11036
Number of heterogen atoms	176
Number of water	223
R factor overall/free	20.76 % / 24.76 %
Overall figure of merit	0.871
RMS bonds/angles	0.0064 Å / $1.292°$
Ramachandran (favored / allowed / outliers)	94.86 % / 5.14 % / 0 % [*]

[*]calculated by Molprobity: www.molprobity.biochem.duke.edu/index.phd

The DYRK1A kinase domain follows the same structural arrangement as the other known DYRK1A structures[16,53,132] with the typical kinase fold and the tyrosine Y321 is phosphorylated in the structure (**Figure 37**).

a)   b)
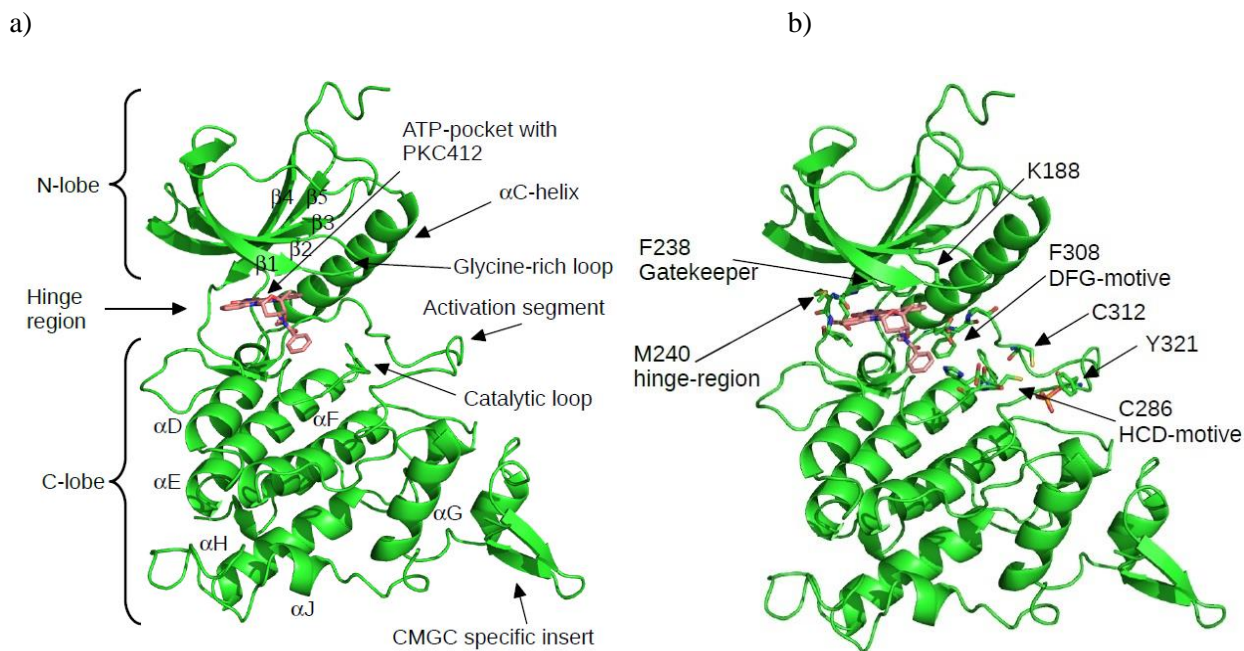
Figure 37. The overview of DYRK1A in the complex with PKC412. a) Overview over the structural elements b) key motifs and residues of the kinase.

PKC412 is clearly visible in the electron density map and with an exception of the phenyl ring, the coverage is nearly complete (**Figure 38**). PKC412 is bound to the ATP pocket via two hydrogen bonds made by the amine and ketone group in the 2-one-3-pyrroline head group of PKC412 to the hinge amino acids E239 and L241. Due to a lack of any hydrogen acceptor or donor on the other side of the PKC412, there is no interference with the catalytic lysine K188 as described in previous DYRK1A/inhibitor structures[16] and the main binding of PKC412 is via hydrophobic interaction (**Figure 39**).
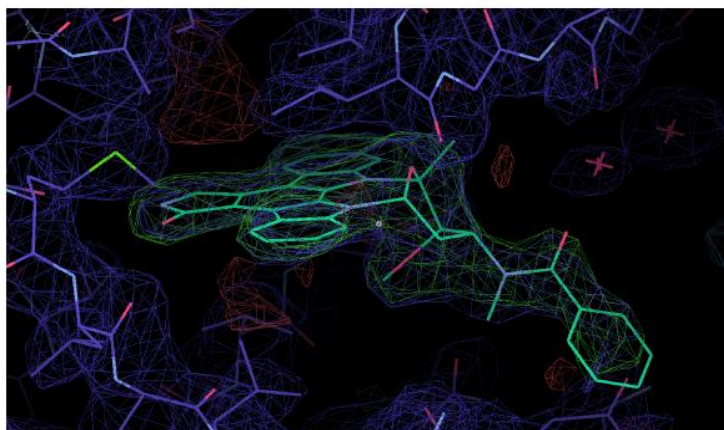
Figure 38. Binding of PKC412 to DYRK1A. The omit map (without PKC412) calculated shows the electron density coverage for PKC412. The DYRK1A and PKC412 molecule represented in stick are after final refinement.
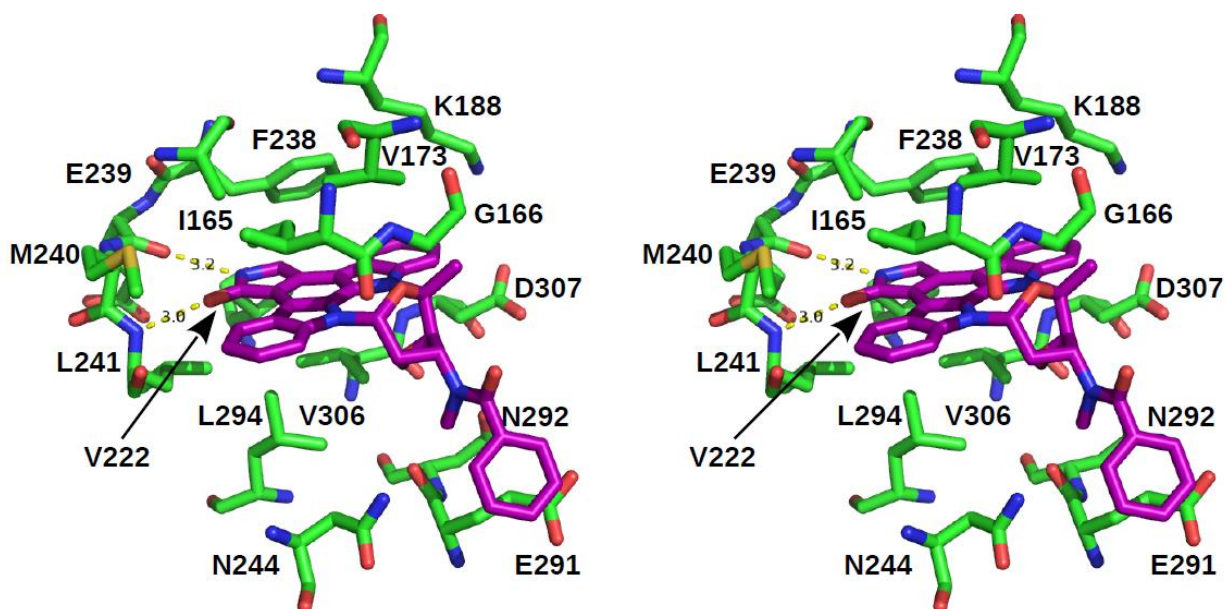
Figure 39. Stereo image of PKC412 bound to DYRK1A. Hydrogen bonds are made to the backbone atoms of E239 and L241. However most of the interactions are via hydrophobic residues. The catalytic Lysine K188 does not participate in the binding of PKC412.

The four individual chains in the asymmetric unit are not identical and differ slightly from each other. In all, chain A has the best density fit and is the most complete chain. The three other chains have a lower density fit, especially in the CMGC insert. The chain A has no density in the loop AA 409-412, chain B has missing residues AA 213-218 and AA 407-414. Chain C has a gap between AA 408-412 and chain D has missing residues AA 408-414 and AA 437-444. One feature of the structure described here that distinguishes it from the previous DYRK1A crystal structures is the existence of disulfide bridges formed between cysteine C286 of the HCD motive in the catalytic loop and cysteine C312 in the activation segment. These disulfide bridges are present in all the four monomers in the asymmetric unit. The distances between the two cysteines

after refinement in chain A, B, C and D are with ~2.06 Å in an ideal distance for disulfide bridges. The previously published structure 2VX3[53] with an open conformation has a cysteine-cysteine distance of ~4.3Å. The formation of the disulfide bridge does not have an obvious visible major impact on the structure. A superposition of chain A of our structure with chain A from 2VX3 does not show any large changes in the structure caused by the disulfide bridge, nor does the disulfide bridge interfere with the binding of PKC412. However, it locks the activation segment making the loop more rigid (**Figure 40)** by pulling residue C312 towards the catalytic motif HCD. The activation loop is differently folded after the C312, however this part of the DYRK1A kinase is flexible and the activation segment adopts different conformations based on the crystal packing. In comparison of 4NCT with 2VX3 the loop differs due to a difference in crystal packing (C2 symmetry). The structures with INDY and harmine 3ANQ and 3ANR have the same crystal packing (P212121) and have identical loop conformation like 4NCT. Since the disulfide bridge is also missing in these two structures, the local folding around C312 differs too compared to 4NCT. The HCD motive is rather rigid and does not move upon the disulfide bridge formation.
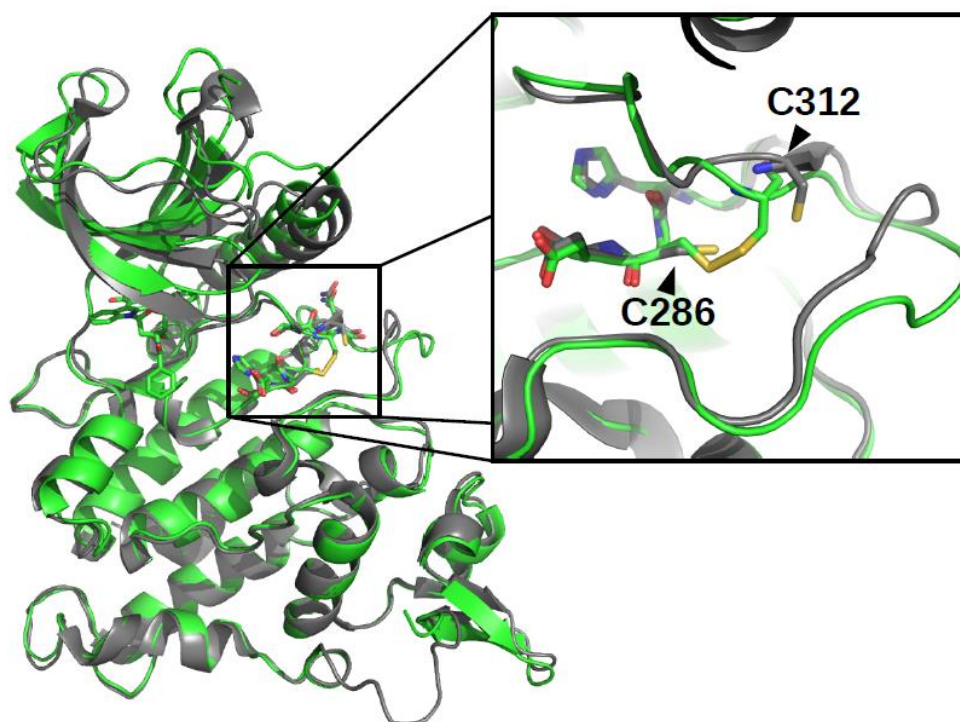
Figure 40. Structure of DYRK1A in the complex with PKC412 (green) is superimposed with DYRK1A (2VX3, grey). In the box is shown a close up picture; the disulfide bridge is formed between C286 and C312 in the DYRK1A in complex with PKC412 (green), but is absent in the 2VX3 structure (grey).

The formation of the disulfide bridge has however a local effect on the hydrogen network between the catalytic loop residues I^{283}IHCD^{287} and the activation segment D^{307}FGSSCQ^{313}. The hydrogen bond between the backbone carbonyl of I284 and the backbone amid C312 keeps the

same length (so the angle changes, **Figure 41**), however the hydrogen bond between the backbone amide I284 to backbone carbonyl C312 gets stretched by ~18% from 2.8 Å to 3.3 Å and in the case of the hydrogen bond between the backbone carbonyl H285 and the backbone amide S311 the distance increase is ~20% from 3.5 Å to 4.2 Å indicating that this hydrogen bond is practically non-existent in the structure with the disulfide bridge.
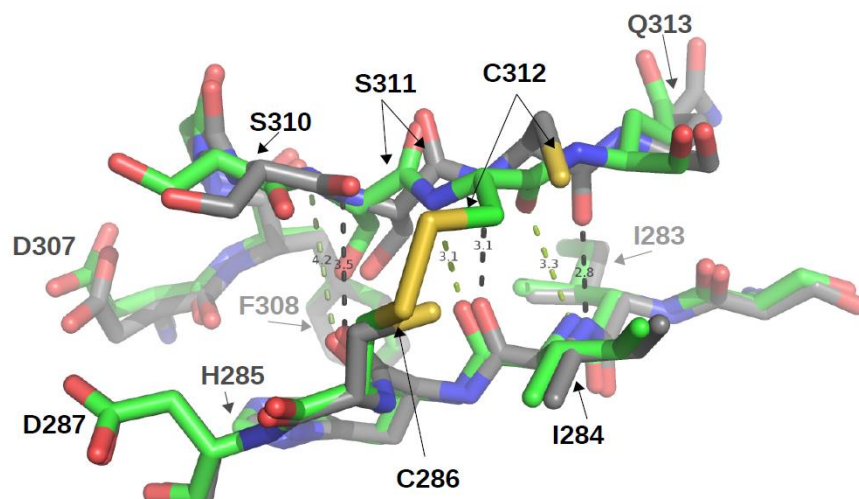
Figure 41. Superposition of chain A (4NCT, green) with chain A (2VX3, gray) showing the hydrogen bond network between the catalytic loop and the activation segment. The formation of the disulfide bridge weakens the hydrogen interactions.

One final feature of the 4NCT structure that further distinguishes it from the previously published DYRK1A structures is chain C has a phosphoserine at position S301. This phosphorylation is unique to chain C and it is not observed in the other three chains. It is so far not known in the literature that S301 can be phosphorylated by DYRK1A and the fact that it is only present in one chain indicates that this phosphorylation occurs in only 25% of the protein and might be a rare event (**Figure 42**).
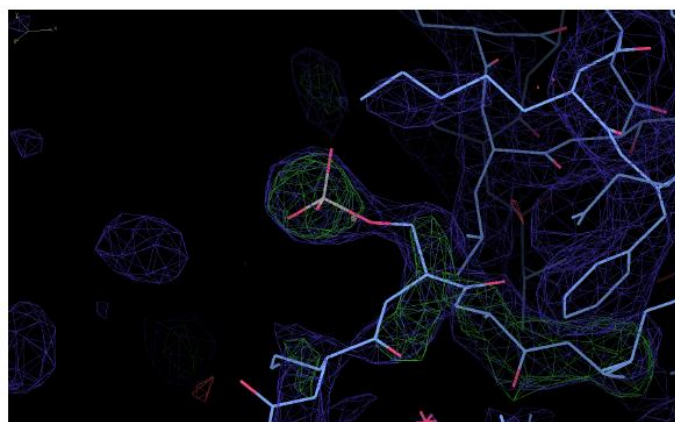
Figure 42. Omit map for serine S301 of chain C (4NCT). The map clearly shows an electron rich group next to the serine that can be interpreted as a phosphorylation. A phosphorylation of DYRK1A on serine S301 is so far not known in the literature.

4. DISCUSSION

4.1 Comparison of DYRK1A and DYRK1B

4.1.1 Expression and purification

DYRK1A and DYRK1B are the closest related kinases in the DYRK family. The sequence identity of the kinase domain is 85% and in the ATP pocket there is just one amino acid difference: a methionine to leucine exchange. Besides the high similarity, the two proteins behave differently when expressed in *E. coli*. Overexpressed DYRK1B accumulated mostly in inclusion bodies and phosphate based buffers have a highly destabilizing effect on DYRK1B, while DYRK1A was expressed in high quantities as soluble protein and is less sensitive to different buffers. The overall amount of DYRK1A after purification was on average 20 mg per liter culture while DYRK1B had a much lower yield of 2 mg per liter of bacterial culture. It should be mentioned that the expression of DYRK1B was high, but the solubility of the protein itself was low, causing inclusion body formation, leading to the overall lower amount of purified protein. DYRK1B is sensitive to different buffers. Surprisingly it is not the pH that causes the differences, but rather the buffering compound and the presence of alkali salts like KCl. The effect of this was clearly seen in the thermal shift experiment where the protein had an around 10 degrees lower melting temperature in phosphate buffer compared to a HEPES buffer at the same pH. Besides these differences, both proteins are expressed as active kinases. The mass spectrometry analysis shows that they are phosphorylated on the second tyrosine of the YQY motif in the activation segment. This was also true for the DYRK1B L192M and Q164K mutant. The third mutant C238R was however not phosphorylated in the activation segment.

The expression of the mutants followed the protocol for DYRK1B wt. The Q164K mutant expressed in a more soluble form and the yield was on average higher compared to the wild type DYRK1B. The L192M mutant could be only obtained in a lower yield compared to the wild type and Q164K mutant. However it might be possible to optimize the expression of L192M mutant by optimizing expression time, temperature and media and using parameters optimal for this mutant. Due to the limited time the expression protocol was kept identical for all the mutants.

Interestingly, DYRK1B L192M elutes as dimer and monomer in the gel filtration in the absence of reducing agents. This was also the case for the Q164K mutant in absence of reducing agents. DYRK1B has six cysteines in the expression construct. Three of them are buried within

the hydrophobic core of the kinase and are not accessible. Besides C238 and C264 that are accessible but rather would form an intramolecular disulfide bridge between them, as seen in the crystal structure 4NCT, the most likely candidate for an intermolecular disulfide bridge formation is C248. It was observed that the lack of reducing agent destabilizes DYRK1B and the mutants and they are more likely to precipitate and cannot be concentrated higher than 5 mg/ml. It was therefore important to purify DYRK1B in the presence of reducing agents; however, a point mutation of C248S might be beneficial for future work.

The mutant C238R did not express very well and the purification that was done before the buffer optimization showed that this kinase is not active. Since the mutant was not phosphorylated and the phosphorylation is a posttranslational step during the translation it can be speculated that the formation of the disulfide bridge might be essential for this step and proper folding of the protein and the lack of activity can be due to a miss-folding in addition to the inactive activation segment. Literature data shows that DYRK mutants with phenylalanine instead of tyrosine in the activation segment can still be active[18,19], however with a lower activity. The Cook assay used in this thesis might be not sensitive enough to detect very low levels of kinase activity. The C238R mutant has, beside its inactivity, interesting properties and offers a way to study the mechanism of autoactivation and the necessity of the disulfide bridge for stability and kinase activity.

4.1.2 Enzyme kinetics

The kinetic studies were performed by the Cook assay. One primary observation was that DYRK1B phosphorylates DYRKtide faster than DYRK1A. The K_m value is with 80 μM compared to 118μM in DYRK1A lower which means that DYRK1B has a higher affinity to ATP. The K_m value for DYRK1B correlates strongly with the Kd value for ATP obtained by microscale thermophoresis (NanoTemper). Our observation with the kinase activity assay indicates that DYRK1B is more active than DYRK1A which is shown in the K_m values, however since our assays were performed at room temperature the kinases were most probably not operating at a their temperature optima. The K_m values measured in this thesis for DYRK1A differ from the K_m value reported in the literature which was 35 μM[29]; i.e., four times lower. A direct comparison might be so not valid since the K_m values were determined with different assays and at different temperatures. The higher temperature of 30 degree used in the radiometric assay by Himpel et al.[29] might be closer to a temperature optimum. This higher activity of the kinases at higher temperatures could explain the difference in the K_m value.

The only difference in the ATP pocket between DYRK1A and DYRK1B is the more bulky but unbranched methionine in DYRK1A compared to the smaller leucine in DYRK1B in the hinge region. (P+2 from gatekeeper residue) The methionine in the crystal structure points away from the binding pocket and it does not give the impression that methionine could block the ATP pocket. It is however possible that since the amino acid is flexible it causes some steric hindrance in the path for ATP to the pocket which could explain the lower activity of DYRK1A compared with DYRK1B. However, a mutant of DYRK1B where the leucine in the hinge is replaced by a methionine has a reduced activity even lower than DYRK1A. The K_m value for the L192M mutant was 1400 nM, ten times weaker than DYRK1A. There is no obvious explanation for this unexpected weaker K_m value. If correct, an additional mechanism that influences the kinase activity must exist. Since there are not many other residues close by that are different between DYRK1A and DYRK1B that could be responsible for this effect it could be a simple problem of stability of the L192M mutant in the assay conditions. However, neither DYRK1A nor DYRK1B wt have stability problems in the activity assay. One other possibility is a tryptophan (W184) at the beginning at β-sheet 3 in DYRK1A that could hold the methionine residue away from the ATP pocket via hydrophobic interactions. In DYRK1B this residue is a leucine, a small hydrophobic residue that might not be able to do so. It needs however more investigation whether this is a possible mechanism. The distance (in the structure of DYRK1A (4NTC)) between W184 and L240 is, with around 5-8 Å, large for hydrophobic interactions. A double mutant of DYRK1B with L192M and L137W might be needed to investigate the potential role of the tryptophan. The IC_{50} value of PKC412 for DYRK1B L192M is 2.5 times weaker compared to the wild type kinases DYRK1A and DYRK1B which also would indicate that additional factors are involved in the selectivity for ATP and inhibitor interaction with these kinases.

4.1.3 Comparison in inhibitor screen

The inhibitors, provided by a private pharmaceutical company, were originally designed for the inhibition of DYRK1A. However the close relation between DYRK1A and DYRK1B makes it obvious to test these inhibitors also for DYRK1B and derive a selectivity profile. The experimental results demonstrate that the potency of inhibitors is, in general, higher for DYRK1A than for DYRK1B; however exceptions exist. The graphical representation of the **Table 7** and **Figure 48** (appendix) shows that there are three inhibitors (15, 26 and 48) that are significant better for DYRK1B compared to DYRK1A. An additional ten inhibitors (23, 25, 27, 37, 39, 40, 41, 44, 47 and 49) have a preference for DYRK1B, however the difference is less significant. On

the other hand, 21 inhibitors are significantly more selective for DYRK1A and the remaining 16 inhibitors have a minor preference for DYRK1A or do not distinguish between the two kinases.

The screening assay for the 50 inhibitors was performed at a fixed concentration of inhibitor (20 µM). For a more detailed analysis of inhibitor potency, the determination of IC_{50} followed by Ki calculation was performed for some inhibitors using the Cook assay and a serial dilution of inhibitor concentrations. In the case of harmine, the IC_{50} determination for DYRK1B wt and the L192M mutant show similar IC_{50} values, however if the L192M mutant has lower affinity for ATP (K_m is 1,4 mM) compared to DYRK1B wt (K_m is 80 µM), then for L192M a lower concentration of inhibitor is required to reduce the kinase activity to 50%. The calculation of Ki for harmine shows that harmine binds stronger to DYRK1B wt by a factor of two (Ki is 337 nM) compared to the L192M mutant (Ki is 601 nM). We would expect that harmine binds stronger to the L192M mutant since it mimics DYRK1A and in the scientific literature a stronger affinity of harmine towards DYRK1A over DYRK1B was shown[133]. Nevertheless the ~10 fold lower K_m of L192M compared to DYRK1A and almost ~20 times lower K_m towards DYRK1B would result in a decrease in Ki value for this mutant. The fact that the order for the binding strength is reversed when comparing IC_{50} values to Ki values makes it important in competitive inhibitor assays to not only determine the binding strength of the inhibitor but also to take into consideration the binding strength of the substrate that has to be replaced. The IC_{50} determination gives the inhibitor concentration at which 50% of the protein is inactive, but to compare actual binding strength of inhibitors the Ki values might be more suitable and independent of the ATP substrate concentration. The difference in IC_{50} values and Ki values are most prominent in cases where the K_m values for ATP are significantly different. The closer similarity of the K_m values between DYRK1A and DYRK1B wt do not influence the Ki determination that much and the IC_{50} values are more comparable with the Ki values meaning that the affinity arose from the IC_{50} is direct proportional to the affinities determined by the Ki values. This is seen in the PKC412 titration for DYRK1A and DYRK1B which have similar affinities by comparing IC_{50} values or Ki values.

In addition to harmine, four inhibitors synthesized and provided by the company were selected for IC_{50} determination and Ki calculation for DYRK1B. A more precise determination of inhibitor potency by Ki calculation revealed that the most potent inhibitor, among the inhibitors synthesized and provided by the private company, was inhibitor 4 (Ki is 625 nM) which was in the third place in the rank of inhibitors, based on the initial screen at a fixed inhibitor concentration, after inhibitor 47 and harmine. Inhibitor 47, based on the result of the inhibitor screen, was the best one, but in the ranking according to the Ki values it binds weaker (685 nM) than harmine (337 nM) and inhibitor 4 (625 nM). The difference in Ki between inhibitor 4 and 47 is however

only 9%. This shows, in conclusion, that the testing of inhibitors with one particular inhibitor concentration is efficient for fast screening for the strongest inhibitors, but ranking inhibitors solely based on one inhibitor concentration can only be a preliminary step. For full verification a more precise analysis of inhibitor binding or determination of Ki value is required. Nevertheless is an inhibitor screen based on one inhibitor concentration is practical and useful to rapidly eliminate inhibitors that do not, or only marginally, inhibit the target enzyme. In this way the more time consuming IC_{50} determinations can be avoided for non-binders and weak inhibitors.

4.2 Crystallography

4.2.1 Structure of DYRK1A

It was unfortunately not possible to crystalize DYRK1B, however due to the close similarity between DYRK1A and DYRK1B, the structure of DYRK1A in complex with PKC412 crystallized and solved in this thesis offers a good model for DYRK1B. The kinetic data for PKC412 show that both kinases are inhibited equally well by PKC412 and it can be assumed that the binding of PKC412 is identical in both kinases. DYRK1A crystallized with disulfide bridges formed which is a novel finding since the previously published DYRK1A structures do not have disulfide bridges. It was speculated so that the formation of disulfide bridges is involved in tweaking the activity of the kinase. The structure with the disulfide bridge does not show any major structural rearrangements. As discussed in the results section, it weakens the hydrogen bond network between the activation segment and the catalytic loop and replaces it with a stronger covalent S-S-bond. Our observation from the expression of the C238R mutant which is not phosphorylated at tyrosine Y273 might suggest that the disulfide bridge formation is essential during the autophosphorylation in the translation step. It needs however more research to settle this problem. Another finding in the DYRK1A structure was a phosphoserine S301. This phosphorylation site was previously not described in the literature. It is only present on chain C in the asymmetric unit. One of the tested crystals of DYRK1A/PKC412 solved by us diffracted to 3Å and, had a high twinning fraction of 0.6 to 0.4 (H, K, L/ K, H, -L) while there was no twinning in the 4NCT structure. The two crystals came from different protein batches, and it might be possible that the phosphorylation on S301 in 25% of the protein helped to orientate the asymmetric unit in the crystal packing and by that avoiding the twinning.

4.2.2 Disulfide bridge

The HCD motif in the catalytic loop in DYRK kinases is rare in the human kinome (**Figure 43**). Besides the DYRK family it is only found in a few other kinases like the PKD family (protein kinase D faimily), the Tyrosine-protein kinase SgK269 (sugen kinase 269), ULK4 (uridine kinase-like protein 4) and LRRK1 (Leucine-rich repeat serine/threonine-protein kinase 1) that have a cysteine at this position. (ULK4 and LRRK1 have a FCD motif). Among these, only UKL4 has a second cysteine in the activation segment between the DFG and APE motifs that could act like a partner for disulfide bridge formation as in DYRK1A. The PKD kinases have no cysteine in the activation segment between the residues DFG and APE however they have a cysteine right in front of the DFG, and the CDFG motif is conserved among the three PKD kinases. Whether these kinases are able to form disulfide bridges to the cysteine in the extended activation segment or to other cysteines in the kinase domain can only be speculated upon due to the lack of structural information. Preliminary observations of the DYRK1B mutant with the HCD motif mutated to HRD (C238R) show that the *E. coli* expressed protein was not enzymatically active in the kinase assay. However as discussed above the Cook assay might not be sensitive enough to detect low activity, and a radiometric assay might be more accurate in this respect. It needs further studies to investigate whether the HCD and the disulfide bridge are mandatory for tyrosine phosphorylation and autoactivation, or whether the disulfide bridge plays a role in the kinase activity.
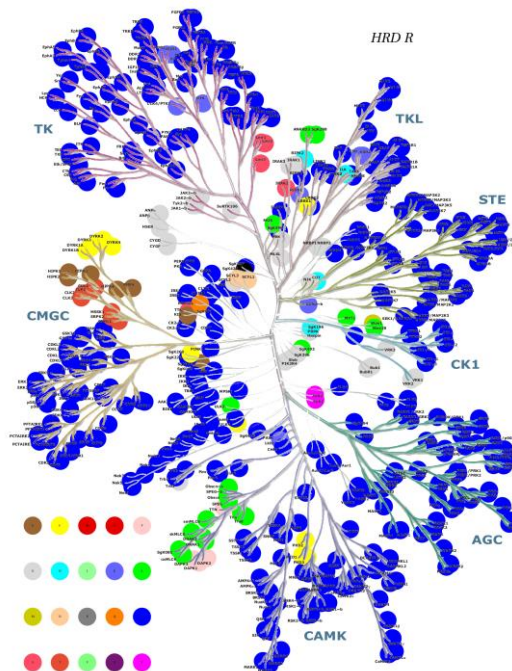
Figure 43. Distribution of the second residue of the HRD catalytic motif in human kinome. Cysteine residue is in yellow. Figure from R. Engh, including kinome representation from Manning G. *et al.*[4]

4.2.3 PKC412

The DYRK1A structure 4NCT is the first kinase in the protein data bank which has a PKC412 molecule bound to the ATP pocket. There exists however several kinase structures with staurosporine the original isolated natural compound from which PKC412 was derived. Like staurosporine PKC412 inhibits many kinases in the kinome, however its inhibitory profile is more selective. The structure of DYRK1A with PKC412 might help to understand this profile and can serve as a starting point to develop more selective inhibitors for DYRK kinases. Some modification that might lead to a stronger binder would be to introduce a hydrogen acceptor opposite of the hinge to bind to K188 as it is seen in the inhibitors INDY and harmine[16]. Another modification could be an extension of the "tail" to anchor the inhibitor via hydrogen bonds to E291 or N244 (**Figure 44**). Additional extensions to introduce hydrogen bonds to D305 from the DFG motive are possible.
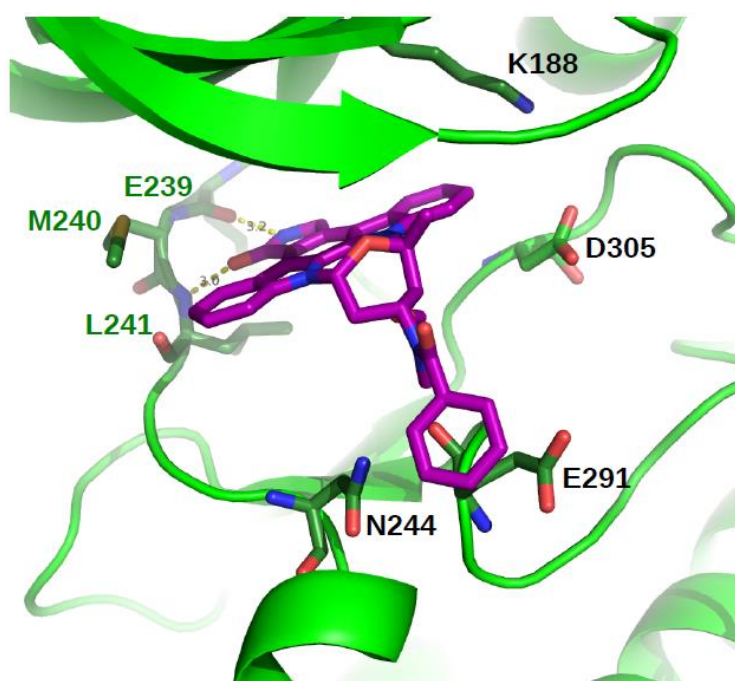
Figure 44. The PKC412 (purple) bound to the ATP-pocket of DYRK1A (4NCT). The green residues are involved in hydrogen bond formation, the black residues are amino acids in close proximity that could serve as hydrogen bond partners.

PKC412 is widely used in clinical trials to treat acute myeloid leukemia and other cancers and it is currently in clinical trials as an inhibitor for FLT3[71]. A possible application in neurological disease is not established. Since DYRK1A is a kinase involved in neurological disease it may be possible to expand the clinical trials to neurological diseases.

5. FUTURE WORK

Many questions could be answered by obtaining a crystal structure of DYRK1B. For this purpose it would be necessary to try new constructs with different lengths compared to the construct used in this master project. The different constructs could contain the point mutations at the position of the possible crystal contact like Q164K used, but also include new point mutations like C248S, a residue most probably involved in dimerization in the absence of reducing agent. For each mutant and construct it would be necessary to optimize the buffers in order to obtain the most stable protein. Another option would be to focus on the inclusion bodies. DYRK1B is highly expressed but most of the protein stays in the insoluble fraction after lysis. Finding a protocol for refolding would overcome the shortage of protein and would allow for more numerous and extensive crystallization screens.

For the kinetics it would be interesting to further study the inhibitor selectivity profile. It is necessary to make DYRK1A mutants that mimic DYRK1B like a DYRK1A M240L where the hinge methionine in DYRK1A is replaced by a leucine found in DYRK1B at this position. It would be the reverse mutation to the DYRK1B L192M used in this thesis. Also, the potential role of W184 (L137 in DYRK1B) could be investigated by a point mutation.

Finally, the HCD could be investigated in more detail. Point mutation of the HCD motif to HSD or mutagenesis of the cysteine binding partner C264 (C312 in DYRK1A) could be performed.

In addition to the Cook assay, a second binding assay should be established. Since most of the company's provided inhibitors are poorly water soluble and the Biacore did not work due to instability of the protein on the chip, the microthermophoresis technology could be an alternative and a supplement to the kinetic assay.

And finally, it can be proposed to continue the research on PKC412 as a drug candidate for neurological diseases (e.g. Alzheimer disease) and maybe expand the ongoing clinical trials for PKC412.

SUMMARY

The research within this thesis describes the biophysical characterization of DYRK1B, a member of the dual-specificity tyrosine phosphorylation-regulated kinase family (DYRKs) which have recently emerged as new therapeutic targets for various kinds of cancer and neurodegenerative diseases. DYRK1B plays a key role for cancer cell survival, and its inhibition induces apoptosis of cancer cells. This thesis describes the cloning of the kinase domain of DYRK1B. The construct contains a $(His)_6$-tag, TEV protease cleavage site and the kinase domain (AA 78-451). DYRK1B was expressed and purified by affinity chromatography (HisTrap Ni-NTA columns) followed by a TEV cleavage - to remove the Histag - during dialysis and a second HisTrap purification. For the crystallization trails a size exclusion chromatography (SEC) was used as last step resulting in production of to 98% pure protein.

To study the stability and solubility of DYRK1B two buffer screens were designed. The buffer screens, carried out by Thermofluor, showed that HEPES buffer increased the melting temperature by 12 ℃ compared to initially used phosphate buffer. The buffer optimization improved the yield of DYRK1B by 10 fold. In the absence of reducing agent, DYRK1B dimerizes and these dimers could be separated from the monomers via SEC. Three mutants of DYRK1B were cloned in this master project to investigate different aspects of enzymatic activity (C238R), selectivity (L192M) and crystallisability (Q164K). DYRK1B C238R was not autophosphorylated at Y273 and did not show activity in the cook assay; however this mutant needs to be further investigated with a more sensitive assay. DYRK1B L192M and DYRK1B Q164K were expressed as active enzymes and were used for their designed purposes: inhibitor selectivity profiling and crystallization trials, respectively.

50 inhibitors were screened to determine the selectivity of DYRK1B versus DYRK1A. The best inhibitors were chosen for IC_{50} determination and Ki calculation. The point mutation DYRK1B L192M that mimics DYRK1A in the ATP pocket was used to study the influence of methionine in the hinge region on the selectivity profile of the inhibitors. The Michaelis-Menten constant K_m was determined by Cook assay for DYRK1A, DYRK1B wt and DYRK1B L192M. DYRK1B has the highest affinity for ATP with a K_m of 81 µM, DYRK1A has a weaker affinity of $K_m = 119$ µM. In contrast to the two wild type kinases, the K_m value for DYRK1B L192M drops by almost 20 times to 1400 µM. This significantly weaker K_m, if correct, leads to the conclusion that DYRK1A probably has additional residues close to the ATP pocket that could compensate for

a weaker ATP affinity. As a possible candidate, a tryptophan W184, was identified that is close to M240 and probably interacts with methionine. In DYRK1B this residue is L137.

Crystallization trials with DYRK1B wt, DYRK1B Q164K and DYRK1A were performed with commercially available inhibitors. Unfortunately, DYRK1B did not crystallize but DYRK1A was crystallized in complex with inhibitor PKC412. The diffraction data were collected at BESSY II beamline 14.1 (Helmholz Zentrum Berlin). The crystal diffracted at resolution 2.6 Å. The structure was solved by molecular replacement in Molrep (CCP4) and refined by Refmac5 and Phenix. The crystal structure demonstrates a formation of the disulfide bridge between C286 in the catalytic motif HCD and C312 in the activation segment. This crystal structure is the first DYRK1A structure with a disulfide bridge and it is the first kinase with the staurosporine analog PKC412.

APPENDIX

Figure 45. Expression plasmid of DYRK1B wt
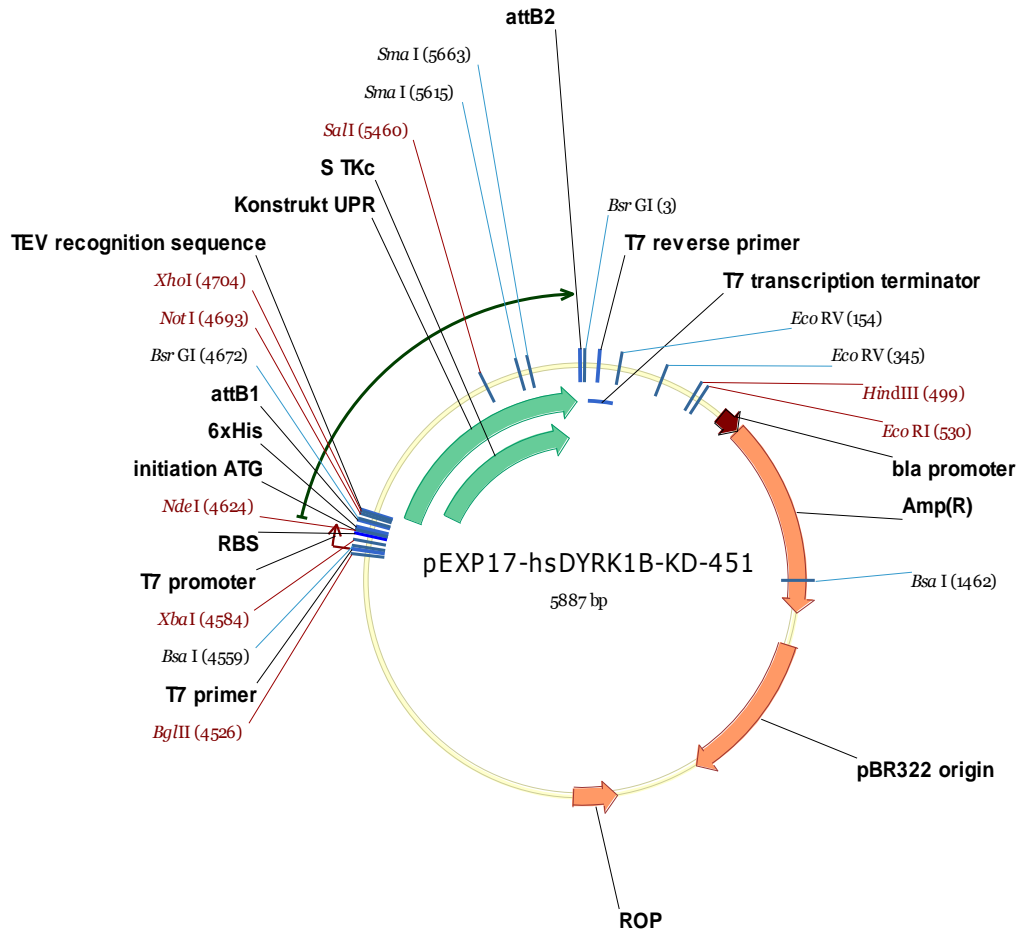
Figure 46. Scheme of the DYRK1B wt protein construct

Translation of pEXP17-hsDYRK1B-KD-451

411 aa
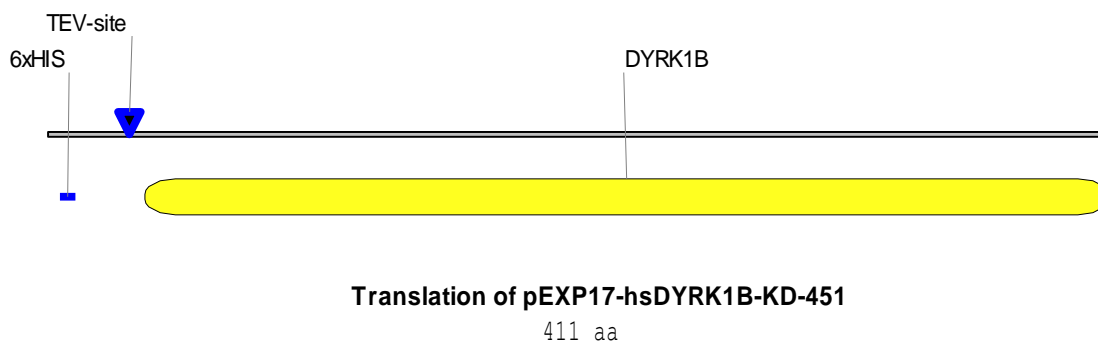
Figure 47. Gateway destination vector pDEST17.

Pst I (5896)

Amp(R)

bla promoter

Eco RI (5140)

Hin dIII (5109)

Eco RV (4955)

Eco RV (4764)

T7 transcription terminator

T7 reverse primer

attR2

Sal I (4495)

Pst I (4493)

ccdB

Sma I (4238)

Bam HI (3820)

Bgl II (3814)

Cm(R)

Eco RI (3367)

pBR322 origin

ROP

pDEST17

6354 bp

Bgl II (2782)

T7 primer

Xba I (2840)

T7 promoter

RBS

Nde I (2880)

initiation ATG

6xHis

attR1

Not I (3047)

Bam HI (3117)
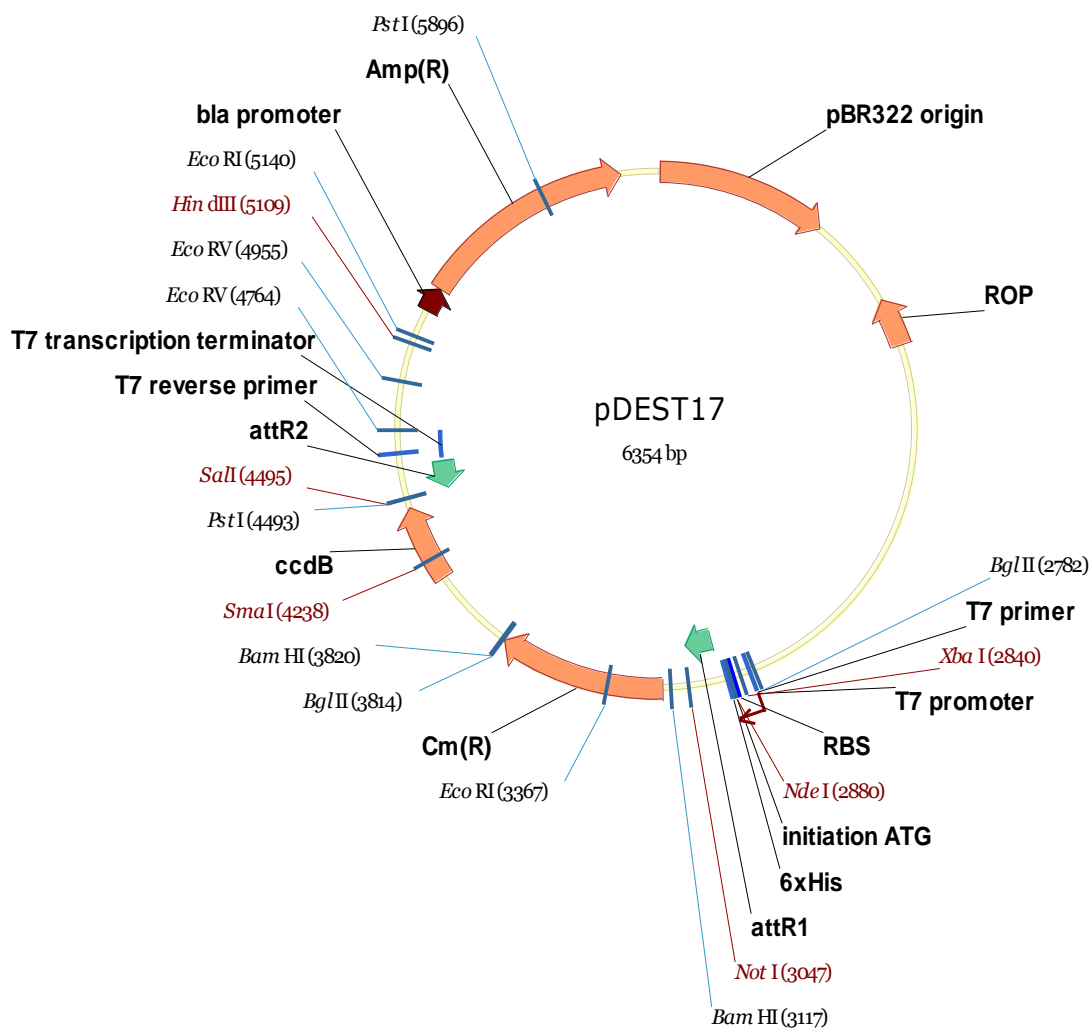
Table 13. Stability and Solubility Screen 1.

| well	Buffer			Salt		Additive	
#	name	mM	pH	name	mM	name	mM
A01	TricCl	100	7				
A02			7	NaCl	800		
A03			7	KCl	800		
A04			7	LiCl	800		
A05	TricCl	100	8				
A06				NaCl	800		
A07				KCl	800		
A08				LiCl	800		
A09	MOPS	100	6,5				
A10				NaCl	800		
A11				KCl	800		
A12				LiCl	800		
B01	MOPS	100	7				
B02				NaCl	800		
B03				KCl	800		
B04				LiCl	800		
B05	MOPS	100	7,5				
B06				NaCl	800		
B07				KCl	800		
B08				LiCl	800		
B09	MOPS	100	8				
B10				NaCl	800		
B11				KCl	800		
B12				LiCl	800		
C01	Tris	100	7,5				
C02				NaCl	800		
C03				KCl	800		
C04				LiCl	800		
C05	Tris	100	8,5				
C06				NaCl	800		
C07				KCl	800		
C08				LiCl	800		
C09	HEPES	100	6,5				
C10				NaCl	800		
C11				KCl	800		
C12				LiCl	800		
D01	HEPES	100	7				
D02				NaCl	800		
D03				KCl	800		
D04				LiCl	800		
D05	HEPES	100	7,5				
D06				NaCl	800		
D07				KCl	800		
D08				LiCl	800		
D09	HEPES	100	8				
D10				NaCl	800		
D11				KCl	800		
D12				LiCl	800		
E01	MES	100	5,5				
E02				NaCl	800		
E03				KCl	800		
E04				LiCl	800		
E05	MES	100	6				
E06				NaCl	800		
E07				KCl	800		
E08				LiCl	800		
E09	MES	100	6,5				
E10				NaCl	800		
E11				KCl	800		
E12				LiCl	800		
F01	Bistris	100	5,5				
F02				NaCl	800		
F03				KCl	800		
F04				LiCl	800		

F05	Bistris	100	6				
F06				NaCl	800		
F07				KCl	800		
F08				LiCl	800		
F09	Bistris	100	6,5				
F10				NaCl	800		
F11				KCl	800		
F12				LiCl	800		
G01	Bistris	100	7				
G02				NaCl	800		
G03				KCl	800		
G04				LiCl	800		
G05	TricCl	100	7	NaCl	800	Chaps	20
G06	TricCl	100	8	NaCl	800	Chaps	20
G07	MOPS	100	6,5	NaCl	800	Chaps	20
G08	MOPS	100	7	NaCl	800	Chaps	20
G09	MOPS	100	7,5	NaCl	800	Chaps	20
G10	MOPS	100	8	NaCl	800	Chaps	20
G11	Tris	100	7,5	NaCl	800	Chaps	20
G12	Tris	100	8,5	NaCl	800	Chaps	20
H01	HEPES	100	6,5	NaCl	800	Chaps	20
H02	HEPES	100	7	NaCl	800	Chaps	20
H03	HEPES	100	7,5	NaCl	800	Chaps	20
H04	HEPES	100	8	NaCl	800	Chaps	20
H05	MES	100	5,5	NaCl	800	Chaps	20
H06	MES	100	6	NaCl	800	Chaps	20
H07	MES	100	6,5	NaCl	800	Chaps	20
H08	Bistris	100	5,5	NaCl	800	Chaps	20
H09	Bistris	100	6	NaCl	800	Chaps	20
H10	Bistris	100	6,5	NaCl	800	Chaps	20
H11	Bistris	100	7	NaCl	800	Chaps	20
H12	H2O						

Table 14. Stability and Solubility Screen 2

well	Buffer			Salt	
#	name	mM	pH	name	mM
A01	TricCl	100	7	+KCl	100
A02				+KCl	200
A03				+KCl	300
A04				+KCl	400
A05	TricCl	100	8	+KCl	100
A06				+KCl	200
A07				+KCl	300
A08				+KCl	400
A09	MOPS	100	6,5	+KCl	100
A10				+KCl	200
A11				+KCl	300
A12				+KCl	400
B01	MOPS	100	7	+KCl	100
B02				+KCl	200
B03				+KCl	300
B04				+KCl	400
B05	HEPES	100	6,5	+KCl	100
B06				+KCl	200
B07				+KCl	300
B08				+KCl	400
B09	HEPES	100	7	+KCl	100
B10				+KCl	200
B11				+KCl	300
B12				+KCl	400
C01	HEPES	100	7,5	+KCl	100
C02				+KCl	200
C03				+KCl	300
C04				+KCl	400
C05	HEPES	100	8	+KCl	100
C06				+KCl	200
C07				+KCl	300
C08				+KCl	400
C09	MES	100	5,5	+KCl	100
C10				+KCl	200
C11				+KCl	300
C12				+KCl	400
D01	MES	100	6	+KCl	100
D02				+KCl	200
D03				+KCl	300
D04				+KCl	400
D05	MES	100	6,5	+KCl	100
D06				+KCl	200
D07				+KCl	300
D08				+KCl	400
D09	Bistris	100	5,5	+KCl	100
D10				+KCl	200
D11				+KCl	300
D12				+KCl	400
E01	Bistris	100	6	+KCl	100
E02				+KCl	200
E03				+KCl	300
E04				+KCl	400
E05	Bistris	100	6,5	+KCl	100
E06				+KCl	200
E07				+KCl	300
E08				+KCl	400
E09	PBS	100	7	+KCl	100
E10				+KCl	200
E11				+KCl	300
E12				+KCl	400
F01				+KCl	800

Figure 48. The comparison of remaining activity (%) of 50 inhibitors between DYRK1A (red) and DYRK1B (Blue)
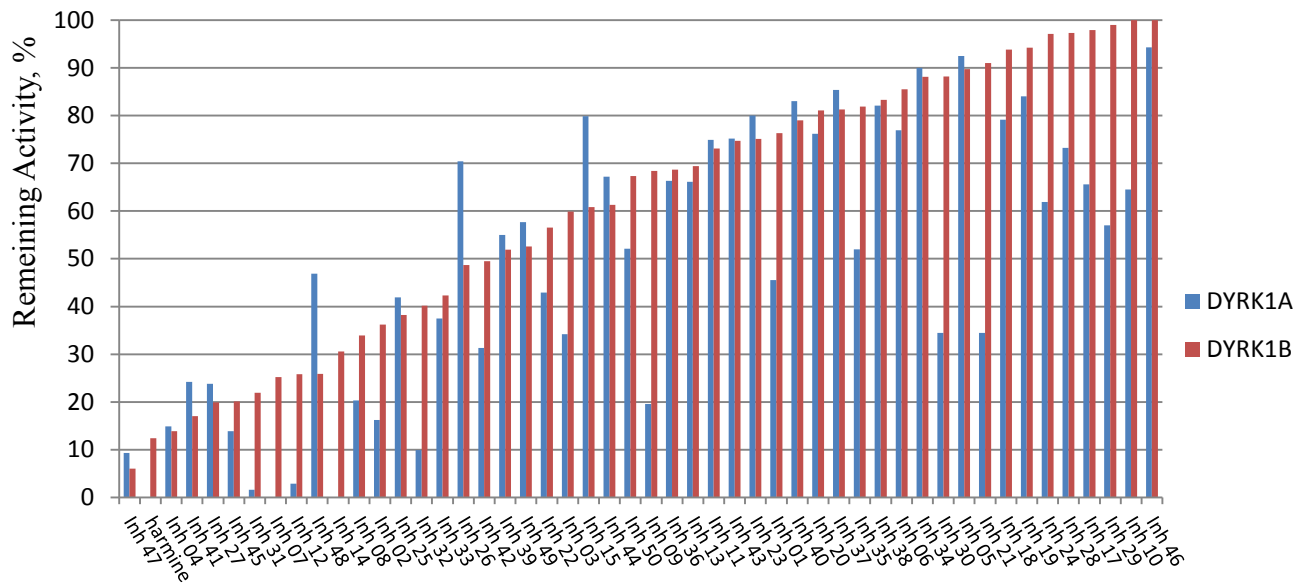
REFERENCES

1   Klebl, B., Müller, G. & Hamacher, M. *Protein kinases as drug targets*. (Wiley-VCH, 2011).
2   Montminy, M. Transcriptional regulation by cyclic AMP. *Annual review of biochemistry* **66**, 807-822, doi:10.1146/annurev.biochem.66.1.807 (1997).
3   Tasken, K. *et al.* Structure, function, and regulation of human cAMP-dependent protein kinases. *Advances in second messenger and phosphoprotein research* **31**, 191-204 (1997).
4   Manning, G., Plowman, G. D., Hunter, T. & Sudarsanam, S. Evolution of protein kinase signaling from yeast to man. *Trends in biochemical sciences* **27**, 514-520 (2002).
5   Hanks, S. K. & Hunter, T. Protein kinases 6. The eukaryotic protein kinase superfamily: kinase (catalytic) domain structure and classification. *FASEB journal : official publication of the Federation of American Societies for Experimental Biology* **9**, 576-596 (1995).
6   Lindberg, R. A., Quinn, A. M. & Hunter, T. Dual-specificity protein kinases: will any hydroxyl do? *Trends in biochemical sciences* **17**, 114-119 (1992).
7   Weinberg, R. A. *The biology of cancer*. Second edition. edn.
8   Alberts, B. *Molecular biology of the cell*. 4th edn, (Garland Science, 2002).
9   Cohen, P. The Croonian Lecture 1998. Identification of a protein kinase cascade of major importance in insulin signal transduction. *Philosophical transactions of the Royal Society of London. Series B, Biological sciences* **354**, 485-495, doi:10.1098/rstb.1999.0399 (1999).
10   Monaco, E. A., 3rd & Vallano, M. L. Role of protein kinases in neurodegenerative disease: cyclin-dependent kinases in Alzheimer's disease. *Frontiers in bioscience : a journal and virtual library* **10**, 143-159 (2005).
11   Cheshenko, N. *et al.* HSV activates Akt to trigger calcium release and promote viral entry: novel candidate target for treatment and suppression. *FASEB journal : official publication of the Federation of American Societies for Experimental Biology* **27**, 2584-2599, doi:10.1096/fj.12-220285 (2013).
12   Noble, M. E., Endicott, J. A. & Johnson, L. N. Protein kinase inhibitors: insights into drug design from structure. *Science* **303**, 1800-1805, doi:10.1126/science.1095920 (2004).
13   Martin, E. D., De Nicola, G. F. & Marber, M. S. New therapeutic targets in cardiology: p38 alpha mitogen-activated protein kinase for ischemic heart disease. *Circulation* **126**, 357-368, doi:10.1161/CIRCULATIONAHA.111.071886 (2012).
14   Endicott, J. A. & Noble, M. E. Structural characterization of the cyclin-dependent protein kinase family. *Biochemical Society transactions* **41**, 1008-1016, doi:10.1042/BST20130097 (2013).
15   Eswaran, J. & Knapp, S. Insights into protein kinase regulation and inhibition by large scale structural comparison. *Biochimica et biophysica acta* **1804**, 429-432, doi:10.1016/j.bbapap.2009.10.013 (2010).
16   Ogawa, Y. *et al.* Development of a novel selective inhibitor of the Down syndrome-related kinase Dyrk1A. *Nature communications* **1**, 86, doi:10.1038/ncomms1090 (2010).
17   Johnson, L. N., Noble, M. E. & Owen, D. J. Active and inactive protein kinases: structural basis for regulation. *Cell* **85**, 149-158 (1996).
18   Becker, W. & Sippl, W. Activation, regulation, and inhibition of DYRK1A. *The FEBS journal* **278**, 246-256, doi:10.1111/j.1742-4658.2010.07956.x (2011).
19   Lochhead, P. A., Sibbet, G., Morrice, N. & Cleghon, V. Activation-loop autophosphorylation is mediated by a novel transitional intermediate form of DYRKs. *Cell* **121**, 925-936, doi:10.1016/j.cell.2005.03.034 (2005).
20   Lochhead, P. A. *et al.* A chaperone-dependent GSK3beta transitional intermediate mediates activation-loop autophosphorylation. *Molecular cell* **24**, 627-633, doi:10.1016/j.molcel.2006.10.009 (2006).
21   Kornev, A. P., Haste, N. M., Taylor, S. S. & Eyck, L. F. Surface comparison of active and inactive protein kinases identifies a conserved activation mechanism. *Proceedings of the National*

Academy of Sciences of the United States of America **103**, 17783-17788, doi:10.1073/pnas.0607656103 (2006).

22   Vulpetti, A. & Bosotti, R. Sequence and structural analysis of kinase ATP pocket residues. *Farmaco* **59**, 759-765, doi:10.1016/j.farmac.2004.05.010 (2004).

23   Walte, A. *et al.* Mechanism of dual specificity kinase activity of DYRK1A. *The FEBS journal* **280**, 4495-4511, doi:10.1111/febs.12411 (2013).

24   Garrett, S. & Broach, J. Loss of Ras activity in Saccharomyces cerevisiae is suppressed by disruptions of a new kinase gene, YAKI, whose product may act downstream of the cAMP-dependent protein kinase. *Genes & development* **3**, 1336-1348 (1989).

25   Raich, W. B. *et al.* Characterization of Caenorhabditis elegans homologs of the Down syndrome candidate gene DYRK1A. *Genetics* **163**, 571-580 (2003).

26   Tejedor, F. *et al.* minibrain: a new protein kinase family involved in postembryonic neurogenesis in Drosophila. *Neuron* **14**, 287-301 (1995).

27   Becker, W. *et al.* Sequence characteristics, subcellular localization, and substrate specificity of DYRK-related kinases, a novel family of dual specificity protein kinases. *The Journal of biological chemistry* **273**, 25893-25902 (1998).

28   Aranda, S., Laguna, A. & de la Luna, S. DYRK family of protein kinases: evolutionary relationships, biochemical properties, and functional roles. *FASEB journal : official publication of the Federation of American Societies for Experimental Biology* **25**, 449-462, doi:10.1096/fj.10-165837 (2011).

29   Himpel, S. *et al.* Specificity determinants of substrate recognition by the protein kinase DYRK1A. *The Journal of biological chemistry* **275**, 2431-2438 (2000).

30   Leder, S. *et al.* Cloning and characterization of DYRK1B, a novel member of the DYRK family of protein kinases. *Biochemical and biophysical research communications* **254**, 474-479, doi:10.1006/bbrc.1998.9967 (1999).

31   Lu, J., McKinsey, T. A., Zhang, C. L. & Olson, E. N. Regulation of skeletal myogenesis by association of the MEF2 transcription factor with class II histone deacetylases. *Molecular cell* **6**, 233-244 (2000).

32   Deng, X., Ewton, D. Z., Pawlikowski, B., Maimone, M. & Friedman, E. Mirk/dyrk1B is a Rho-induced kinase active in skeletal muscle differentiation. *The Journal of biological chemistry* **278**, 41347-41354, doi:10.1074/jbc.M306780200 (2003).

33   Mercer, S. E. *et al.* Mirk/Dyrk1B mediates survival during the differentiation of C2C12 myoblasts. *The Journal of biological chemistry* **280**, 25788-25801, doi:10.1074/jbc.M413594200 (2005).

34   Lee, K., Deng, X. & Friedman, E. Mirk protein kinase is a mitogen-activated protein kinase substrate that mediates survival of colon cancer cells. *Cancer research* **60**, 3631-3637 (2000).

35   Mercer, S. E., Ewton, D. Z., Shah, S., Naqvi, A. & Friedman, E. Mirk/Dyrk1b mediates cell survival in rhabdomyosarcomas. *Cancer research* **66**, 5143-5150, doi:10.1158/0008-5472.CAN-05-1539 (2006).

36   Yang, C. *et al.* The kinase Mirk is a potential therapeutic target in osteosarcoma. *Carcinogenesis* **31**, 552-558, doi:10.1093/carcin/bgp330 (2010).

37   Gao, J. *et al.* Mirk/Dyrk1B, a novel therapeutic target, mediates cell survival in non-small cell lung cancer cells. *Cancer biology & therapy* **8**, 1671-1679 (2009).

38   Hu, J. & Friedman, E. Depleting Mirk Kinase Increases Cisplatin Toxicity in Ovarian Cancer Cells. *Genes & cancer* **1**, 803-811, doi:10.1177/1947601910377644 (2010).

39   Friedman, E. Mirk/dyrk1B Kinase in Ovarian Cancer. *International journal of molecular sciences* **14**, 5560-5575, doi:10.3390/ijms14035560 (2013).

40   Friedman, E. The Kinase Mirk/dyrk1B: A Possible Therapeutic Target in Pancreatic Cancer. *Cancers* **2**, 1492-1512 (2010).

41   Zou, Y., Ewton, D. Z., Deng, X., Mercer, S. E. & Friedman, E. Mirk/dyrk1B kinase destabilizes cyclin D1 by phosphorylation at threonine 288. *The Journal of biological chemistry* **279**, 27790-27798, doi:10.1074/jbc.M403042200 (2004).

102

42   Deng, X., Mercer, S. E., Shah, S., Ewton, D. Z. & Friedman, E. The cyclin-dependent kinase inhibitor p27Kip1 is stabilized in G(0) by Mirk/dyrk1B kinase. *The Journal of biological chemistry* **279**, 22498-22504, doi:10.1074/jbc.M400479200 (2004).

43   Jin, K., Park, S., Ewton, D. Z. & Friedman, E. The survival kinase Mirk/Dyrk1B is a downstream effector of oncogenic K-ras in pancreatic cancer. *Cancer research* **67**, 7247-7255, doi:10.1158/0008-5472.CAN-06-4099 (2007).

44   Hu, J., Deng, H. & Friedman, E. A. Ovarian cancer cells, not normal cells, are damaged by Mirk/Dyrk1B kinase inhibition. *International journal of cancer. Journal international du cancer* **132**, 2258-2269, doi:10.1002/ijc.27917 (2013).

45   Guimera, J. *et al.* A human homologue of Drosophila minibrain (MNB) is expressed in the neuronal regions affected in Down syndrome and maps to the critical region. *Human molecular genetics* **5**, 1305-1310 (1996).

46   Park, J., Song, W. J. & Chung, K. C. Function and regulation of Dyrk1A: towards understanding Down syndrome. *Cellular and molecular life sciences : CMLS* **66**, 3235-3240, doi:10.1007/s00018-009-0123-2 (2009).

47   Teipel, S. J. & Hampel, H. Neuroanatomy of Down syndrome in vivo: a model of preclinical Alzheimer's disease. *Behavior genetics* **36**, 405-415, doi:10.1007/s10519-006-9047-x (2006).

48   Kim, E. J. *et al.* Dyrk1A phosphorylates alpha-synuclein and enhances intracellular inclusion formation. *The Journal of biological chemistry* **281**, 33250-33257, doi:10.1074/jbc.M606147200 (2006).

49   Kang, J. E., Choi, S. A., Park, J. B. & Chung, K. C. Regulation of the proapoptotic activity of huntingtin interacting protein 1 by Dyrk1 and caspase-3 in hippocampal neuroprogenitor cells. *Journal of neuroscience research* **81**, 62-72, doi:10.1002/jnr.20534 (2005).

50   Smith, B., Medda, F., Gokhale, V., Dunckley, T. & Hulme, C. Recent advances in the design, synthesis, and biological evaluation of selective DYRK1A inhibitors: a new avenue for a disease modifying treatment of Alzheimer's? *ACS chemical neuroscience* **3**, 857-872, doi:10.1021/cn300094k (2012).

51   *LALIGN pairwise sequence alignment software*, <http://www.ebi.ac.uk/Tools/psa/lalign/>

52   *Uniprot*, <http://www.uniprot.org>

53   Soundararajan, M. *et al.* Structures of Down syndrome kinases, DYRKs, reveal mechanisms of kinase activation and substrate recognition. *Structure* **21**, 986-996, doi:10.1016/j.str.2013.03.012 (2013).

54   ClustalW2. <http://www.ebi.ac.uk/Tools/msa/clustalw2/>

55   *ESPript*, <http://espript.ibcp.fr/ESPript/ESPript/>

56   Cohen, P. Protein kinases--the major drug targets of the twenty-first century? *Nature reviews. Drug discovery* **1**, 309-315, doi:10.1038/nrd773 (2002).

57   Kurzrock, R., Kantarjian, H. M., Druker, B. J. & Talpaz, M. Philadelphia chromosome-positive leukemias: from basic mechanisms to molecular therapeutics. *Annals of internal medicine* **138**, 819-830 (2003).

58   Buchdunger, E. *et al.* Inhibition of the Abl protein-tyrosine kinase in vitro and in vivo by a 2-phenylaminopyrimidine derivative. *Cancer research* **56**, 100-104 (1996).

59   Capdeville, R., Buchdunger, E., Zimmermann, J. & Matter, A. Glivec (STI571, imatinib), a rationally developed, targeted anticancer drug. *Nature reviews. Drug discovery* **1**, 493-502, doi:10.1038/nrd839 (2002).

60   Li, R. & Stafford, J. A. *Kinase inhibitor drugs*. (John Wiley & Sons, Inc, 2009).

61   Eswaran, J. & Knapp, S. Insights into protein kinase regulation and inhibition by large scale structural comparison. *Biochimica et biophysica acta* **1804**, 429-432, doi:10.1016/j.bbapap.2009.10.013 (2010).

62   Aberg, E. *et al.* Structural origins of AGC protein kinase inhibitor selectivities: PKA as a drug discovery tool. *Biological chemistry* **393**, 1121-1129, doi:10.1515/hsz-2012-0248 (2012).

63   Davis, M. I. *et al.* Comprehensive analysis of kinase inhibitor selectivity. *Nature biotechnology* **29**, 1046-1051, doi:10.1038/nbt.1990 (2011).

64   Ewton, D. Z. *et al.* Inactivation of mirk/dyrk1b kinase targets quiescent pancreatic cancer cells. *Molecular cancer therapeutics* **10**, 2104-2114, doi:10.1158/1535-7163.MCT-11-0498 (2011).

65   Ormerod, M. G. *Flow cytometry : a practical approach*. 3rd edn, (Oxford University Press, 2000).

66   *Maestro, version 9.3, Schrödinger, LLC, New York, NY, 2012.*, <http://www.schrodinger.com/productpage/14/12/>

67   Omura, S. *et al.* A new alkaloid AM-2282 OF Streptomyces origin. Taxonomy, fermentation, isolation and preliminary characterization. *The Journal of antibiotics* **30**, 275-282 (1977).

68   Podar, K., Raab, M. S., Chauhan, D. & Anderson, K. C. The therapeutic role of targeting protein kinase C in solid and hematologic malignancies. *Expert opinion on investigational drugs* **16**, 1693-1707, doi:10.1517/13543784.16.10.1693 (2007).

69   Millward, M. J. *et al.* The multikinase inhibitor midostaurin (PKC412A) lacks activity in metastatic melanoma: a phase IIA clinical and biologic study. *British journal of cancer* **95**, 829-834, doi:10.1038/sj.bjc.6603331 (2006).

70   Weisberg, E. *et al.* Inhibition of mutant FLT3 receptors in leukemia cells by the small molecule tyrosine kinase inhibitor PKC412. *Cancer cell* **1**, 433-443 (2002).

71   Fischer, T. *et al.* Phase IIB trial of oral Midostaurin (PKC412), the FMS-like tyrosine kinase 3 receptor (FLT3) and multi-targeted kinase inhibitor, in patients with acute myeloid leukemia and high-risk myelodysplastic syndrome with either wild-type or mutated FLT3. *Journal of clinical oncology : official journal of the American Society of Clinical Oncology* **28**, 4339-4345, doi:10.1200/JCO.2010.28.9678 (2010).

72   Stone, R. M. *et al.* Phase IB study of the FLT3 kinase inhibitor midostaurin with chemotherapy in younger newly diagnosed adult patients with acute myeloid leukemia. *Leukemia* **26**, 2061-2068, doi:10.1038/leu.2012.115 (2012).

73   Berg J.M. & J.L., T. *Biochemistry, 5th edition*. (W. H. Freeman and Company, 2002).

74   Schwender, J. r. *Plant metabolic networks*. (Springer, 2009).

75   Bisswanger, H. *Enzyme kinetics : principles and methods*. 2nd. rev. and updated edn, (Wiley-VCH, 2008).

76   Zhang, J., Yang, P. L. & Gray, N. S. Targeting cancer with small molecule kinase inhibitors. *Nature reviews. Cancer* **9**, 28-39, doi:10.1038/nrc2559 (2009).

77   Cook, P. F., Neville, M. E., Jr., Vrana, K. E., Hartl, F. T. & Roskoski, R., Jr. Adenosine cyclic 3',5'-monophosphate dependent protein kinase: kinetic mechanism for the bovine skeletal muscle catalytic subunit. *Biochemistry* **21**, 5794-5799 (1982).

78   Cheng, Y. & Prusoff, W. H. Relationship between the inhibition constant (K1) and the concentration of inhibitor which causes 50 per cent inhibition (I50) of an enzymatic reaction. *Biochemical pharmacology* **22**, 3099-3108 (1973).

79   Michaelis, L. & Menten, M. L. Die Kinetik der Invertinwirkung. *Biochemische Zeitschrift* **49**, 333-369 (1913).

80   Briggs, G. E. & Haldane, J. B. S. A note on the kinetics of enzyme action. *Biochem J* **19**, 338-339 (1925).

81   Segel, I. H. *Enzyme Kinetics: Behavior and Analysis of Rapid Equilibrium and Steady-State Enzyme Systems*. (Wiley Classics Library, 1993).

82   Adams, J. A. Kinetic and catalytic mechanisms of protein kinases. *Chemical reviews* **101**, 2271-2290 (2001).

83   Szafranska, A. E. & Dalby, K. N. Kinetic mechanism for p38 MAP kinase alpha. A partial rapid-equilibrium random-order ternary-complex mechanism for the phosphorylation of a protein substrate. *The FEBS journal* **272**, 4631-4645, doi:10.1111/j.1742-4658.2005.04827.x (2005).

84   *DYRK1B (NM_004714) Human cDNA Clone (OriGene)*, <http://www.origene.com/1/1/158040-dyrk1b-nm-004714-human-cdna-clone-dyrk1b-clone-trueclone-np-004705.html>

85   *Uniprot database: DYRK1B, code Q9Y463.*, <http://www.uniprot.org/uniprot/Q9Y463>

86   *Gateway® Cloning Technology*, <http://www.lifetechnologies.com/no/en/home/life-science/cloning/gateway-cloning.html>

104

87   *Directional Topo® Cloning*,
      <http://www.lifetechnologies.com/no/en/home/references/protocols/nucleic-acid-amplification-and-expression-profiling/pcr-protocol/directional-topo-cloning.html>

88   *pENTR™ Directional TOPO® Cloning Kits*,
      <http://tools.lifetechnologies.com/content/sfs/manuals/pentr_dtopo_man.pdf>

89   Shuman, S. Recombination mediated by vaccinia virus DNA topoisomerase I in Escherichia coli is sequence specific. *Proceedings of the National Academy of Sciences of the United States of America* **88**, 10104-10108 (1991).

90   *Vector NTI® Express Designer Software*,
      <http://tools.lifetechnologies.com/content/sfs/manuals/VectorNTIExpress_Designer_UG.pdf>

91   *Plasmid 23761: pDONR223-DYRK1B*, <http://www.addgene.org/23761/>

92   *DH5α™ Competent Cells user guide*,
      <http://tools.lifetechnologies.com/content/sfs/manuals/subcloningefficiencydh5alpha_man.pdf>

93   *QIAprep Spin Miniprep Kit*, <http://www.qiagen.com/products/catalog/sample-technologies/dna-sample-technologies/plasmid-dna/qiaprep-spin-miniprep-kit#resources>

94   *PCR Protocol for Phusion® High-Fidelity DNA Polymerase*,
      <https://www.neb.com/protocols/1/01/01/pcr-protocol-m0530>

95   *QIAquick® Gel Extraction Kit user guide*

96   *One Shot® TOP10 Chemically Competent E. coli*,
      <http://www.lifetechnologies.com/order/catalog/product/C404010>

97   *BigDye® Terminator v3.1 Cycle Sequencing Kit*,
      <http://www.lifetechnologies.com/order/catalog/product/4337455>

98   Katzen, F. Gateway((R)) recombinational cloning: a biological operating system. *Expert opinion on drug discovery* **2**, 571-589, doi:10.1517/17460441.2.4.571 (2007).

99   *Gateway® Recombination Cloning Technology*,
      <http://www.lifetechnologies.com/no/en/home/life-science/cloning/gateway-cloning/gateway-technology.html>

100   QuikChange Primer Design online software by Agilent Technologies.

101   *QuikChange II Site-Directed Mutagenesis Kit (Agilent Technologies), Instruction manual*
      <http://www.chem.agilent.com/library/usermanuals/Public/200555.pdf>

102   *PfuTurbo DNA Polymerase (Agilent Technologies), Instruction manual*,
      <http://www.chem.agilent.com/library/usermanuals/Public/600250.pdf>

103   *XL10-Gold Ultracompetent Cells (Agilent Technologies)*,
      <http://www.chem.agilent.com/library/usermanuals/Public/200315.pdf>

104   *BL21-CodonPlus Expression Competent Cells - Details & Specifications*,
      <http://www.genomics.agilent.com/article.jsp?pageId=484>

105   Affinity Chromatography Principals and Methods, Handbook from GE Healthcare. (2007).

106   Gelfiltration Principal and Method, Handbook by GE Healthcare. (2010).

107   *Nanodrop 2000c*, <http://www.nanodrop.com/productnd2000coverview.aspx>

108   Ericsson, U. B., Hallberg, B. M., Detitta, G. T., Dekker, N. & Nordlund, P. Thermofluor-based high-throughput stability optimization of proteins for structural studies. *Analytical biochemistry* **357**, 289-298, doi:10.1016/j.ab.2006.07.027 (2006).

109   Pantoliano, M. W. *et al.* High-density miniaturized thermal shift assays as a general strategy for drug discovery. *Journal of biomolecular screening* **6**, 429-440, doi:10.1089/108705701753364922 (2001).

110   Dupeux, F., Rower, M., Seroul, G., Blot, D. & Marquez, J. A. A thermal stability assay can help to estimate the crystallization likelihood of biological samples. *Acta crystallographica. Section D, Biological crystallography* **67**, 915-919, doi:10.1107/S0907444911036225 (2011).

111   Thermal Shift (FTS) Assay, A. N. L.

112   (HR2-072), S. S. S. u. g. b. H. r. <http://hamptonresearch.com/documents/product/hr003755_2-072_user_guide.pdf>

113 Ludwig, C. Diffusion zwischen ungleich erwärmten Orten gleich zusammengesetzter Lösungen. *Sitzungsbericht. Kaiser. Akad. Wiss. (Mathem.-Naturwiss. Cl.), Wien* **65** (1856).

114 Baaske, P., Wienken, C. J., Reineck, P., Duhr, S. & Braun, D. Optical thermophoresis for quantifying the buffer dependence of aptamer binding. *Angewandte Chemie* **49**, 2238-2241, doi:10.1002/anie.200903998 (2010).

115 Wienken, C. J., Baaske, P., Rothbauer, U., Braun, D. & Duhr, S. Protein-binding assays in biological liquids using microscale thermophoresis. *Nature communications* **1**, 100, doi:10.1038/ncomms1093 (2010).

116 *MicroScale Thermophoresis (MST)*, <http://www.nanotemper-technologies.com/technology/microscale-thermophoresis/article/background/>

117 Jerabek-Willemsen, M., Wienken, C. J., Braun, D., Baaske, P. & Duhr, S. Molecular interaction studies using microscale thermophoresis. *Assay and drug development technologies* **9**, 342-353, doi:10.1089/adt.2011.0380 (2011).

118 Rhodes, G. *Crystallography made crystal clear : a guide for users of macromolecular models*. 3rd edn, (Elsevier/Academic Press, 2006).

119 *JCSG-plus™ initial crystallization screen* <http://www.moleculardimensions.com/shopexd.asp?id=2541>

120 *Wizard I and II Crystallization screen (Emerald Bio) instruction sheet*, <http://www.rigakureagents.com/UploadDocuments/Wizard%20Classic%20Screen_Instruction_Sheet_Rigaku.pdf>

121 Hui, R. & Edwards, A. High-throughput protein crystallization. *Journal of structural biology* **142**, 154-161 (2003).

122 *Hampton Reasearch. Additive Screen HT (HR2-428) User Guide* <http://hamptonresearch.com/documents/product/hr003789_binder1.pdf>

123 Krug, M., Weiss, M. S., Heinemannb, U. & Muellera, U. XDSAPP: a graphical user interface for the convenient processing of diffraction data using XDS. *Applied Crystallography*, 568-572 (2012).

124 Vagin, A. & Teplyakov, A. MOLREP: an automated program for molecular replacement. *J. Appl. Cryst.* **30**, 1022-1025 (1997).

125 Vagin, A. & Teplyakov, A. An approach to multi-copy search in molecular replacement. *Acta crystallographica. Section D, Biological crystallography* **56**, 1622-1624 (2000).

126 Winn, M. D. *et al.* Overview of the CCP4 suite and current developments. *Acta crystallographica. Section D, Biological crystallography* **67**, 235-242, doi:10.1107/S0907444910045749 (2011).

127 Potterton, E., Briggs, P., Turkenburg, M. & Dodson, E. A graphical user interface to the CCP4 program suite. *Acta crystallographica. Section D, Biological crystallography* **59**, 1131-1137 (2003).

128 Murshudov, G. N., Vagin, A. A. & Dodson, E. J. Refinement of macromolecular structures by the maximum-likelihood method. *Acta crystallographica. Section D, Biological crystallography* **53**, 240-255, doi:10.1107/S0907444996012255 (1997).

129 Adams, P. D. *et al.* PHENIX: a comprehensive Python-based system for macromolecular structure solution. *Acta crystallographica. Section D, Biological crystallography* **66**, 213-221, doi:10.1107/S0907444909052925 (2010).

130 Li, J. *et al.* [Research on the selective kinetics of HIV-1 nucleoside reverse transcriptase inhibitor drug resistance-associated mutations among 4 AIDS patients receiving highly active antiretroviral therapy]. *Zhonghua liu xing bing xue za zhi = Zhonghua liuxingbingxue zazhi* **29**, 794-800 (2008).

131 *Mercaptoethanol - compound Summary (Pubchem)*, <http://pubchem.ncbi.nlm.nih.gov/summary/summary.cgi?cid=1567>

132 Tahtouh, T. *et al.* Selectivity, cocrystal structures, and neuroprotective properties of leucettines, a family of protein kinase inhibitors derived from the marine sponge alkaloid leucettamine B. *Journal of medicinal chemistry* **55**, 9312-9330, doi:10.1021/jm301034u (2012).

133 Gockler, N. *et al.* Harmine specifically inhibits protein kinase DYRK1A and interferes with neurite formation. *The FEBS journal* **276**, 6324-6337, doi:10.1111/j.1742-4658.2009.07346.x (2009).